Summer 2013

Improving the Stability of High and Low Bandgap Polymers Organic Photovoltaic Devices Using a Solution Based Titanium Sub-Oxide Interfacial Layer

Kurniawan Foe
Old Dominion University

IMPROVING THE STABILITY OF HIGH AND LOW BANDGAP POLYMERS ORGANIC PHOTOVOLTAIC DEVICES USING A SOLUTION BASED TITANIUM SUB-OXIDE INTERFACIAL LAYER

by

Kurniawan Foe
B.Sc. May 1998, Physics, University of Indonesia, Indonesia
M.Sc. May 2000, Physics, University of Indonesia, Indonesia
M.S. May 2006, Physics, Old Dominion University

A Dissertation Submitted to the Faculty of
Old Dominion University in Partial Fulfillment of the
Requirements for the Degree of

DOCTOR OF PHILOSOPHY

ELECTRICAL AND COMPUTER ENGINEERING

OLD DOMINION UNIVERSITY
August 2013

Approved by:

Gon Namkoong (Director)

Helmut Baumgart (Member)

Sylvain Marsillac (Member)

Tarek Abdel-Fattah (Member)

ABSTRACT

IMPROVING THE STABILITY OF HIGH AND LOW BANDGAP POLYMERS ORGANIC PHOTOVOLTAIC DEVICES USING A SOLUTION BASED TITANIUM SUB-OXIDE INTERFACIAL LAYER

Kurniawan Foe
Old Dominion University, 2013
Director: Dr. Gon Namkoong

The improvement in device efficiency has brought organic photovoltaic (OPV) devices closer to commercial viability, highlighting the importance of studying the lifetime and stability of OPV devices. At present, the lifetime and stability of OPV devices is much shorter and poor mainly caused by oxygen, moisture, and light resulting in the oxidation on low work function electrodes and the degradation of the morphology of the photoactive layer. To improve the lifetime and stability of the OPV devices, we used newly developed low bandgap polymer, PCDTBT, as the electron acceptor material and a solution based titanium sub-oxide (TiO_x) interfacial layer inserted between the active layer and the cathode.

In our experiment, we fabricated unencapsulated bulk heterojunctions OPV devices based on the high and low bandgap polymers of P3HT:PC61BM and PCDTBT:PC71BM, respectively. We synthesized a solution based TiO_x by using a sol-gel chemistry method. We performed stability tests on the OPV devices: (1) with and without the TiO_x layer (Case (I)) to test the effectiveness of the TiO_x layer in protecting the photoactive layer from degradation, (2) with and without a protection cover (a high research grade opaque Al foil) to observe the device performance in a dark/light environment (Case (II)), and (3) in different storage media conditions: (a) air, (b) glove box, (3) ante-chamber of a glove

box, and (4) (Case (III)). We spent significant time and effort in optimizing the fabrication processing steps including; the thickness of the active layer, pre-annealing and post-annealing treatments. We fabricated the OPV devices by using the optimal fabrication procedure.

We found that the best PCE value of 4.1% achieved for the P3HT:PC61BM OPV cell and 5.1% for the PCDTBT:PC71BM OPV cell. On the air stability test, we found that the OPV cell of P3HT:PC61BM materials showed good air stability performance resulting in the PCE only dropping 26% over a period of 70 days (stored in a glove box). The PCDTBT:PC71BM devices stored in the glove box over a period of 30 days showed relatively good air stability performances; (1) the device with a TiO_x layer and an opaque Al cover the PCE dropped only 16%, (2) the device with the TiO_x layer and without an opaque Al cover PCE dropped 34%, and (3) the device without a TiO_x layer and with an Al cover PCE dropped 48%. While the PCDTBT:PC71BM devices stored in the air; (1-2) with a TiOx layer and with/without opaque Al covers the PCE values dropped 92% after 18 days, and (3) without the TiO_x layer and with an opaque Al cover, the PCE dropped 100% after 3 days. These results highlight the effectiveness of the TiO_x layer in protecting the active layer from degradation. We concluded that the TiO_x layer effectively improved the stability the OPV devices.

With love and humble admiration, I dedicate this thesis to
my God and Savior, Lord Jesus,
to my wife, Lian, and our children, Joshua, Micah, and Nehemiah, and
to my parents, brothers, and sisters.

ACKNOWLEDGMENTS

"*To everything there is a season, and a time to every purpose under the heaven*" (Ecclesiastes 3:1). This academic life has been a long journey. I thank God for all people whom He has brought to help, to inspire, to teach, and to support me in the journey.

I want to thank my research advisor, Dr. Gon Namkoong, for his guidance, for inspiring me to work so hard in the research lab, for introducing me so many exciting nanoscale research projects, in particular, the organic photovoltaic devices that I have never imagined before, and for the invaluable input to finish this dissertation. I want to thank my doctoral committee, Dr. Helmut Baumgart, Dr. Tarek Abdel-Fattah, and Dr. Sylvain Marsillac, for their valuable discussions and guidance in this dissertation.

I want to thank faculties at Department of Physics and Department of Electrical and Computer Engineering at Old Dominion University for teaching me wonderful lessons in science and technology during my academic studies there. I want to thank the Chairs and Graduate Program Directors from both departments, especially Dr. Gail Dodge and Dr. Oscar Gonzalez, for their support in the transition and the completion of my doctoral studies, respectively. Also I want to thank to the staff from both departments for their help.

I enjoyed my time working in the ODU Applied Research Center Laboratories. I want to thank Dr. Hani Elsayed-Ali as the Director of ODU ARC, Dr. Wei Cao and Dr. Diefeng Gu for their help in characterizing my samples and their valuable input, and the

ODU-ARC staff. I also want to thank staff at the Applied Research Center of the William and Mary College, Dr. Fattah and the staff at Christopher Newport University, Dr. Sham-Shajing Sun from The Center for Materials Research at Norfolk State University, and Dr. In-Wook Hwang from Gwangju Institute of Science and Technology for their help in characterizing my samples and sharing their knowledge in organic photovoltaic devices.

I want to thank my research lab mates, Sri Sabarinadh, Sampath Chennuri, Arda Akman, Kevin Latimer, Matthew Sampson, and Dr. Patrick Boland Jr. for making the work around the lab so much fun. I appreciate their friendship, hard work, and support in maintaining the research equipment and facility in good condition, sharing their brilliant ideas, and working until late at night sometimes either to fix equipment or to conduct experiments.

I could not be thankful enough for the late Prof. Darmadi Kusno and Prof. Yohanes Surya who encouraged me to study in the US. They had encouraged me greatly to pursue my academic dream. They are more than just mentors who had inspired me immensely; they have become great models and friends to me.

I appreciate greatly the help from staff at the ODU Writing Center, Mr. Bill Thompson, and Mrs. Linda Jones in writing this dissertation. I want to thank them for working with my English and for making time out of their busy schedules to read and edit my dissertation.

I greatly appreciate the support from the former ODU President, Dr. Roseann Runte, the current ODU President, President John R. Broderick, Vice President, Dr. Ellen Neufeldt, and ODU administrations. They have been encouraging me during my studies and are great supporters and partners in serving the international community at ODU.

There are so many great friends in many different paths of life that really helped me during my study in the US. I also want to thank my international and American friends in Hampton Roads area. In particular, I want to thank the individuals who worked and have been working along with me in Global Student Friendship. I want to thank Pastor Rich and Kathy Hardison, Sundeep Bodapati, Swetha Gali, Senthilraja Singaravelu, Frency and Kavitha Varghese, Soyoung and Sanghoon Son, Ron and JoAnn Evers, Charlie and Gail Woolford, Gordon and Ruth Paulson, Scott and Kathy Strickland, Jimmy and Barbara King, Martin and Edwina Morgan, Tom and Ellen Biro, Mrs. Helena Garrick, Dr. Hap Struthers, Dr. Lytton and Mrs. Libby Musselman, Danya Horton, Semuel Rompis, Diana Thomas, and Nick and Gail Rerras. I want to thank friends from the local churches especially from Tabernacle Church of Norfolk for their support and prayer.

I am forever grateful for the unconditional love that I am blessed with my parents, Men Than Foe and Sinjorita Foe, and my siblings; Joesmiati Stevanus, Fadjarawati Lahey, Sastra August Kurniawan, Setiawan Kurniawan, and their families. I also want to thank my parent-in-laws, David and Esther Sutanto. I am thankful to God for my children; Joshua, Micah, and Nehemiah. They are wonderful children and gifts from God. Most of all, I want to thank God for my wife, Lian, for her love, her sacrifice, endless support, encouragement, and believing in me. This dissertation is certainly not possible without God. I thank Lord Jesus Christ for His blessing and provision, for giving me the opportunity to study in the US, for loving me unconditionally, for allowing me to finish my work, and for His divine guidance. I pray that my work will bring glory to Him and His name alone.

NOMENCLATURE

AFM	atomic force microscope/microscopy
AM1.5G	air mass 1.5 global
a.u.	arbitrary unit
BHJ	bulk heterojunction
DI	de-ionized water
e	electron charge, C
eV	electron volt
e-beam	electron beam
HOMO	the highest occupied molecular orbital
IPCE	incident photon-to-current collection efficiency
IQE	internal quantum efficiency
J-V	current density – voltage
LUMO	the lowest unoccupied molecular orbital
NREL	National Renewable Energy Laboratory
OPV	organic photovoltaic
OLED	organic light emitting diode
PTFE	polytetrafluoroethylene
PV	photovoltaic
TEM	transmission electron microscope
UV-Vis	ultraviolet visible
V_C	Coulombic potential

XPS	x-ray photoelectron spectroscope/spectroscopy
XRD	x-ray diffraction/diffractometer

MATERIALS

CB	chlorobenzene
DCB	1,2-dichlorobenzene
ITO	indium tin oxide
P3HT	poly(3-hexylthiophene)
PC61BM	[6,6]-phenyl-C_{61}-butyric acid methyl ester
PCDTBT	poly[N-9″-hepta-decanyl-2,7-carbazole-*alt*-5,5-(4′,7′-di-2-thienyl-2′,1′,3′-benzo-thiadiazole)]
PC71BM	[6,6]-phenyl-C_{71}-butyric acid methyl ester
PEDOT:PSS	poly(3,4-ethylene dioxythiophene) : poly(styrene sulfonate)
TiO_x	titanium sub-oxide

CONSTANTS and VARIABLES

E_g	bandgap energy, eV
FF	fill factor, %
J_{SC}	short circuit current density, mA cm^{-2}
PCE	power conversion energy, %
T_g	the glass-transition temperature, °C
μ_e	the electron mobility, $cm^2\ V^{-1}\ s^{-1}$
V_{OC}	open circuit voltage, V

TABLE OF CONTENTS

LIST OF TABLES

LIST OF FIGURES

Chapter 1

Organic Photovoltaic Devices

1.1. Photovoltaic technology

According to the first law of thermodynamics, any human activity requires energy input. With strong economic growth and continued heavy reliance of the energy demand on fossil fuels, it is projected that there will be a significant increase in carbon dioxide (CO_2) emissions. Today, about 20×10^{12} kg of CO_2 are put into the atmosphere every year, mainly by burning fossil fuel [1]. International discourse on climate change has been emphasizing the need for clean (near zero carbon-emission) and renewable energy technologies. Photovoltaic (PV) technology is the most attractive solution to modern energy demands. It has the ability to meet some of these demands by directly converting sunlight into electricity, while minimizing detrimental effects on the environment. The first oil crisis in the 1970's prompted a surge of interest in PV energy and other alternative energy sources and led to increased funding and research in these areas. In particular, this led to the development of the first non-single crystal PV devices such as polycrystalline silicon, amorphous silicon, and thin film and organic semiconductors [2]. This technology produces near-zero carbon emissions and limits the concentration of greenhouse gases in the atmosphere which is potentially slowing the global climate change [3]. Moreover, PV technology can potentially generate power anywhere there is light.

1.2. Organic photovoltaics

Alexandre Becquerel first observed the photovoltaic effect in an electrolyte solution in 1839 [4]. The basis for organic photovoltaic (OPV) technology was the discovery of dark conductivity in halogen doped organic compounds at Bell Laboratories in 1954, although many of them were not stable [5]. The first breakthrough in modern solid state PV based on organic materials was performed by C.W. Tang during his time at Eastman Kodak in the 1980s [6]. In 2000, Shirakawa, Heeger, and MacDiarmid were each awarded the Nobel Prize in Chemistry for "the discovery and development of conductive polymers" [7].

OPVs promise potential as a novel type of a renewable, delocalized, and competitive energy source. All properties of organic semiconductor materials are directly derived from the chemical properties of a carbon atom. The conductivity in organic semiconductors is due to conjugation, the alternation of single and double bonds between the carbon atoms [8]. Thin film photovoltaic devices based on organic semiconductors are interesting for several reasons. First, organic semiconductor materials have relatively strong absorption coefficients (usually $\geq 10^5$ cm^{-1}), which partly balances low mobility, giving high absorption in even thin devices (< 100 nm). Second, the electrical and chemical properties of organic semiconductors can be tailored by modifying the chemical structure of the compounds in endless combinations. Third, inorganic semiconductors have a relatively small diffusion length of excitons in these rather amorphous and disordered organic materials [9]. Fourth, organic semiconductors can be deposited at low temperatures with high throughput such as evaporation and solution processing that can lower manufacturing costs. Fifth, the use of very thin organic layers reduces the amount

of active material needed and also makes lightweight and flexible devices possible. For these and other reasons, OPVs have gained great attention.

1.3. State of the art of OPV devices

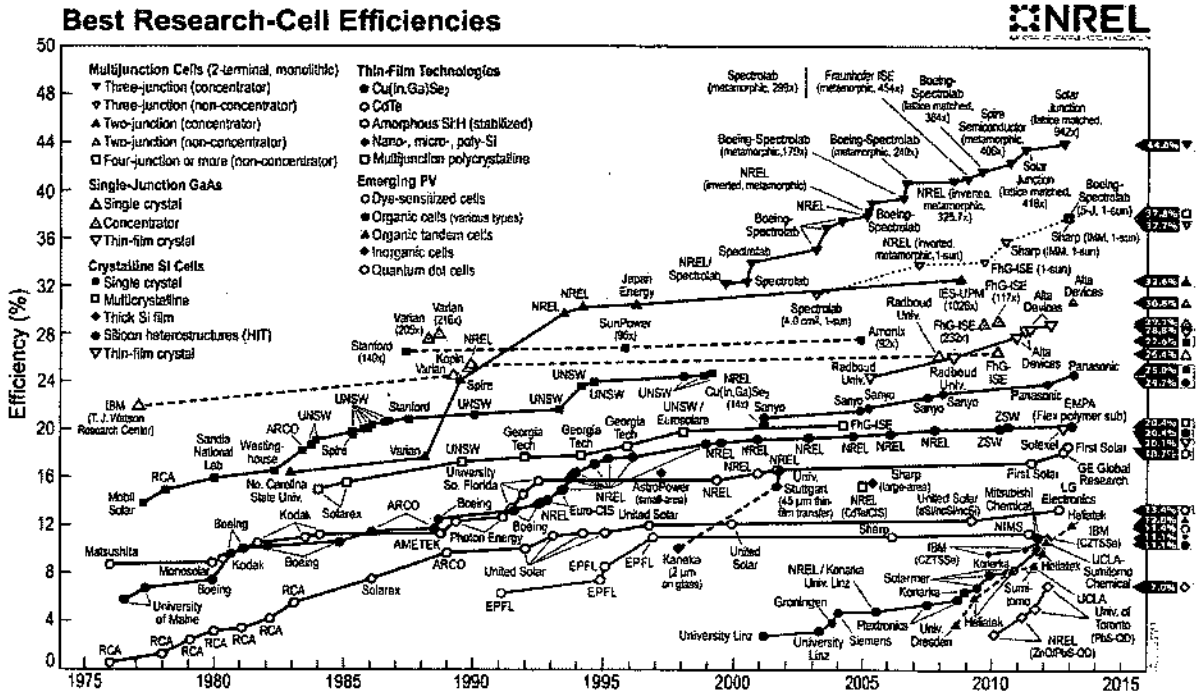

Figure 1.1: Laboratory best device efficiencies for various PV technologies including OPV devices. Reprinted with permission [10]. Copyright (2013) National Renewable Energy Laboratory.

Figure 1.1 summarizes the highest efficiencies in various solar cell technologies obtained throughout the years. It is clear that there are many different approaches to reach the same goal of converting sunlight to electricity, and each approach may be able to fill an appropriate role based on its individual advantages and tradeoffs. Numerous OPV technologies exist that are still not widely available commercially. Dye-sensitized solar cells with efficiencies of 11% have been reported to use an organic dye coated porous electrode with a high surface area to absorb light [11]. Another organic solar cell

technology is thin film solar cells based on solid state organic semiconductors. Recently, smart developments in the area of organic materials and OPV device design engineering made a great achievement by succeeding in the fabrication of OPV devices with PCE values of 10% [12]. Another promising approach to OPV technology is a tandem structure OPV cell which is an effective approach to enhancing the harvest of light by means of stacking multiple cells with complementary absorption spectra [13].

1.4. Motivation

Despite the excellent progress that has been achieved in the area of OPV devices, the lifetime of OPV devices is much shorter (inorganic PV devices have lifetimes in excess of 20 years) and they show poor stability due to photo-degradation of the organic materials [14]. The instability of OPV devices is mainly caused by oxygen, moisture, and light resulting in the oxidation of low work function electrodes and the degradation of the morphology of the photoactive layer [15,16]. These issues have limited OPV technology from becoming a widely spread application. Consequently, it appears that a significant improvement has to be made in terms of lifetime and stability to make OPV technologically attractive for mass production and commercialization. To achieve this goal, knowledge of the source of degradation and a possible solution to overcoming degradation on the OPV devices are very important.

1.5. Goal of this study

The goal of this study is to improve the stability and lifetime of OPV devices by using the solution based titanium sub-oxide (TiO_x) as an interfacial layer. The mechanism of

OPV device instability caused by degradation is not yet fully understood and very complex. The interfacial layer protects the organic materials from a physical or chemical interaction with the electrode materials. The diffusion of metal atoms into polymeric layers during the metallic cathode deposition process causes shunting or electrical shorting of the organic devices and limits their lifetime [17]. We will use a solution based titanium sub-oxide (TiO_x) as the interfacial layer which has been reported to be an efficient approach to improve the lifetime of OPV devices [18]. In the stability study of the OPV devices, we will investigate three different stability conditions. First, we will fabricate OPV devices with and without TiO_x layers by using optimal fabricating conditions (Case (I)). Second, we will store the fabricated OPV devices with and without a protection cover (a high research grade opaque Al foil) to observe the device performance in a dark environment and in an exposure to light environment (Case (II)). Third, we will vary the storage media: (1) in the ambient atmosphere, (2) in the N_2-filled atmosphere, (3) in the ante-chamber of a glove box, and (4) inside a refrigerator. We will observe the OPV device performance in different storage media conditions (Case (III)). We will perform a stability study on the OPV device at a prolonged storage time (over 30 days). Both the organic materials and electrodes need to be stable without any encapsulation.

We also will use the low bandgap polymer, PCDTBT, to improve the stability of the OPV devices. PCDTBT has large ionization potential energy and the highest occupied molecular orbital (HOMO) level below the air oxidation threshold of 5.27 eV, ensuring better air stability [19]. The stability of the fully aromatic backbone and the amorphous structure of PCDTBT are responsible for the remarkable ability of this semiconducting

polymer to withstand exposure to high temperatures.

1.6. Thesis outline

Chapter 1 has given a brief background of photovoltaic technology. The improvement and the trend of PV technologies are likely to face many new opportunities in the years ahead. The goal of the study is also presented. Chapter 2 discusses the degradation issues in the OPV cell which cause the instability of the OPV device and some of smart solutions. Chapter 3 presents literature studies of the state-of-the-art in the use of solution based titanium sub-oxide (TiO_x) materials in OPV devices and explains important functional features of the TiO_x interfacial layer in the OPV research. The experimental method and sol-gel synthesis of the solution based TiO_x material are also discussed.

Chapter 4 and 5 present the results on conventional high and low bandgap OPV devices without TiO_x layer. These two chapters discuss the uniqueness of the organic materials based on high and low bandgap polymers and the optimization processes in fabricating OPV devices. The results of the best high and low bandgap OPV devices achieved in our study by using optimal fabrication conditions are presented as well. Chapter 6 discusses the application and the optimization process of the TiO_x layer in the high bandgap P3HT:PC61BM OPV devices. A brief stability study of a high bandgap P3HT:PC61BM device using a TiO_x layer is presented. Chapter 7 discusses the application and optimization processes of the TiO_x layer in the low bandgap PCDTBT: PC71BM devices. Detailed stability studies based on fabricated OPV devices (1) with and without TiO_x layer (Case (I)), (2) with and without opaque Al covers (Case (II)), and

(3) different storage media conditions (Case (III)) are discussed. Finally, Chapter 8 concludes and suggests the future work of OPV devices.

1.7. Summary

In this chapter, we described the need of a photovoltaic (PV) technology which is a near-zero carbon emissions renewable technology. We discussed one of the PV technologies that we focused in our study which is the organic photovoltaic (OPV) technology. The progress and state of the art of OPV devices were described. The motivation and goal of our study, which is to improve the stability and lifetime of OPV devices, was explained. We described briefly the use of a solution based TiO_x material as the interfacial layer between the active layer and the Al cathode and the plan to perform a stability study to utilize and to test the efficacy of the solution based TiO_x material. Finally, the outline of this thesis was presented.

Chapter 2

Degradation Issues in Organic Photovoltaic Devices

2.1. Loss mechanism in an OPV cell

Photogenerated current in an OPV cell generally occurs in four main steps: (1) light absorption and exciton creation, (2) exciton diffusion, (3) exciton dissociation and charge separation, (4) charge transport and charge collection. The multilayered BHJ OPV structures show a great potential to achieve highly efficient OPV devices. However, the performance of the OPV devices, in reality, decreases due to loss mechanism processes as shown in Figure 2.1. Two key loss mechanisms operative in OPVs are geminate pair and bimolecular recombination losses [20]. Recombination of excess charge through localized states or trap states occurs radiatively or non-radiatively. In the radiative recombination mechanism, an electron transitioning into a relaxed state releases transition energy via a photon. In the non-radiative recombination mechanism, an electron's relaxation is mediated via a phonon emission.

The disordered nature of solution processed films of a BHJ OPV cell results in low charge carrier mobilities. The mobility of the slower charge carriers limits the photocurrent and efficiency of the OPV cells due to accumulation and concomitant high carrier concentration. If during charge transport, the charge carrier meets another carrier with an opposite sign, it recombines and does not contribute to the photocurrent thereby creating another photocurrent loss mechanism. Recombination of photogenerated charge

carriers in BHJ OPV cells reduces the short circuit current density (J_{SC}) and the fill factor (FF) of the OPV devices [21]. Smart electron and hole blocking materials have been used as an interfacial layer between the active layer and the metal electrode in OPV devices in order to protect the photoactive area of the device from the metal electrode.

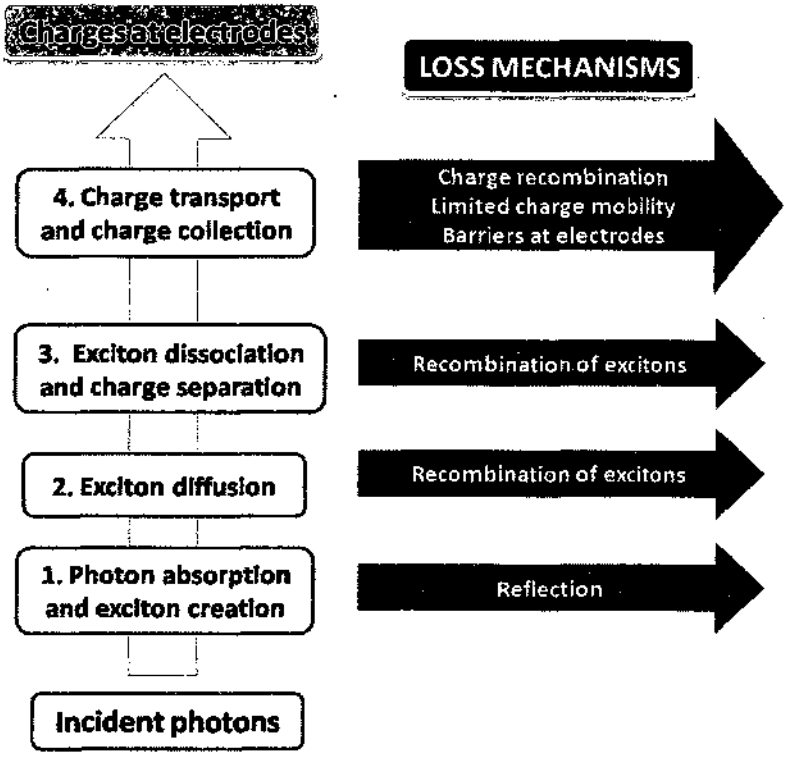

Figure 2.1: Possible loss mechanism processes in an OPV device.

2.2. Degradation issues in OPV devices

In general, degradation refers to the natural process of the declining qualities or certain properties of a given material over a period of time. At this time, the mechanism of OPV device degradation is not yet fully understood. A number of studies on degradation show that the degradation issue is rather complicated and might occur at multiple sites inside an OPV cell as shown in Figure 2.2 [14,16,22]. The critical problem

in the device degradation is related to the deterioration quality of the BHJ active layer due to the time dependent evolution toward the sub-optimal morphology and the device performance with time [23,24]. Physical and/or chemical degradation modes of OPV devices can be divided in two main categories:

- Degradation caused by the internal modification of the materials used and due to changes in the characteristics of the interface between orderly stacked thin film layers including the electrodes.
- Degradation caused by changes in the cell behavior induced by external triggers, such as oxygen, moisture, light, etc.

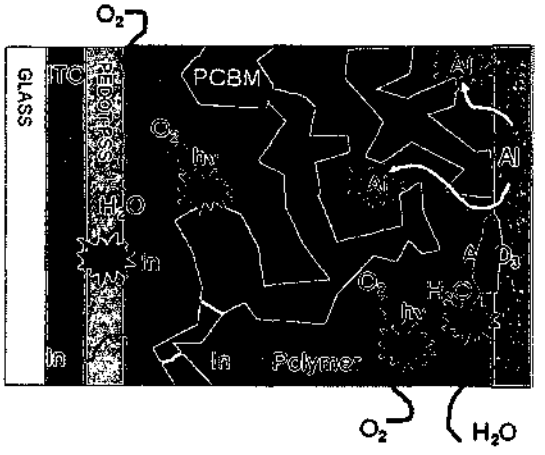

Figure 2.2: Cross-sectional view of a BHJ OPV cell with possible degradation processes. Reprinted with permission [22]. Copyright (2008) Elsevier.

All degradation processes ultimately lead to a decline or loss in the OPV cell's performance. Since many different issues can lead to the same degradation trend of OPV cells, it is generally strenuous to determine specifically the exact cause of degradation. By observing the changes in the important OPV device's parameters, such as short circuit current density (J_{SC}), open circuit voltage (V_{OC}), fill factor (FF), and power conversion

efficiency (PCE) values as a function of time, we can make some intelligent guesses concerning the type of degradation taking place. For example, a decrease in J_{SC} values during the OPV operation corresponds to a decrease in the number of charges collected at the OPV electrodes. Understanding and combating various loss mechanisms that occur in processes from optical excitation to charge collection and developing new materials (particularly donor materials) should lead to OPV's efficiencies of approximately 10% in the near future [12].

2.3. Degradation at the active layer

Organic materials such as P3HT, PC61BM, PCDTBT, and PC71BM are by nature more susceptible to chemical degradation from, for example, O_2 and H_2O, than they are to inorganic materials [25]. Fullerene materials are air sensitive once they have been in contact with O_2. The oxidative polymerization on the organic materials would take place under thermal treatments, even when no additional O_2 is present [26]. This polymerization is greatly accelerated when it occurs in an environment containing oxygen. Exposure to O_2 will also lower the conductivity of fullerene films. Upon O_2 uptake, the electron mobility is reduced by several orders of magnitude because the inserted oxygen acts as an electron trap [27].

2.4. Degradation at the electrodes

A typical metal used for a low work-function electrode (in the case of a conventional OPV structure, in which the metal electrode is the electron collecting electrode) is aluminum. At the organic-inorganic interface, metal atoms interact with carbon atoms

from the organic materials and create an Al-polymer complex interlayer [28,29]. When the Al evaporates onto organic materials, it also preferentially interacts with the carbon atoms in the conjugated backbone, which leads to a significant charge transfer from the metal atoms to some carbon and sulfur sites [30]. Thus, the control of the organic-inorganic interface is becoming an important issue in organic electronics [31].

Degradation of these negative electrodes is mainly caused by metal oxidation. Small amounts of O_2 and H_2O can be introduced unintentionally during the device fabrication absorbed in the different layers through the microscopic holes in the electrode [32]. As a result, a chemical reaction with O_2 and H_2O takes place. Krebs and his coworkers reported that radical species formed in the active layer may react with the Al electrode, leading to a gradual deterioration of the active layer/electrode interface quality [16]. Furthermore, light appeared to accelerate the degradation of the metal electrode as well [33].

2.5. Degradation at the PEDOT: PSS layer

Though the poly(3,4-ethylene dioxythiophene):poly(styrene sulfonate) or PEDOT: PSS has been used extensively in organic semiconductor devices, its acidic nature could cause interface instability to the active layer [34], corrosion to the ITO film [35], electrical inhomogeneities [36], and degradation to the interfacial layer of ITO/PEDOT: PSS [37]. It has also been reported that indium ions migrated into the PEDOT:PSS layer [38]. PEDOT:PSS also has a relatively low work function of 5.2 eV, showing that the hole injection could be a limiting factor in the OPV device [39].

2.6. Solutions to degradation issues

2.6.1. Inverted structure OPV device

To avoid the aforementioned degradation issues, as especially posted by PEDOT: PSS, an inverted structure of the OPV device was introduced. In an inverted OPV device structure, it is important to determine the appropriate energy level of the collecting electrode to match the active layer [40]. Different metal oxide semiconductor materials are introduced in device fabrication as a substitution for PEDOT:PSS. Cs_2CO_3, ZnO, TiO_2, WO_3, MoO_3, or V_2O_5 has been used to effectively substitute PEDOT:PSS and inserted between the active layers and top electrode [41,42,43,44]. In an inverted OPV structure, an air-stable high work function metal such as Au or Ag as the top anode, a transparent ITO is used as the bottom cathode, and air-stable solution interfacial layer metal oxides (between the active layer and the electrodes) have been used. Significant improvement of the lifetime of inverted OPV devices has been reported [45,46,47]. However, the use of expensive metals such as Au and Ag as the anodes would greatly increase the production cost.

2.6.2. Encapsulation technique

Encapsulation research in OPV devices is more particularly aimed to protecting OPV devices from degradation triggers such as oxygen and moisture. Thin film encapsulation layers such as Al_2O_3 [48], SiO_x/Al_2O_3/parylene [49], and Al_2O_3/Hf_2O [50] on top of OPV devices also demonstrated significant improvement in the lifetime of the devices. The inorganic barrier layer plays a significant role in reducing moisture and oxygen penetration and in increasing the thermal stability of the OPV cells [51].

2.6.3. Interfacial layer

To improve the stability and lifetime of OPV devices, an interfacial layer is inserted between the active layer and the electrodes. The interfacial layer has proven to slow down the degradation between the active layer and the electrode [52]. The interfacial layer is used to extract photogenerated carriers from the active layer to the electrode. One of the functional features of the interfacial layer is to determine the polarity of the OPV device. Depending on whether the bottom electrode forms the anode or the cathode, there are two different geometries of OPV devices; conventional and inverted structures. Therefore, the order of insertion of an interfacial layer in each case matters. Different solution based metal oxides (TiO_x, MoO_3, and ZnO) have been used as the interfacial layers [53,54]. In our study, we focused on the conventional structure. The interfacial layer was also effective in adjusting the energy level between the active layer and the electrode, to form a selective contact for charge carriers, and to act as an optical spacer. More detailed discussion about the TiO_x interfacial layer will be presented in the following chapter.

2.7. Summary

We have learned that oxygen, water, and light are major degradation sources of OPV devices. They could be introduced into the OPV system during the preparation of active solutions, fabrication processes, and in the storage environment of the OPV devices. Several alternative solutions to improve air-stability of OPV devices have been introduced such as inverted OPV device structures, encapsulation techniques, and metal oxide interfacial layers. At present, the exact degradation mechanism in OPV devices is

still unclear and an ongoing research topic. We can also study the degradation trend of OPV cells by observing the changes in the important OPV device's parameters, such as the J_{SC}, V_{OC}, FF, and PCE values as a function of time.

Chapter 3

A Solution Based Titanium Sub-oxide Interfacial Layer

3.1. Introduction

Titanium dioxide (TiO_2) belongs to the family of transition metal oxides [55]. TiO_2 has received a great deal of attention due to its chemical stability, non-toxicity, low cost, and other advantageous properties. Today, the primary use for the annual production of TiO_2 is as white pigment in paints [56,57,58], while the remaining production is used in various applications such as textiles, food additives, toothpaste, sunscreen cream, cosmetic products, medicine, plastic, paper, sensors, and semiconductors [59,60,61,62]. TiO_2 has also become a photocatalyst in the environmental decontamination [63,64] and semiconductor industry [65]. Due to its high refractive index, TiO_2 is also used as anti-reflection coating in inorganic PV cells and in many thin film optical devices [66].

In 1972, Fujishima and Honda [67] pioneered and studied the effect of TiO_2 as oxygen/water protection and as an oxygen scavenging agent originating from a combination of photocatalysis and inherent oxygen deficiency [68,69,70]. TiO_2 has also been reported as an electron acceptor and transport material and has been used in dye-sensitized photovoltaic devices [71,72], hybrid polymer/TiO_2 devices [73,74], and multilayer Cu-phthalocyanine/dye/TiO_2 devices [75,76]. TiO_2 is also a good hole blocking and electron selective contact in inverted photovoltaic devices [40].

3.2. Literature studies of the state-of-the-art research in the use of TiO_x layers in OPV devices

3.2.1. TiO_x layer as an interfacial layer

The incorporation of TiO_2 into organic semiconductor devices would seem to be a useful approach toward reducing the sensitivity of such devices to oxygen and water vapor. Kim and his coworkers used a low temperature sol-gel method to synthesize TiO_2 thin film for OPV application [77]. By using X-ray photoelectron spectroscopy (XPS), they found that the TiO_2 thin film exhibited an oxygen deficiency and the stoichiometric ratio of titanium and oxygen of 42.1:56.4 in percent or 1:1.34 rather than the 1:2 for TiO_2. It was therefore referred as titanium sub-oxide or TiO_x. It is well known that deficient oxygen sites act as electron donors providing a relatively high density of electron carriers for *n*-type transport [78].

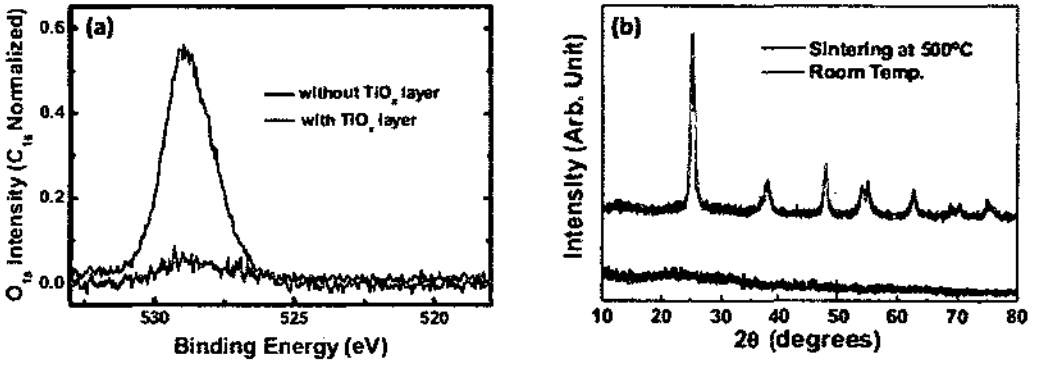

Figure 3.1: (a) XPS evidence of the oxygen scavenger effect of the TiO_x layer. Reprinted with permission [18]. Copyright (2007) John Wiley and Sons. (b) XRD patterns of two different TiO_x thin films deposited at room temperature and sintered at 500 °C. Reprinted with permission [77]. Copyright (2006) John Wiley and Sons.

The XPS analysis also showed the relative ratio of oxygen O_{1S}/ carbon C_{1S} inside the polymers, with and without the TiO_x layer as shown in Figure 3.1(a). The polymer without the TiO_x layer shows a high intensity peak with an asymmetric feature, whereas

this signal is hardly detectable in the polymer covered with the TiO_x layer. These results were attributed to the O_2/H_2O vapor protection and scavenging ability of the TiO_x material.

X-ray diffraction (XRD) patterns of two different TiO_x thin film conditions are shown in Figure 3.1(b). As a comparison, the TiO_x thin film deposited at room temperature exhibits an amorphous structure, while another one sintered at 500 °C showed an anatase crystalline peak [77]. At such high temperatures, organic semiconductors will be completely damaged. By using XRD analysis on the amorphous TiO_x films prepared by typical sol-gel processes, time-of-flight measurements indicate that the electron mobility (μ_e) was approximately 1.7×10^{-4} cm^2 V^{-1} s^{-1}, which is somewhat higher than mobility values obtained through other synthetic methods [18].

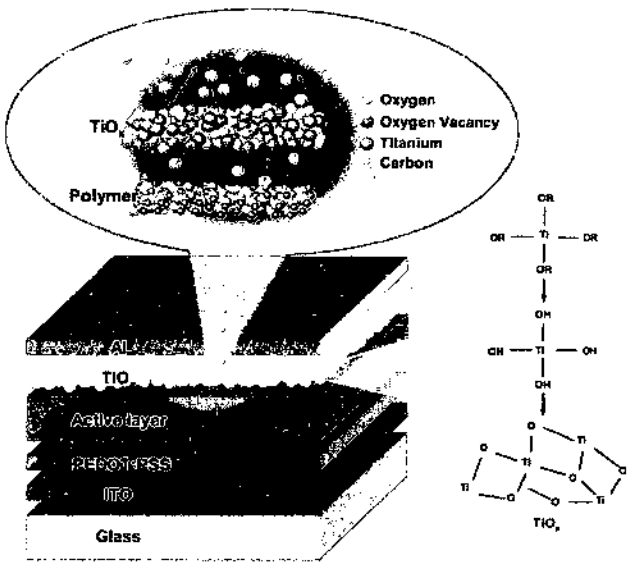

Figure 3.2: A schematic illustration of the device structure with a TiO_x layer. Reprinted with permissions [18]. Copyright (2007) John Wiley and Sons.

The OPV device architecture with a TiO_x layer is shown in Figure 3.2. As an interfacial layer, the TiO_x layer also protects the organic layer from physical or chemical interaction with the electrode materials. Gratzel reported that the energies of the bottom

of the conduction band (LUMO) and the top of the valence band (HOMO) of the TiO_x material, -4.4 eV and -8.1 eV respectively, were determined by using optical absorption and cyclic voltametry data [79]. This allows TiO_x to function as a good interfacial layer between the ITO and the BHJ active layer blend. The TiO_x layer deposited on the top of the organic-based active layers serves as an electron transport/injection layer for organic light emitting diodes (OLEDs) [80] and as a collector for OPVs [77].

PV devices ideally are operated at temperatures higher than ambient conditions (especially during the summer); therefore it is necessary to improve their high-temperature long-term stability. Wang and his coworkers reported that the operational lifetime of solar cells at elevated temperatures worsened because of their significant morphological change during high-temperature operations [81]. This problem could deteriorate the interface between the cathode (Al) and the active layer. They found that by introducing a TiO_x layer, the interfacial and morphological stability were improved at high temperature operations and improved the lifetime of OPVs.

3.2.2. TiO_x layer as an optical spacer

In a typical OPV device, light enters through the transparent electrode and is reflected by the back electrode, forming a standing wave. At the boundary of the reflective electrode, electric field strength diminishes, $|\boldsymbol{E}|^2 = 0$, while its peak is somewhere in the bulk heterojunction of the active layer, depending on the refractive index and the thicknesses of the layers as shown in Figure 3.3(a). Moreover, a relatively large fraction of the active layer is in a dead zone in which the photogeneration of carriers is significantly reduced. These problems also reduce the PCE of OPV significantly [82,83].

Two approaches have been introduced to solve the dead zone problems: (1) the use of a sufficiently thick active polymer layer so that the light is completely absorbed despite the existence of the dead layer and (2) keeping the active polymer layer thin and inserting an optical spacer to enable better light absorption. The first solution would simply increase the internal resistance of thicker films and will inevitably lead to a reduced fill factor.

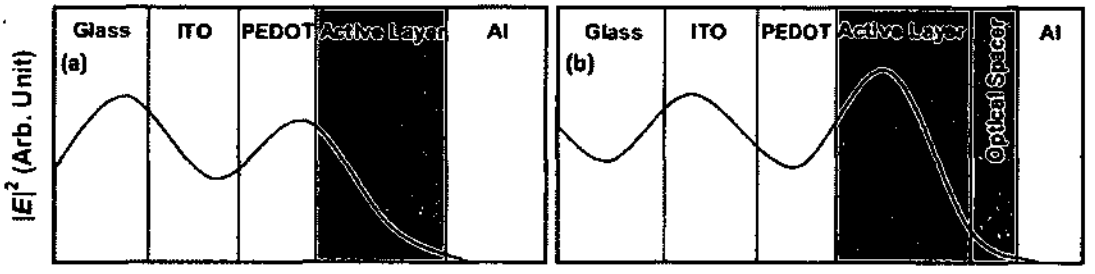

Figure 3.3: Schematic representation of the spatial distribution of the squared optical electric field strength $|E|^2$ inside the devices without optical spacer (left) and with optical spacer (right). Reprinted with permission [77]. Copyright (2006) John Wiley and Sons.

An optical spacer is a novel concept to optimize the absorption within the active layer as shown in Figure 3.3(b). In this approach, the optical spacer changes the device's architecture with the goal of spatially redistributing the light intensity inside the device between the active layer and the reflecting electrode [18,84]. To function as an optical spacer, a candidate material should fulfill a specific set of requirements: (1) the layer must be a good acceptor and an electron transport material with a conduction band edge lower in energy than that of the LUMO of the fullerene derivative (or the electron acceptor material); (2) the material's LUMO must be above (or close to) the Fermi energy of the collecting metal electrode; and (3) the material must be transparent to light with wavelengths within the solar spectrum [18]. Roy and his coworkers reported that the TiO_x layer was a great optical spacer material because it was a non-absorbing material in

the visible and infrared, the interference between the incident and reflected waves was changed and therefore the position of maximum intensity was shifted [85]. The efficacy of the TiO_x layer depended not only on its optical constants and thickness, but also on the optical constants and thickness of other layers within the device. Kim and his coworkers have reported that the OPV device with the TiO_x layer demonstrated a substantial enhancement of about 40% in the incident photon-to-current efficiency (IPCE) over the entire excitation spectral range [77]. The IPCE is defined as the number of photo-generated charge carriers contributing to the photocurrent per incident photon. This enhancement was attributed to increased absorption in the BHJ layer as a result of using a solution based TiO_x layer as the optical spacer.

3.2.3. TiO_x layer as an oxygen scavenger agent

As previously demonstrated in Chapter 2, the degradation behavior of OPV cells includes the direct photo-oxidation of BHJ active layer components. This problem leads to a loss of conjugation and irreversible deterioration of the light absorbing properties, the photochemical reduction of the organic constituents by the Al electrode and a subsequent chemical reaction between the organo-aluminum species and oxygen atoms [86]. The solution based TiO_x layer was also found to passivate the OPV device against intrusion of oxygen and moisture into the electronically active polymers and to improve device operating lifetimes [80,81,84,87]. The TiO_x layer allows the flow of electrons and blocks transport of holes.

Direct evidence of the oxygen barrier and scavenging effects came from the XPS measurements as shown in Figure 3.1(a). Heeger's group proposed two possible

mechanisms to explain the high stability of the TiO_x layer in OPV cells: (1) oxygen deficiencies in the TiO_x film providing adsorption sites for O_2, and (2) the TiO_x layer acting as a photochemically activated oxygen scavenger [77,88]. The TiO_x layer contains both Ti-OR (OR=alkoxide) functionalities and Ti-OH groups. The Ti-OR functionalities are photo-oxidized, consuming O_2 and generating CO_2, H_2O gas products, and [HCOO-] and Ti-OH moieties. The photo-activation of these TiO_x films leads to O_2 scavenging and forms the basis for thin films, which remove TiO_x when exposed to light, thereby protecting the underlying surface from O_2 gas. Furthermore, Cho and his coworkers demonstrated that by depositing a thin film of TiO_x layer, a significant improvement in field effect transistor device lifetime was achieved [88].

The effect of the TiO_x layer on the performance and stability of OPV is seen in Figure 3.4(a). It is observed that the OPV device with the TiO_x layer, J_{SC} values do not show any significant variation as the storage time increases up to 5 h with exposure to air, while with the device without the TiO_x layer, J_{SC} values decrease as the storage time increases [18]. Figure 3.4(b) shows that the lifetime of the OPV devices in the air is enhanced by the TiO_x layer by two orders of magnitude. It shows that the devices with the TiO_x layer again exhibit an excellent air-stability; the efficiency of the unencapsulated TiO_x devices remains almost unchanged after five-hour-exposure to air without any extra packaging, in remarkable contrast to the device without the TiO_x layer. This study further highlights the importance of the TiO_x layer in improving the stability and lifetime of OPV devices.

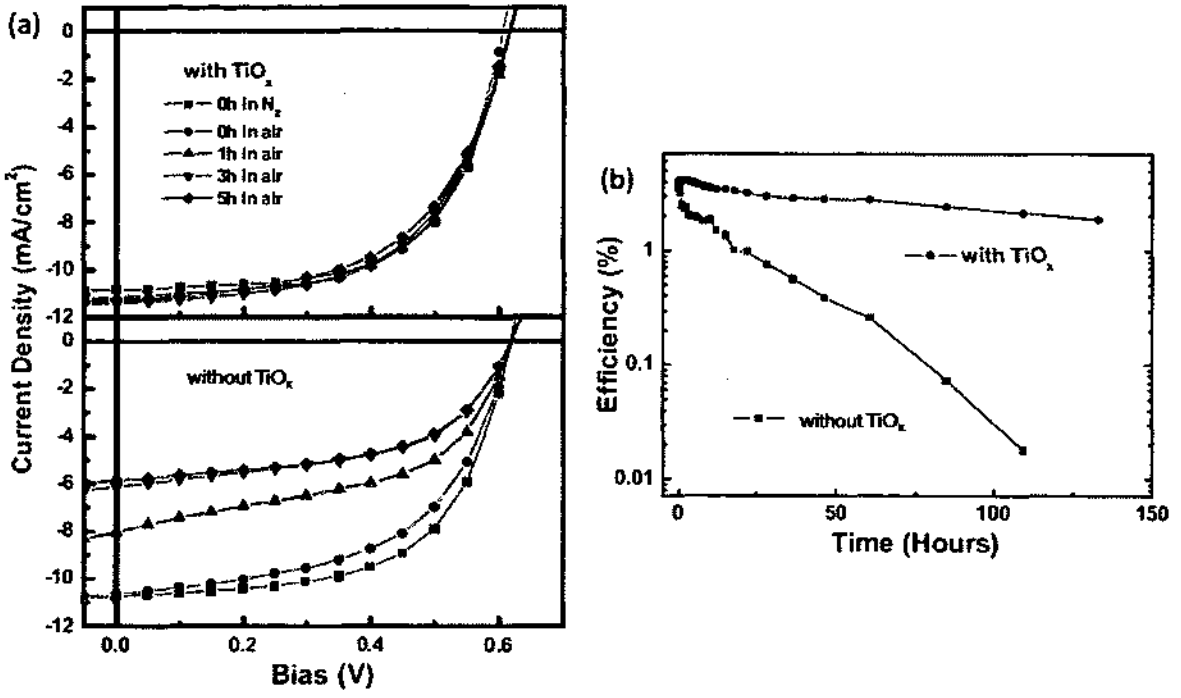

Figure 3.4: (a) *J-V* characteristics of P3HT:PC61BM OPV devices fabricated with and without TiO_x layers measured after various storage times in the air. The same devices were characterized periodically with increasing storage times. (b) Comparison of efficiencies of OPV devices fabricated with and without TiO_x layers as a function of storage time. Reprinted with permission [18]. Copyright (2007) John Wiley and Sons.

3.3. Experimental method of the solution-based TiO_x synthesis

Finally in this section we report our own experimental synthesis of solution based TiO_x materials using sol-gel chemistry [77,84]. For this study, sol-gel processing was performed by using an IKA rotary evaporator system developed by Boland in our laboratory as shown in Figure 3.5 [89]. Prior to use, rotary and condensation flasks were cleansed using the standard method (trichloroethylene, acetone, methanol, ethanol, and DI water rinse between each solvent), blown dry with N_2 gas, and placed in an oven to dry for one hour. These flasks were then installed on the condenser column. An empty flask was also allowed to rotate at 50 rpm and 120 °C in a silicon oil bath under an N_2

environment for one hour to ensure all moisture was removed from the system. The schematic diagram of the sol-gel TiO_x synthesis is shown in Figure 3.6.

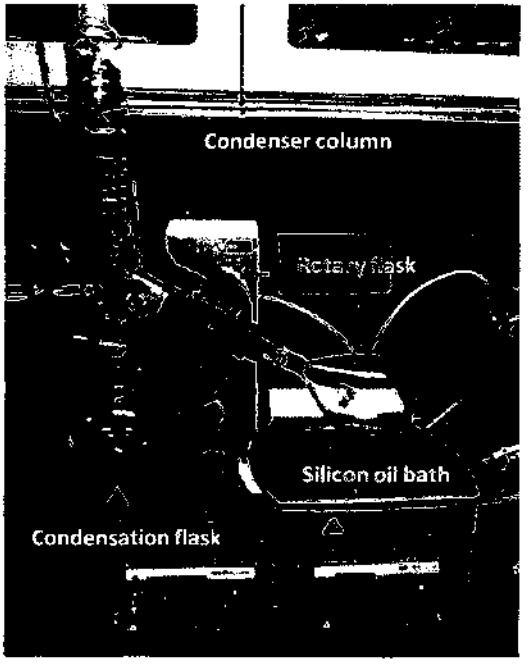

Figure 3.5: An IKA rotary evaporator system.

The sol-gel procedure started with an injection of the precursor, in the following order: (1) titanium (IV) isopropoxide ($Ti(OCH(CH_3)_2)_4$, 5 ml), (2) 2-methoxyethanol ($CH_3OCH_2CH_2OH$, 20 ml), and (3) ethanolamine ($H_2NCH_2CH_2OH$, 2 ml) into the rotary flask connected with a water condenser and nitrogen gas inlet/outlet at room temperature [84]. Figure 3.7(a) shows the fresh initial solution. After stirring for one hour at room temperature, the mixed solution was heated at 80 °C (using a silicon oil bath) for one hour resulting in a dark orange colored solution as observed in Figure 3.7(b). During this process, the inside of the flask must be in a dry N_2 environment and the mixed solution must be stirred continuously (600 – 800 rpm). The final step was to stir the mixed solution at the same speed at an elevated temperature of 120 °C for another hour. At the

end of the stirring process, we observed that the solution was transformed into a dark wine color as seen in Figure 3.7(c).

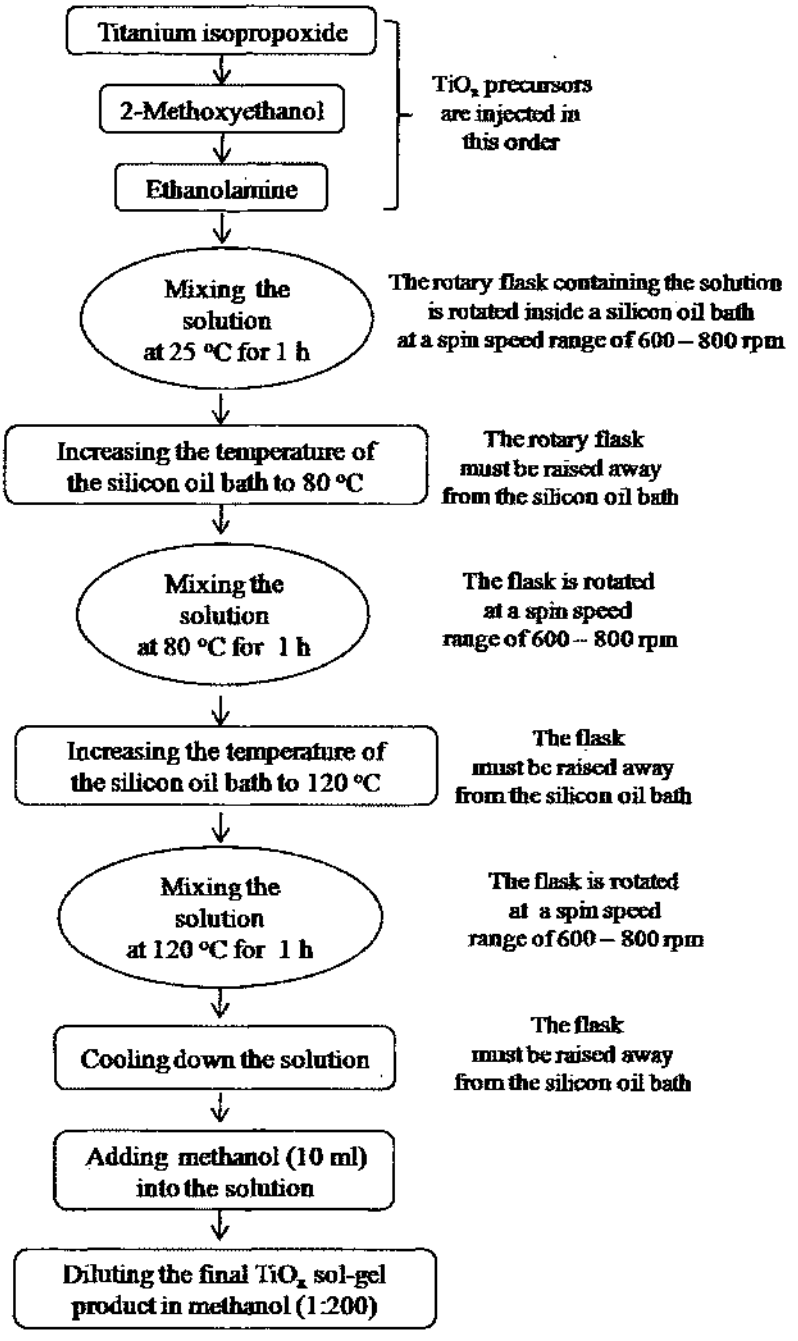

Figure 3.6: A schematic diagram of the sol-gel TiO_x synthesis.

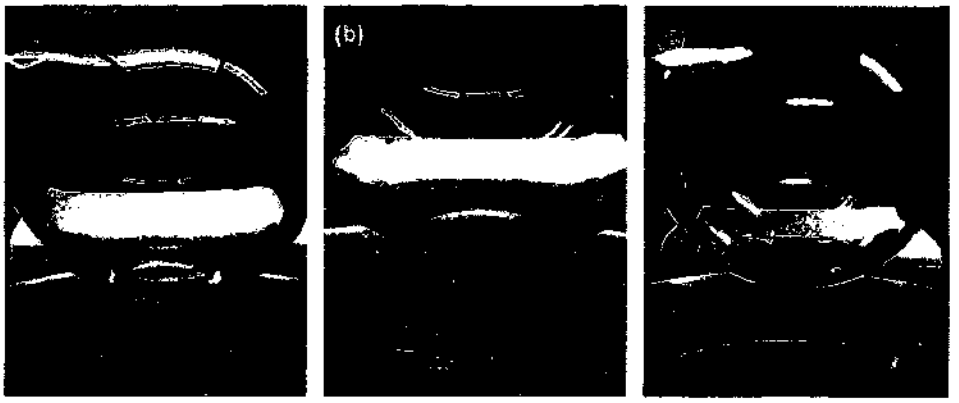

Figure 3.7: (a) A fresh mixture solution of TiO_x precursor and solvents. The mixed solution appeared (b) after stirring for 1 h at 80 °C (dark orange color) and (c) after stirring for another 1 h at 120 °C (dark red wine color).

As a final step after cooling to room temperature, 10 ml of methanol was injected to extract the final solution of TiO_x sol-gel product (see Figure 3.8). Prior to applying the TiO_x layer on the active layer, the TiO_x sol-gel product was diluted by 1:200 in methanol [77,84,90]. When the TiO_x layer deposited on the substrate was dried in the air, the condensation process started immediately resulting in the formation of Ti-O-Ti linkages [81,91,92]. These reactions occurred very slowly because the alcohol solution inhibits contact of the TiO_x with moisture. The condensation was significantly accelerated after spin casting forming solid TiO_x films.

Figure 3.8: The final TiO_x sol-gel product (right).

3.4. Summary

In section 3.2 we conducted a literature study of the state-of-the-art research results of solution based TiO_x layers. Lee and his coworkers [18] performed XPS measurements showing that the TiO_2 thin film exhibited an oxygen deficiency and a stoichiometric ratio of titanium and oxygen of 42.1:56.4 in percent or 1:1.34 rather than the 1:2 for TiO_2. Furthermore by using XRD analysis, Kim and his coworkers established that their films were completely recrystallized into polycrystalline TiO_x at the annealing temperatures of 500 °C [77]. Gratzel reported that the conduction and the valence energy levels of the TiO_x material, -4.4 eV and -8.1 eV respectively, satisfied the electronic structure requirements of an interfacial layer [79]. The solution based TiO_x interfacial layer has been reported to be significantly effective in enhancing photon absorption, in protecting damaging reactions between the active layer with oxygen and moisture, therefore in improving the lifetime and stability of OPV devices.

Finally in Section 3.3, we performed and showed an experimental procedure to synthesize a solution based TiO_x using sol-gel method in our laboratory. An IKA rotary evaporator system developed by Boland in our experiment was utilized to synthesize the TiO_x precursor under an N_2-filled atmosphere with a silicon bath as the heating bath and water to cool down any excessive heat. The synthetic process of a TiO_x material from the initial stage until the final stage was discussed.

Chapter 4

Results on the Fabrication of P3HT:PC61BM Based OPV Devices

4.1. OPV device fabrication

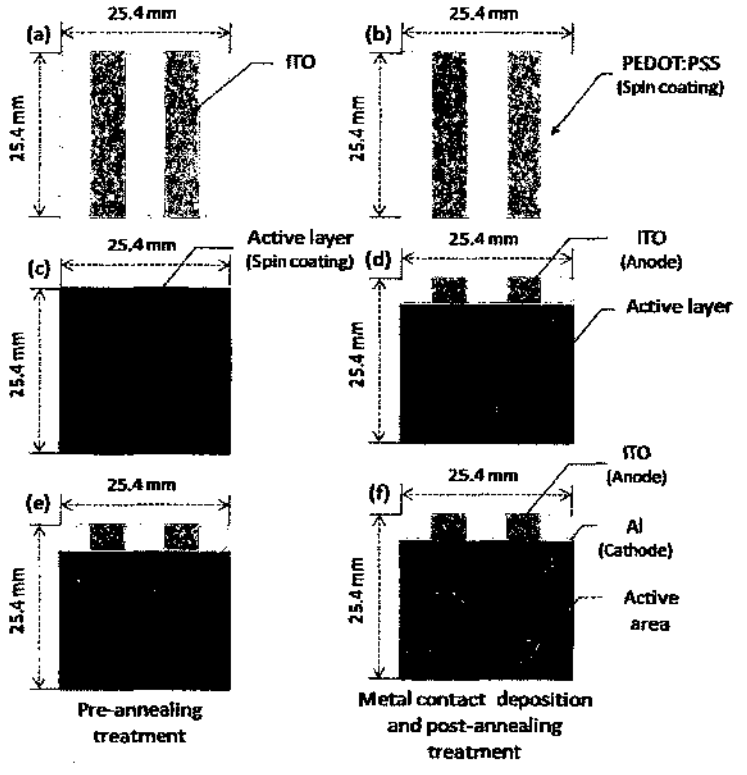

Figure 4.1: A diagram of typical fabrication processes on a 25.4 × 25.4 mm^2 OPV device. (a) Patterning an ITO glass substrate, (b) depositing a PEDOT:PSS layer, (c) depositing an active layer, (d) cleaning ITO anode films, (e) a pre-annealing treatment, and (f) depositing an Al cathode layer and a post-annealing treatment.

The typical fabrication steps of a 25.4 × 25.4 mm^2 OPV device are shown in Figure 4.1. OPV device fabrication processes are as follows: (1) patterning an ITO glass substrate using a combination of acidic solutions, (2) depositing a PEDOT:PSS solution

by a means of spin coating in the air, (3) depositing the active solution inside a glove box, (4) cleaning the ITO anodic layer, (5) a pre-annealing treatment, and (6) depositing Al metal contact using an *e*-beam evaporator and a post-annealing treatment. High quality fabrication processing conditions play a key role in realizing a high efficient OPV device.

4.2. Standard of OPV device characterizations

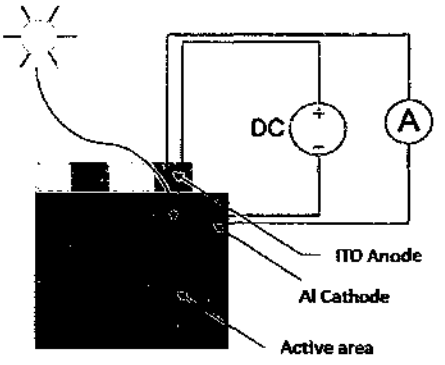

Figure 4.2: An OPV device characterization set up.

The physical layout of an OPV device showing 4 cells on each column or a total of 8 fabricated organic solar cells is shown in Figure 4.2. In our experiment, the solar cells were characterized under 100 mW cm^{-2} using a relatively uniform Oriel® Arc Lamp solar illuminator (outputting AM1.5G). I-V characterization curves were measured with a Keithley 2400 source meter. ITO was connected to the positive electrode, Al to the negative. The curves were recorded by continuously sweeping from -2V to +2V and recording data points in 10 mV steps.

The OPV results depended on the quality and the purity of the processing and fabricating conditions. It has been reported that the morphology of the active layer (and

the ability to control the morphology) has significantly led to the best performance of OPV devices [93,94].

Each OPV device fabricated in our experiment consists of 8 OPV cells displayed in Figure 4.2 (also see Figures 7.6 and A.7). This study comprises early basic research on OPV devices and as a consequence variability of the fabrication process for the devices was excessive. In some cases, although all OPV cells in an OPV device were processed with the same fabrication conditions, their performances might be different. In general, the top 6 cells were somewhat similar in their performances but subject to large random variability, while the last bottom cells away from the ITO anode were systematically less superior in their performance. In addition to the random variability, this indicates among others a location effect affecting the outcome either due to the mask design or process design. In an attempt to highlight the potential of the current OPV device architecture and the specific design we decided to report only the best 20 – 25 devices out of the 200 OPV devices processed during this thesis research. In practice that means only those OPV devices scoring in the 90^{th} percentile were selected for reporting. We adopted an approach to use only single measurements of the best cell on the 8 cell slide and to discard the data of the other 7 cells on the 8-cell OPV device. Because of the excessive process variability this dissertation focused only on the best case scenario of the absolute best devices. This is not a mature process but a very early research state. The performance and OPV parameters on a regular basis of our specific OPV devices are of course lower. The excessive process variability, the resulting low average performance, and yield are attributed to the difficult fabrication processes and limitations in a university laboratory. As a consequence we obtain a reduced mean PCE value on

average. In order to allow the reader a meaningful comparison of the regular capability of our current process and device design at this stage, and in order to preserve the integrity of the full data set, we also disclose the overall mean PCE value averaged over all 200 devices with a standard deviation, σ [95].

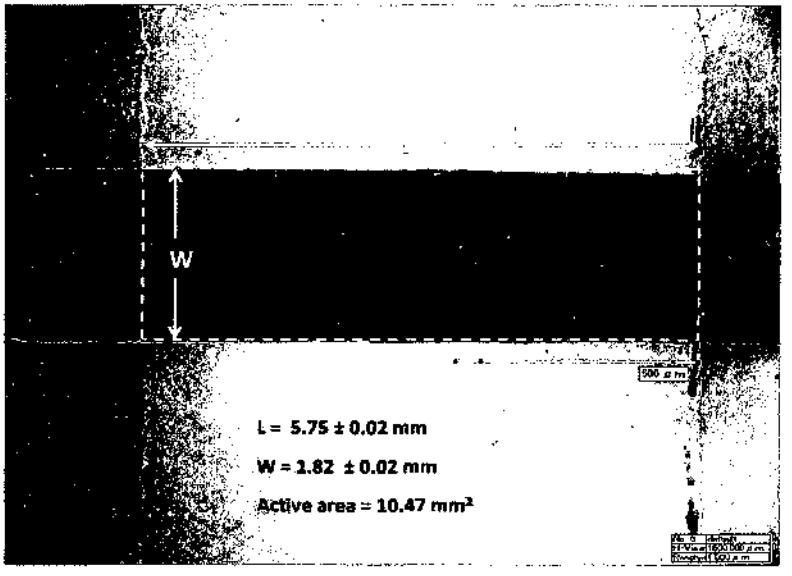

Figure 4.3: The back side image of an OPV cell captured by Hirox KH-3000 VD. The dotted rectangular area is an active area of the OPV device with a structure of ITO/PEDOT:PSS/ P3HT:PC61BM/Al.

We measured the physical active area of the OPV cell by using a Hirox KH-3000 VD equipped with a high resolution CCD camera. Figure 4.3 shows the back side of an OPV cell with a structure of ITO/PEDOT:PSS/P3HT:PC61BM/Al on a glass substrate. We measured the length and width of the active area of the OPV device at multiple locations by using the Hirox's software. We found a length of 5.75 ± 0.02 mm and a width of 1.82 ± 0.02 mm. The active area of the HIROX high resolution image is 10.47 mm^2. We used this active area for calculating the J_{SC} values of the device.

4.3. P3HT:PC61BM OPV devices

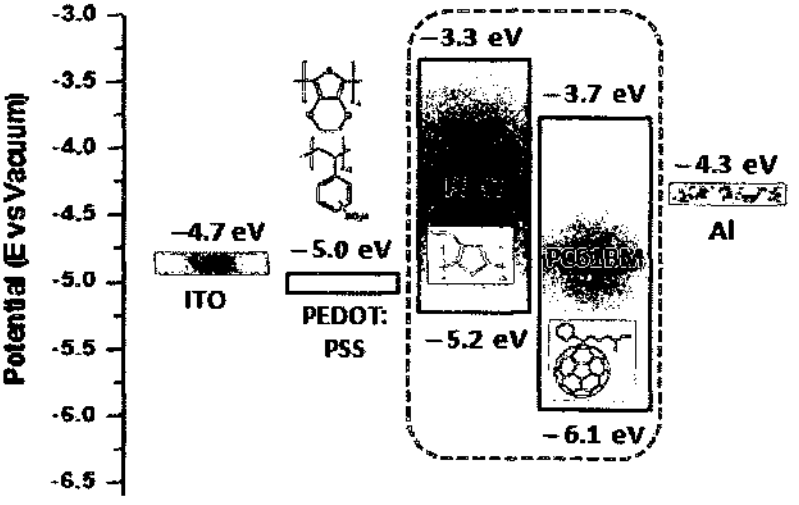

Figure 4.4: Energy levels of an OPV device of P3HT:PC61BM (with respect to the vacuum level).

We fabricated OPV devices using BHJ materials with P3HT as the electron donor and PC61BM as the acceptor. The composition of the active blend of P3HT:PC61BM was kept at a ratio of 1:0.8. The device structure for a high bandgap polymer OPV device is ITO/PEDOT:PSS/P3HT:PC61BM/Al. The energy levels of an OPV device of P3HT: PC61BM with respect to the vacuum level are shown in Figure 4.4. Aluminum with a thickness of 80 nm was used as the metal contact. It was deposited by using an *e*-beam evaporating system at a pressure of 2.0×10^{-7} Torr. The influence of selected control fabrication parameters, including the film thickness of the active layer, the pre- and post-annealing treatments on the structure evolution of polymer based BHJ systems is important in achieving an optimal morphology of the active layer as discussed in this chapter. Studies investigating the performance of polymer based BHJ systems based on fabrication parameters were taken into account.

Optimization steps such as the active layer thickness and the annealing treatment are important in OPV device fabrication. Since P3HT:PC61BM BHJ OPV devices have been explored extensively in past decades, we focused on the optimization of experimental conditions to achieve an excellent OPV device performance within the limitations of our laboratory facility and environment.

4.4. Absorption study on the P3HT:PC61BM layer

We examined the annealing effect on the absorption of the P3HT:PC61BM thin film. First, we deposited the active layer solution of P3HT:PC61BM onto two separate pre-cleaned glass substrates. Second, one of the coated substrates was annealed at a temperature of 140 °C for 2 min inside a N_2-filled glove box atmosphere (O_2, H_2O < 0.1 ppm), while the other was not. At a temperature slightly higher than the glass-transition temperature (T_g) of P3HT, the polymer chains become soft and modify their matrix to make an interpenetrating network of P3HT and PC61BM [96,97]. Thermal annealing increases inter-diffusion and mutual mixing of P3HT and PC61BM. Mixing of acceptor and donor materials results in improved charge transport and device performance [96]. The PC61BM molecules diffuse out of the polymer matrix to form percolated paths upon the annealing treatment on the P3HT:PC61BM composite film, resulting in an increase in the carrier mobility in the active layer. Phase segregation between P3HT and PC61BM also took place upon thermal treatment [98].

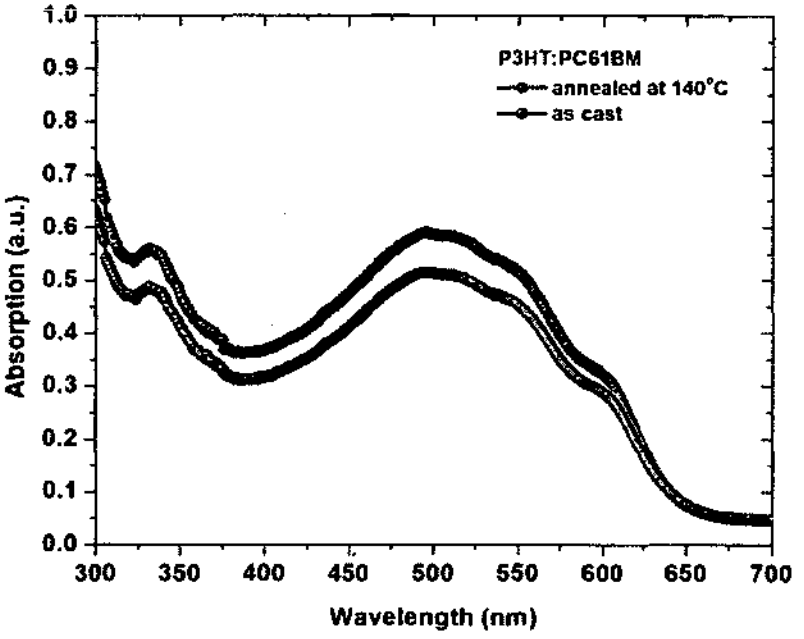

Figure 4.5: The UV-Vis absorption profile of P3HT:PC61BM active layers: as cast (black) and annealed at 140 °C for 2 min (red).

The intensity of the absorption spectrum for P3HT:PC61BM film, as expected, showed a considerable increase after the thermal annealing treatment, as shown in Figure 4.5. The absorption spectrum of the composite film of P3HT:PC61BM is a simple superposition of two spectra, one for P3HT and the other for PC61BM [99]. We observed a stronger intensity of the absorption peak for the annealed substrate at an approximate wavelength of 330 nm, which corresponds to PC61BM, while a broad absorption band peak between 450 nm – 600 nm was due to the $\pi - \pi^*$ transition of the P3HT backbone. An increase in the absorption strength after heat treatment normally means increased packing of the P3HT domains [100].

We also observed the peak absorption wavelength was at 500 nm with two visible shoulders at approximately 545 nm and 600 nm. In particular, the broaden shoulder at 600 nm corresponds to the vibronic transition that is enhanced in planarized P3HT. The latter indicates increased crystallinity within the P3HT domains and is consistent with

previous studies [101,102]. The increased inter-chain interaction among the P3HT chains due to thermal treatment results in more delocalized conjugated π electrons, the lowering of the bandgap between π and π*, and the increase of the optical $\pi - \pi^*$ transition which results in the observed red shift in the peak absorption wavelength [103]. In summary, the increase in the absorption intensity as a result of the annealing treatment on the active layer increases the number of the photogenerated excitons.

4.5. Active layer thickness

The active layer solution was prepared at a ratio of P3HT (30 mg):PC61BM (24 mg) (1:0.8 wt%) in 2 mL chlorobenzene solvent and was stirred at a temperature of 50 °C and at a low speed, overnight inside a globe box atmosphere (H_2O, O_2 < 0.1 ppm). Due to excellent miscibility and solubility of both P3HT and PC61BM in chlorobenzene results in a much finer domain size [104], which is beneficial for both increasing light absorbance and for better charge transport [105]. For the active layer thickness test, we fabricated four OPV devices with different active layer thicknesses of 87 nm, 98 nm, 115 nm, and 146 nm corresponding to spin coating speeds of 1500 rpm, 1250 rpm, 1000 rpm, and 750 rpm, respectively. Prior to depositing the active layer, a blend active layer of P3HT:PC61BM was run through a 0.45 μm PTFE filter. We measured the active layer thickness by using a Veeco Dektak 6M Stylus profilometer.

Optimum layer thicknesses must be determined to improve the optical field distribution across the cell, as well as to properly balance charge transport and current collection at the electrodes. In general, high efficiency OPV devices have been reported with an active layer thickness of approximately 100 nm [84,106]. Our experiment agrees

with these results. From the current density (J_{SC}) level and high fill factor (FF) values attained in our experiment we know that the OPV devices we fabricated were near an optimum condition.

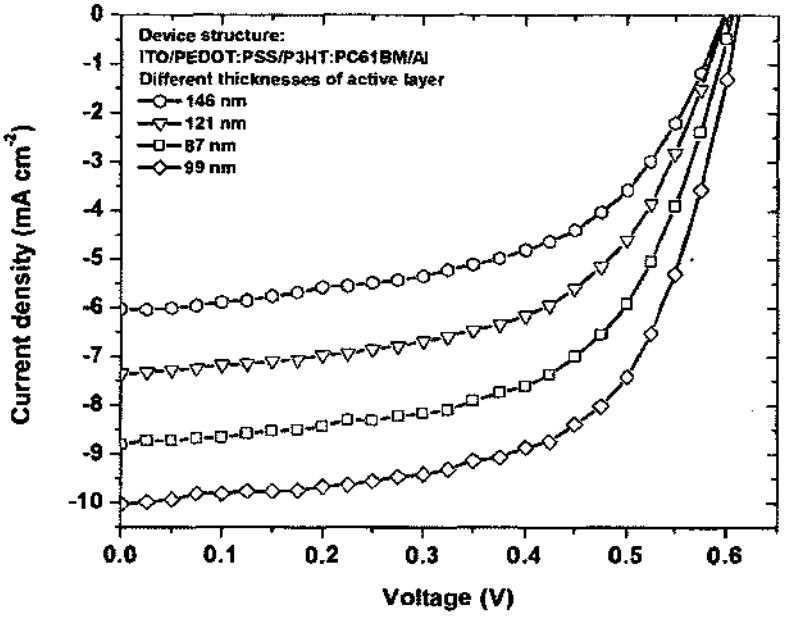

Figure 4.6: *J-V* characteristics of P3HT:PC61BM OPV cells fabricated at different thicknesses of the active layer.

The *J-V* curves of the OPV cells fabricated at different thicknesses of the active layer are shown in Figure 4.6. Each data represents the optimal performance of a single OPV cell in the respected OPV devices. We found that a 98-nm thickness of the active layer yielded the best results with an FF value of approximately 62% and a PCE value of 3.8%. The optimal fabrication condition (the active layer thickness) resulted in an increased photocurrent due to the increase in both charge mobility and absorption (where the space charge limit was reached). As shown in Table 4.1, as the active layer thickness of OPV cells increases, the J_{SC}, FF, and PCE values decrease, due mainly to the build-up of space charge, the increase of the series resistance, and recombination issues [107]. When the active solution was too thin, we observed the PCE value dropping slightly, possibly due

to the condition of organic semiconductor materials producing excitons not in the optimum condition.

Table 4.1: The parameters of P3HT:PC61BM OPV cells fabricated at different active layer thicknesses.

Active layer thickness (nm)	J_{SC} (mA cm^{-2})	V_{OC} (V)	FF (%)	PCE (%)
87	**8.80**	**0.61**	**58.69**	**3.13**
98	**10.07**	**0.61**	**61.69**	**3.80**
121	**7.43**	**0.60**	**56.71**	**2.52**
146	**6.06**	**0.60**	**54.56**	**1.98**

4.6. Pre-annealing treatment

The best annealing temperature achieving the most favorable morphological development of the OPV cell is normally above the glass-transition temperature, T_g, but below the melting point of the polymer [108]. The crystallinity of the polymer could also be improved by using a pre-annealing treatment process. This approach aims at maintaining the polymer ordering during the film formation stage. Reducing the solvent removal accelerates results in self-organization in polymer chains by controlling the active polymer layer growth rate from solution to a solid state. Pre-annealed films consist of highly ordered polymer chains, which cannot be achieved through thermal annealing. The extra step of annealing the films provides further enhancement in device performance [109]. In general, a pre-annealing temperature of 140 °C was used. For the pre-annealing test, we fabricated OPV devices with different pre-annealing times of 2 min, 4 min, and 8 min. We also fabricated a separate OPV device without the pre-annealing treatment as a comparison. In this particular OPV fabrication, other fabrication conditions (the thickness of the active layer and post-annealing treatment parameters) were fixed.

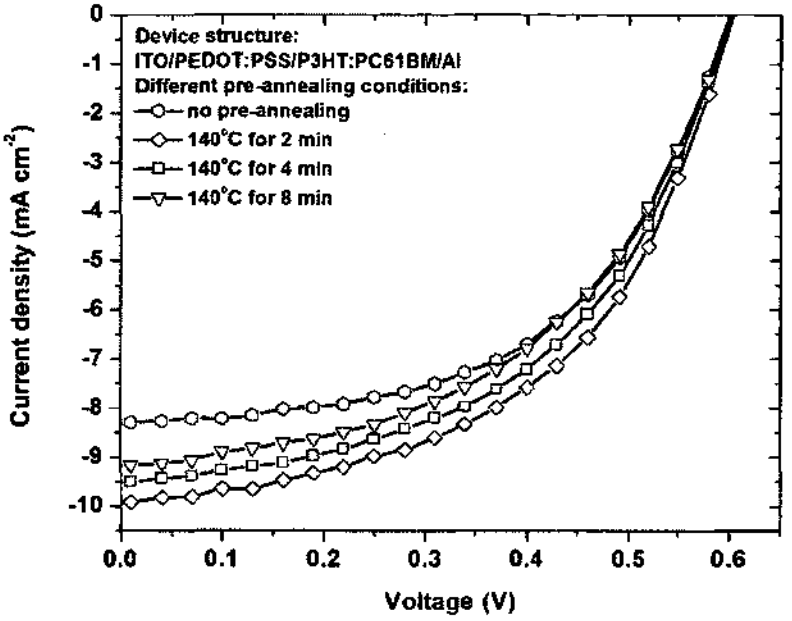

Figure 4.7: *J-V* characteristics of P3HT:PC61BM OPV cells fabricated at different pre-annealing conditions.

Figure 4.7 shows the *J-V* curves of the OPV cells fabricated at a pre-annealing temperature of 140 °C, but at different pre-annealing times. Each data represents the optimal performance of a single OPV cell in the respected OPV devices. As shown in Table 4.2, for the pre-annealing test on a P3HT:PC61BM device, the best OPV performance was obtained at a 2 min pre-annealing time. The effect of the pre-annealing condition was attributed mainly to the short circuit current density (J_{SC}) where the 2 min annealing time yielded the best J_{SC} and PCE values.

Table 4.2: The parameters of P3HT:PC61BM OPV cells fabricated at different pre-annealing conditions.

Pre-annealing condition	J_{SC} (mA cm^{-2})	V_{OC} (V)	FF (%)	PCE (%)
NO	**8.31**	**0.60**	**53.26**	**2.66**
140 °C for 2 min	**9.93**	**0.60**	**51.47**	**3.08**
140 °C for 4 min	**9.52**	**0.60**	**50.66**	**2.90**
140 °C for 8 min	**9.19**	**0.60**	**48.60**	**2.70**

The pre-annealing step has not only improved the blend of active layer by adhering it more strongly to the substrate, but it also enhanced the photocurrent of the device. This finding suggests that a pre-annealing time of 2 min is sufficient to allow optimal reorganization of the morphology, or that thermal annealing provides a more effective driving force for reorganization of the film. Longer annealing times resulted in a decrease in the peak efficiency of this device, likely as a result of phase segregation taking place on a larger than optimal length scale [110]. The OPV device fabricated without pre-annealing treatment did not show good results compared to other OPV devices with pre-annealing treatment.

4.7. Post-annealing treatment

The final optimization step in a P3HT:PC61BM OPV device is the post-production thermal annealing treatment. This step is also known as the post-annealing treatment. The effect of the post-annealing treatment on P3HT:PC61BM OPV devices has been studied and reported elsewhere [34,101,111]. A post-annealing temperature of 150 °C has been reported to be commonly used in fabricating solar cells [81,112]. We fabricated OPV devices with different post-annealing times of 5 min, 10 min, 20 min, and 30 min. As a comparison, we also fabricated a separate OPV device without the post-annealing treatment.

Figure 4.8 shows the *J-V* curves of the P3HT:PC61BM BHJ OPV cells fabricated at different post-annealing conditions. Each data represents the optimal performance of a single OPV cell in the respected OPV devices. The post-annealing treatment on the OPV device showed an increase of the short current density originating from an increase of the

charge carrier mobility [34]. The best performance for the post-annealing study was obtained at a post-annealing temperature of 150 °C for 10 min. While the OPV device fabricated without the post-annealing treatment resulted in collapsing of both the open circuit voltage and the short circuit current. This drawback was related to recombination of the charge carriers [113].

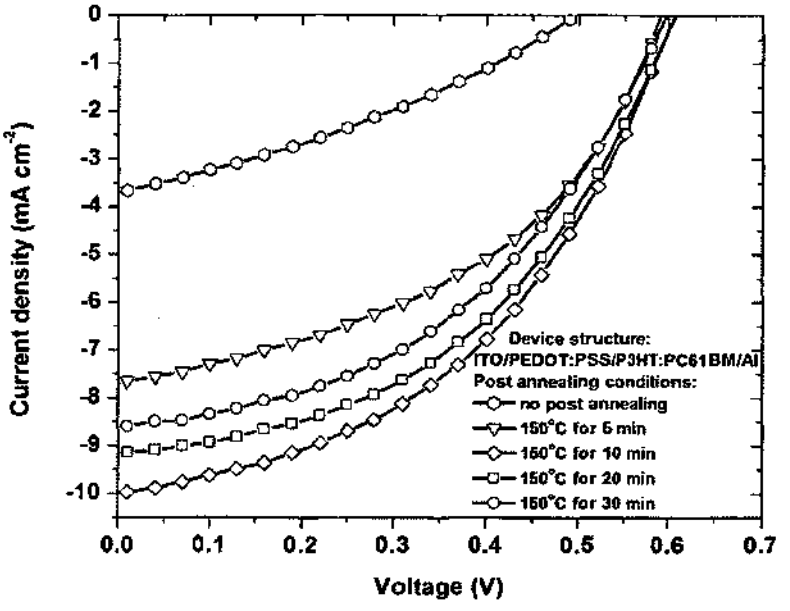

Figure 4.8: *J-V* characteristics of P3HT:PC61BM OPV cells fabricated at different post-annealing conditions.

Table 4.3: The parameters of P3HT:PC61BM OPV cells fabricated at different post-annealing conditions.

Post annealing condition	J_{SC} (mA cm^{-2})	V_{OC} (V)	FF (%)	PCE (%)
NO	**3.70**	**0.50**	**32.18**	**0.59**
150 °C for 5 min	**7.71**	**0.59**	**44.32**	**2.02**
150 °C for 10 min	**10.00**	**0.61**	**44.51**	**2.70**
150 °C for 20 min	**9.17**	**0.61**	**45.25**	**2.52**
150 °C for 30 min	**8.62**	**0.60**	**44.29**	**2.28**

4.8. The best P3HT:PC61BM OPV cell achieved in our experiment

Figure 4.9 shows the best performance of a P3HT:PC61BM BHJ OPV cell with a FF of 63% and a PCE of 4.14% (see Table 4.4). While the average PCE value of

P3HT:PC61BM OPV devices is 2.46 ± 0.97 % (see Appendix C.3). The mean of PCE value was significantly reduced and the standard deviation was large due to data population with a large interval of PCE values and the excessive process variability. The latter issue is attributed to the difficult fabrication processes and limitations in a university laboratory. To achieve the best performance, an OPV project requires a series of optimum conditions from the susbtrate cleaning process, patterning of ITO glass, preparation of active material solutions, depositing organic materials, depositing Aluminum (a good *e*-beam evaporation system's pressure), and the characterization step.

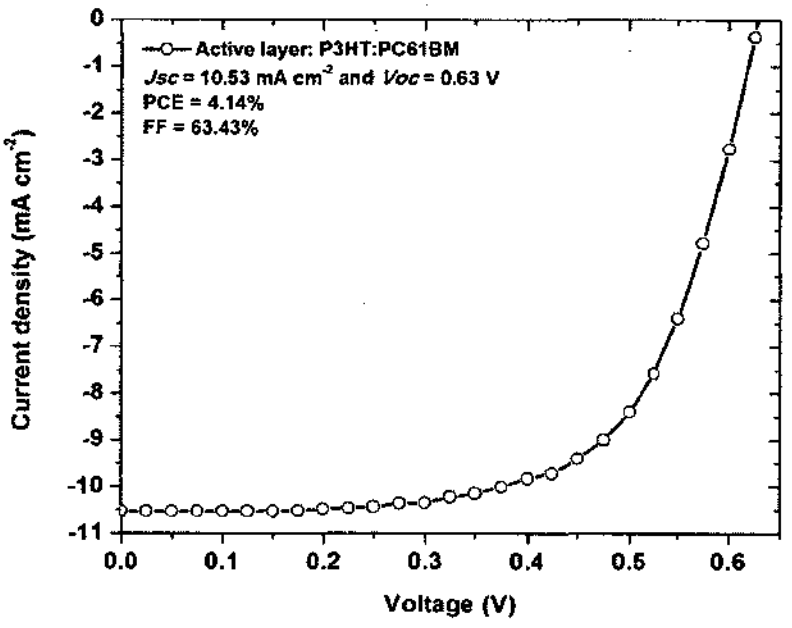

Figure 4.9: *J-V* characteristics of the best P3HT:PC61BM OPV cell achieved in our experiment.

Table 4.4: The parameters of the best P3HT:PC61BM OPV cell achieved in our experiment.

Active layer	J_{SC} (mA cm^{-2})	V_{OC} (V)	FF (%)	PCE (%)
P3HT:PC61BM	**10.53**	**0.63**	**63.43**	**4.14**

The poor performance of OPV devices is generally attributed to a poorly developed morphology that consists of an intimately mixed composite of donor and acceptor

materials rather than a bi-continuous network of well-developed and ordered pathways for the charge transport [114]. The intimate and homogenous mixing of components in spin-coated films confirms that the interaction between P3HT and PC61BM is crucial in the production of OPV devices with excellent performances.

4.9. Summary

We have demonstrated a fabrication procedure of OPV devices based on P3HT:P61BM. We tested and optimized the fabrication procedure on a widely used blend of active solution of P3HT:PC61BM (1:0.8 wt%). The weight concentration used in our experiment was 30 mg of P3HT and 24 mg of PC61BM in a 2 mL chlorobenzene solvent. Optimization steps including the thickness of the active layer, pre- and post annealing treatments were performed in our experiments. The structural order of the organic materials and the device is improved by using annealing treatment processes. We investigated different optimization variables by means of fabricating OPV devices directly. We found that the optimal thickness of the active layer was 100 nm, the optimal pre-annealing condition was at 140 °C for 2 min, and the optimal post-annealing condition was 150 °C for 10 min. Over 200 OPV devices of the blend active layer of P3HT:PC61BM, of less than 10% resulted in PCE values of 4.06 ± 0.04 % (Table C.1). While the average PCE value of P3HT:PC61BM OPV devices is 2.46 ± 0.97 % (see Appendix C.3). In our study, the best OPV cell with the blend active solution of P3HT:PC61BM fabricated using the optimal condition yielded a PCE of 4.14% with a J_{SC} value of 10.53 mA cm^{-2}, a V_{OC} of 0.63 V, and a FF of 63%. These results are compatible with the best OPV in the literature.

Chapter 5

Results on the Fabrication on PCDTBT:PC71BM Based OPV Devices

5.1. PCDTBT:PC71BM OPV devices

Several classes of low band gap polymer have been developed to better harvest the solar spectrum with deeper HOMO energies that could potentially increase V_{OC} [84,115]. These polymers are designed to make use of internal charge transfers from an electron rich unit to an electron deficient moiety within a fundamental repeat unit. The different electron deficient moieties can be used to tune the electronic gap of semiconducting polymer. The implied flexibility of the synthesis can lead to both a smaller band gap that enables the harvesting of a larger fraction of the solar radiation spectrum, and a deeper HOMO energy that increases the V_{OC} of the OPV cell. When a low band gap polymer, poly[*N*-9''-hepta-decanyl-2,7-carbazole-alt-5,5-(4',7'-di-2-thienyl-2',1',3'-benzothiadiazole)] or PCDTBT, was used, a V_{OC} value of approximately 0.9 V was achieved [84].

We fabricated OPV devices using BHJ materials comprising PCDTBT as the electron donor and PC71BM as the acceptor. Unlike the high bandgap polymer BHJ solution, the weight ratio for PCDTBT:PC71BM BHJ solution was kept at a ratio of 1:4. The structure for a low bandgap polymer OPV device is ITO/PEDOT:PSS/PCDTBT:PC71BM/Al. The energy levels of an OPV device of PCDTBT:PC71BM with respect to the vacuum level are shown in Figure 5.1. The thickness of aluminum is 80 nm and deposited by using an *e*-beam evaporating system at a pressure of 2.0×10^{-7} Torr. Since low bandgap polymer

OPV devices are relatively fresh research areas, we will dedicate more studies on the PCDTBT:PC71BM BHJ OPV devices. The influence of selected control fabrication parameters, such as the film thickness of the active layer, pre-annealing, and post-annealing treatments on the structure evolution of polymer based BHJ systems is discussed in this chapter.

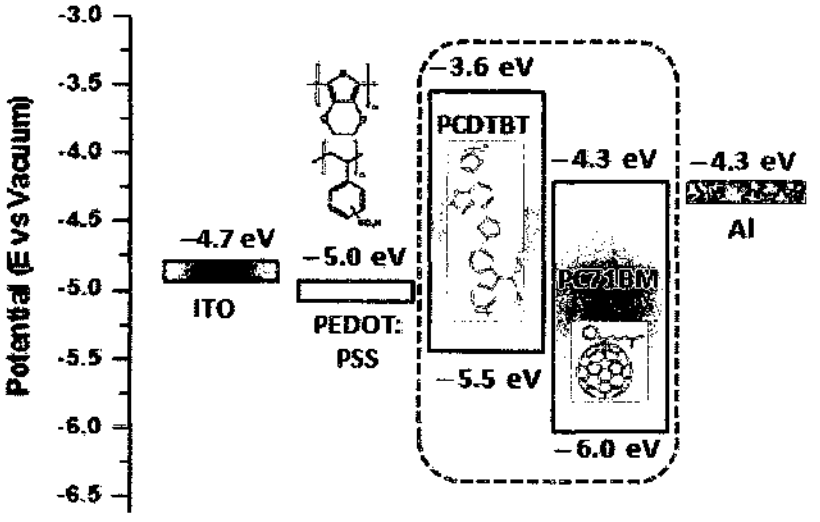

Figure 5.1: Energy levels of OPV device of PCDTBT:PC71BM (with respect to the vacuum level).

5.2. Morphology of PCDTBT:PC71BM composite

We observed the nanomorphology and the nanoscale organization of a blend solution of low bandgap polymer of PCDTBT:PC71BM materials with a weight ratio of 1:4 by using a transmission electron microscope, TEM JEOL-JEM 2100F. The TEM samples were prepared by spin coating the blend of active solution on a clean glass slide substrate. Prior to the TEM characterization, the organic thin film was collected by using a pre-cleaned razor blade to score the thin film coated on the substrate. The film was then

rinsed with DI water using an ultrasonic bath. The film that was floating on the surface of the water was deposited onto a TEM copper grid and then dried at room temperature.

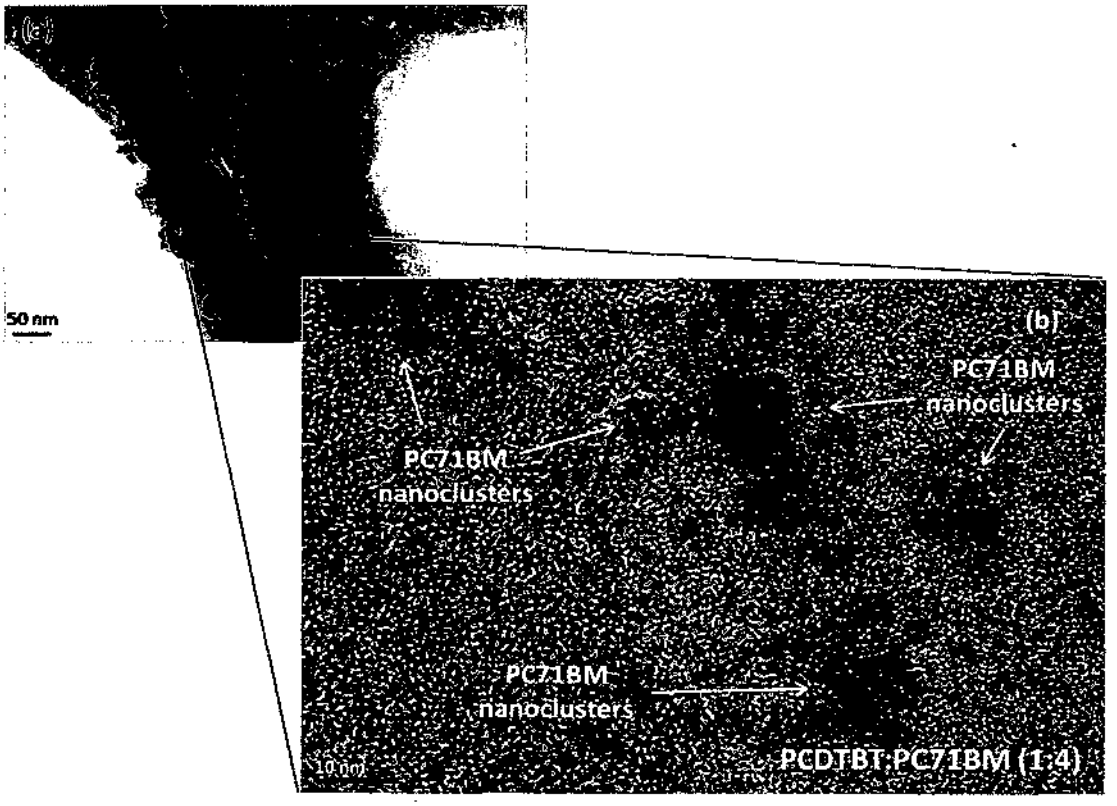

Figure 5.2: TEM images of PCDTBT:PC71BM composite with (a) low and (b) high resolutions.

Figure 5.2(a) shows a low resolution of the composite film of PCDTBT:PC71BM on the TEM copper grid. We observed in Figure 5.2(b) that PC71BM nanoclusters were formed and the 'fibrillar' PCDTBT nanostructures blended smoothly in a composite of PCDTBT:PC71BM with 1:4 weight ratio solutions. The PC71BM molecules can diffuse in the polymer matrix to form nanocluster domains [116]. In the kinetic theory of crystallization, the nucleation of crystal begins at a certain temperature and forms small but unstable clusters [117]. After nucleation of the PC71BM crystals and upon reaching a

certain size, it can provide a growth surface for further crystallization. The diffused PC71BM molecules further growth of the crystal into a nanocluster.

The increasing amount of PC71BM has been reported to cause the PCDTBT network to form longer and better connected pathways [84]. The PC71BM nanoclusters in the active layer provide efficient percolation paths for photogenerated charges. With better electron transportation in the composite film, there is improved photocurrent which facilitates better device performance. The TEM results show clearly that it is very important to consider the nanomorphology of PCDTBT:PC71BM interpenetrating networks resulting in an optimized and stable phase separation for efficient charge separation and transport. In turn this leads to thermal stability, the optimum PCDTBT: PC71BM nanomorphology, which will enhance the efficiency of the BHJ OPV devices.

5.3. Absorption study of the PCDTBT:PC71BM layer

In contrast to the traditional first generation conjugated polymers (polyacetylene, polythiophene, and poly(phenylene-vinylene) [118], the PCDTBT absorption spectrum, as seen in Figure 5.3, exhibits two distinct absorption bands centered at approximately 400 nm and 580 nm. Similar double peak absorption has been observed in other alternating acceptor/donor copolymers [119]. Two absorption peaks were previously attributed to π–π^* transitions with a lower energy peak associated with intra-chain charge transfer [120]. The absorption spectrum for the BHJ film shows additional absorption from the PC71BM in the 2 eV – 3 eV ranges. For PC71BM, the spherical symmetry is broken and forbidden transitions in the visible part of the spectrum become allowed

transitions. The absorption spectrum of the PCDTBT:PC71BM film is a superposition of the polymer and the fullerene absorption spectra.

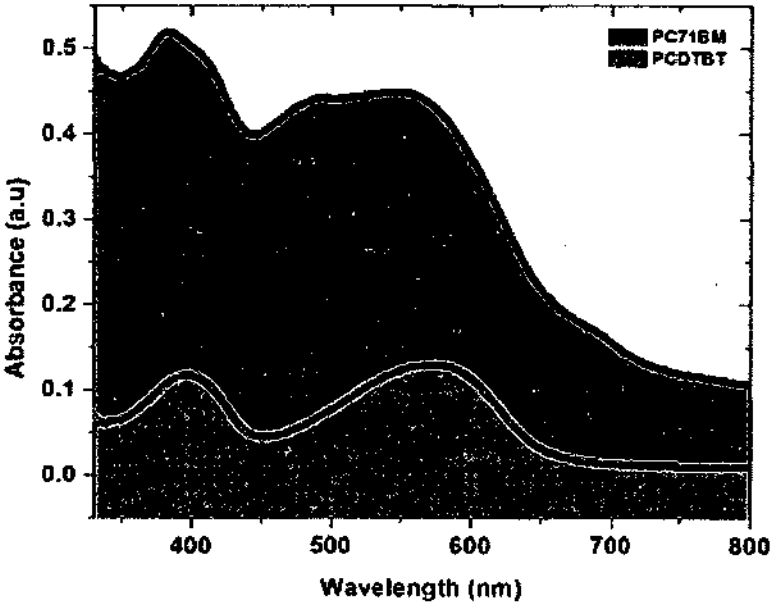

Figure 5.3: The UV-Vis absorption profile of PCDTBT polymer (black) and PC71BM fullerene (red).

Typically, when semi-crystalline conjugated polymers are annealed at temperatures above the glass-transition temperature, T_g, (for PCDTBT, T_g = 130 °C [121]), their degree of crystallinity and the size of the crystallites increases leading to changes in their electronic properties. We began by depositing an active layer solution of PCDTBT: PC71BM onto two separate pre-cleaned glass substrates. Then, one of the spin coated substrates was annealed at a temperature of 140 °C for 2 min inside a N_2-filled glove box atmosphere (O_2, H_2O < 0.1 ppm), while another one was not annealed. The PCDTBT thin films are amorphous when cast and remain amorphous after annealing at high temperatures [122].

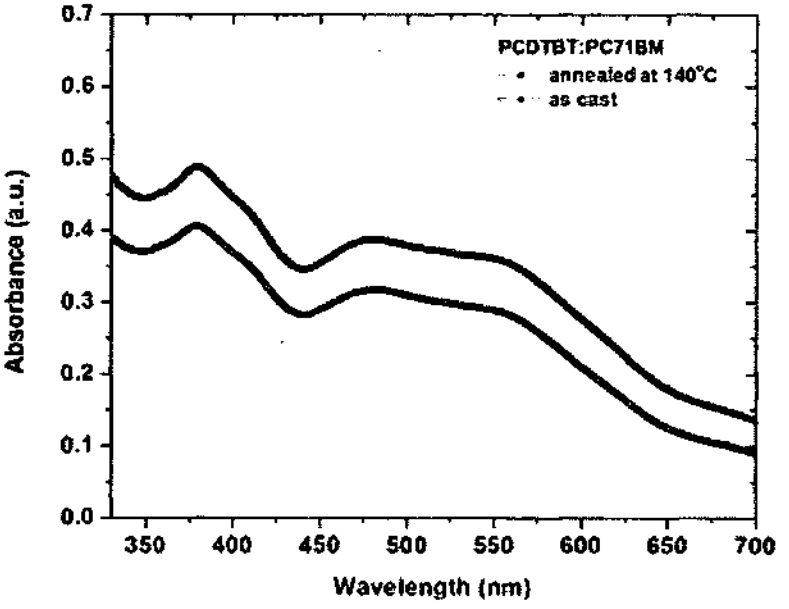

Figure 5.4: The UV-Vis absorption profile of PCDTBT:PC71BM active layers: as cast (black) and annealed at 140 °C for 2 min (red).

The intensity of the absorption spectrum for the PCDTBT:PC71BM film shows a considerable increase after the thermal annealing treatment as shown in Figure 5.4. The absorption spectrum of PCDTBT:PC71BM film is a superposition of the polymer and the fullerene absorption spectra. The increased absorption intensity for the annealed film corresponds to the increase in the number of absorbed photon. We observed a broader absorption with one maximum peaking at 360 nm and another at 560 nm due to the $\pi - \pi^*$ transitions [123,124]. The peak of the PCDTBT thin film at 560 nm decreases in the spectrum of the PCDTBT:PC71BM composite thin film with a new peak appearing around 480 nm.

5.4. Active layer thickness

Several papers reported that the optimized thickness of the active layer of PCDTBT:PC71BM was 70 – 80 nm to achieve maximum efficiency of the OPV devices

[19,125,126]. Thin photoactive layer is required to assure a sweep-out of charge carriers prior to recombination [127]. However, the thin photoactive layer limits absorption, thereby limiting the potential for further improvement in PV efficiencies.

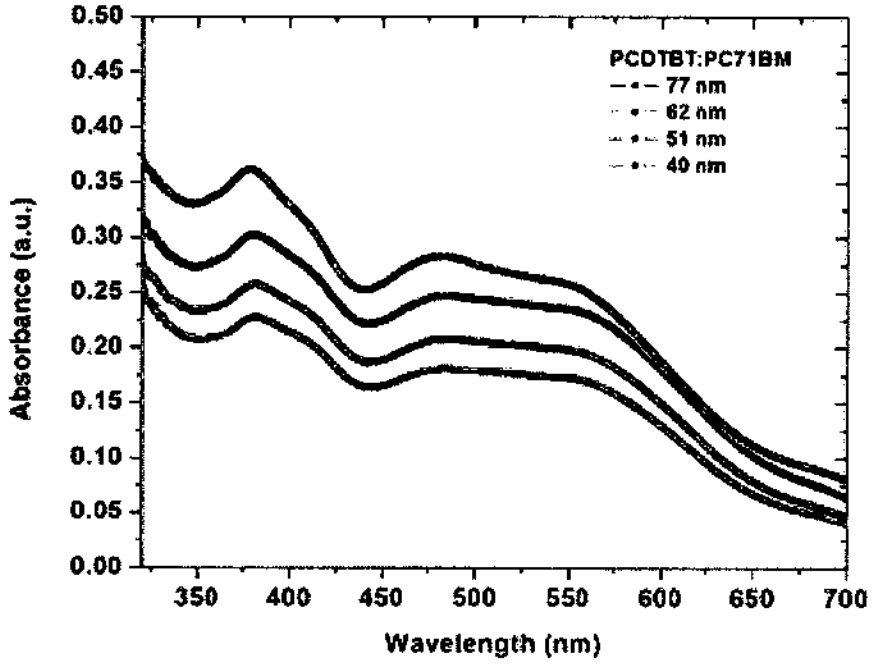

Figure 5.5: The UV-Vis absorption profile of four different thicknesses of PCDTBT:PC71BM active layers; 40 nm (green), 51 nm (blue), 62 nm (red) and 77 nm (black).

To test the optimal thickness of the PCDTBT:PC71BM active layer, we spin coated the active layer on pre-cleaned glass substrates with four different thicknesses of 40 nm, 51 nm, 62 nm, and 77 nm corresponding with spin speeds of 1000 rpm, 800 rpm, 600 rpm, and 400 rpm, respectively. The spin coated glasses were dried inside the glove box without any thermal annealing treatment. We measured the active layer thickness by using a Veeco Dektak 6M Stylus profilometer. Figure 5.5 shows the result of absorption measurements as a function of the wavelength. The active layer of 77 nm thick showed the strongest absorption intensity.

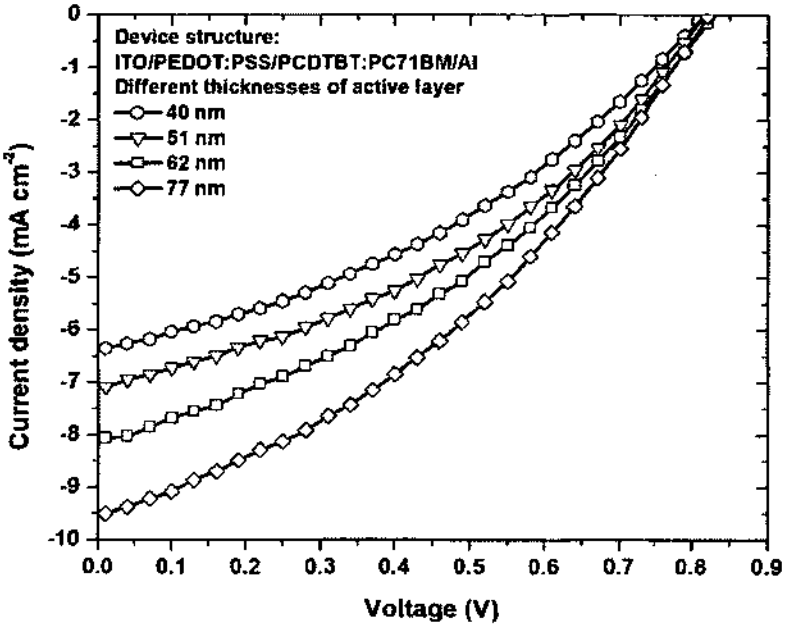

Figure 5.6: *J-V* characteristics of PCDTBT:PC71BM OPV cells fabricated at different thicknesses of the active layer.

We fabricated four OPV devices with different active layer thicknesses and fixed other fabricating parameters (pre- and post-annealing treatments). Figure 5.6 shows the *J-V* characteristic of the PCDTBT:PC71BM BHJ OPV cells fabricated with different active layer thicknesses. Each data represents the optimal performance of a single OPV cell in the respected OPV devices. We discovered that the OPV devices fabricated at an active layer PCDTBT:PC71BM of 77 nm thickness showed the best performance with a FF of 37% and a PCE of 2.9%. This thickness test's results agree with previous studies [19,124].

Table 5.1: The parameters of PCDTBT:PC71BM OPV cells fabricated at different active layer thicknesses.

Active layer thickness (nm)	J_{SC} (mA cm^{-2})	V_{OC} (V)	FF (%)	PCE (%)
40	**6.40**	**0.82**	**36.49**	**1.91**
51	**7.32**	**0.82**	**37.40**	**2.23**
62	**8.12**	**0.83**	**36.85**	**2.47**
77	**9.55**	**0.82**	**36.51**	**2.86**

5.5. Pre-annealing treatment

We performed a pre-annealing thermal test for low bandgap polymer OPV devices. The effect of a pre-annealing treatment on the low bandgap polymer is not well understood. Different pre-annealing parameters (temperature and time) have been reported. At room temperature the spin coated active layer was dried for longer times [128]; at 60 °C for 30 min [129], and at 70 °C for 60 min [84] inside a glove box. We added a pre-annealing condition of 140 °C for 2 min which we used in Section 4.6 for the high bandgap polymer OPV devices. We fabricated different OPV devices based on the aforementioned pre-annealing conditions and other fixed fabricating conditions.

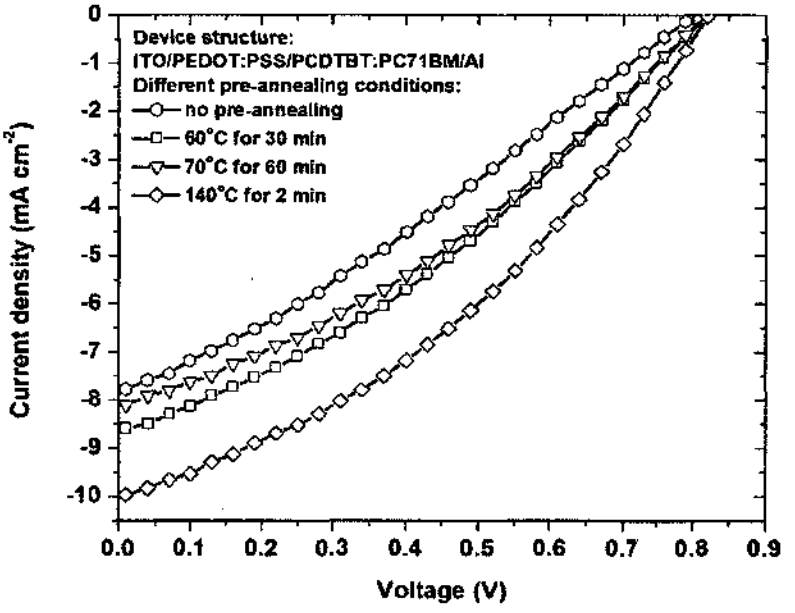

Figure 5.7: *J-V* characteristics of PCDTBT:PC71BM OPV cells fabricated at different pre-annealing conditions.

The *J-V* characteristics of PCDTBT:PC71BM BHJ OPV cells fabricated at different pre-annealing thermal conditions are shown in Figure 5.7. Each data represents the optimal performance of a single OPV cell in the respected OPV devices. Pre-annealing at

a temperature of 140 °C for 2 min produced a FF of 37% and a PCE of 3.0%. The PCDTBT exhibits a high glass-transition temperature (T_g, about 130 °C) and excellent thermal stability [115]. Annealing the active layer of PCDTBT:PC71BM at a temperature of 140 °C for 2 min improves the performance of OPV devices as compared to other pre-annealing conditions. This proves that our experimental conditions for the pre-annealing treatment were optimum for both high and low bandgap polymers OPV devices.

Table 5.2: The parameters of PCDTBT:PC71BM OPV cells fabricated at different pre-annealing conditions.

Pre-annealing condition	J_{SC} (mA cm^{-2})	V_{OC} (V)	FF (%)	PCE (%)
NO	**7.83**	**0.80**	**28.83**	**1.81**
60 °C for 30 min	**8.68**	**0.82**	**30.31**	**2.31**
70 °C for 60 min	**8.16**	**0.82**	**32.61**	**2.18**
140 °C for 2 min	**10.02**	**0.82**	**36.45**	**3.00**

5.6. Post-annealing treatment

We performed the final optimization test; the post-annealing treatment. Post-annealing studies for low bandgap polymers varied from report to report [84,130,131]. We performed our experiment at a post-annealing temperature of 150 °C and at different post-annealing times of 5 min, 10 min, 20 min, and 30 min. As a comparison, we also fabricated a separate OPV device without the post-annealing treatment.

Figure 5.8 shows the *J-V* curves of the PCDTBT:PC71BM BHJ OPV cells fabricated at different post-annealing conditions. Each data represents the optimal performance of a single OPV cell in the respected OPV devices. The best performance for the post-annealing study for the low bandgap polymer was obtained at a post-annealing temperature of 150 °C for 10 min with a PCE of 2.8%. The OPV device fabricated without the post-annealing treatment resulted in collapsing of both the J_{SC} and the FF, primarily due to the recombination of the charge carriers [113]. The post-annealing

results for the low bandgap polymer show the same optimum condition as its high bandgap counterpart. Due to the amorphous nature of PCDTBT and the complex solubility and miscibility properties between PCDTBT and PC71BM, the effect of either pre- or post-annealing treatments on the low bandgap is not well understood [132].

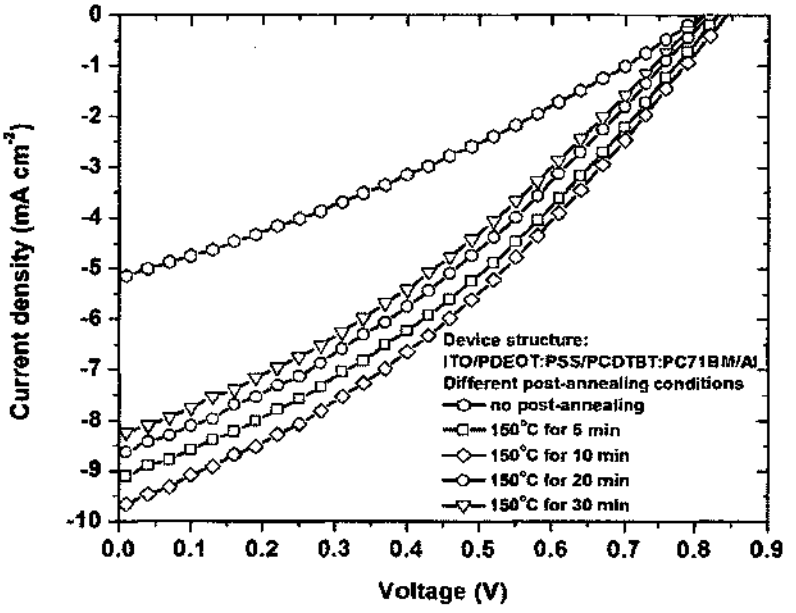

Figure 5.8: *J-V* characteristics of PCDTBT:PC71BM OPV cells fabricated at different post-annealing conditions.

Table 5.3: The parameters of PCDTBT:PC71BM OPV cells fabricated at different post-annealing conditions.

Post-annealing condition	J_{SC} (mA cm^{-2})	V_{OC} (V)	FF (%)	PCE (%)
NO	**5.19**	**0.81**	**30.42**	**1.28**
150 °C for 5 min	**9.17**	**0.83**	**33.76**	**2.58**
150 °C for 10 min	**9.75**	**0.84**	**33.47**	**2.75**
150 °C for 20 min	**8.70**	**0.82**	**32.79**	**2.34**
150 °C for 30 min	**8.29**	**0.81**	**32.64**	**2.20**

5.7. Aged active solution study

The effect of an aged active solution on the performance of low bandgap polymers is rarely reported. The aged active solution reportedly formed organic material aggregates [133]. For a prolonged blend polymer operation, phase separation leads to spatial donor

and acceptor distances exceeding the diffusion length of photogenerated excitons resulting in losses of the photocurrent [134]. However, a good OPV device performance cannot be repeated easily, even in the same laboratory when a new batch material is sourced. The nanomorphology control of the blend polymer and fullerene is at the heart of OPV device research.

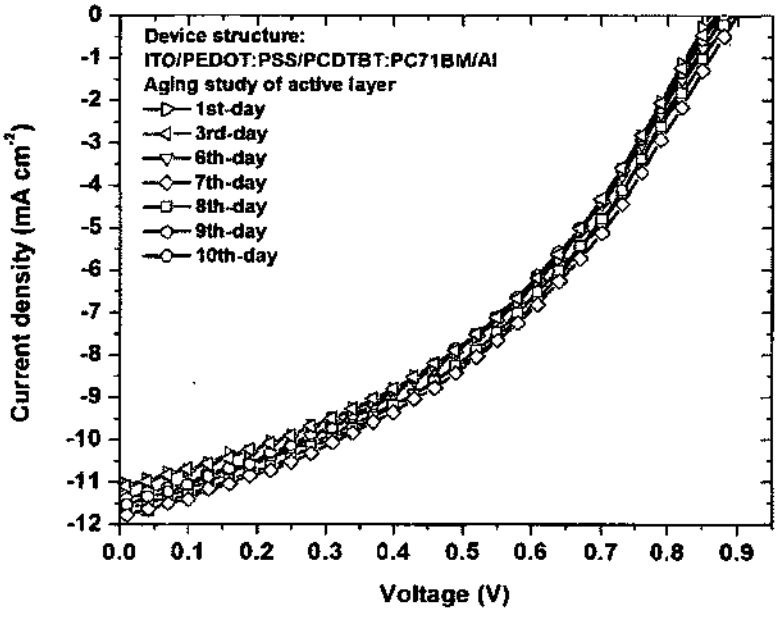

Figure 5.9: *J-V* characteristics of PCDTBT:PC71BM OPV cells fabricated at different aging times of the active solutions of PCDTBT:PC71BM.

We studied the effect of the aging process of the PCDTBT:PC71BM active solution on the performance of OPV devices by fabricating OPV devices with the same processing conditions and by using the aged active solutions of PCDTBT:PC71BM. The active solution was stirred at a temperature of 120 °C and at 400 rpm inside the glove box for several days. During the stirring process, the vial of the active solution was protected from light by wrapping the vial with Al foil. When needed, we used a clean pipette to take the active solution and deposit it onto an ITO glass substrate pre-coated with a PEDOT:PSS solution. We monitored the quality of the aged active solution each time the

newly fabricated OPV device was characterized. Figure 5.9 shows a compilation of the *J-V* characteristics of OPV cells fabricated at different aged active solutions of PCDTBT:PC71BM. In the figure, each data represents the optimal performance of a single OPV cell in the respected OPV devices. In this particular study, the 1st-day, the 3rd-day and the Nth-day refer to the age of the active solution (N× 24 h since the fresh active solution was made).

Table 5.4: The parameters of PCDTBT:PC71BM OPV cells fabricated at different aging times of the active solutions of PCDTBT:PC71BM.

Aging time of the active solution (day)	J_{SC} (mA cm^{-2})	V_{OC} (V)	FF (%)	PCE (%)
1	**11.10**	**0.86**	**40.47**	**3.92**
3	**11.15**	**0.87**	**40.50**	**3.96**
6	**11.67**	**0.88**	**39.65**	**4.07**
7	**11.84**	**0.90**	**39.67**	**4.23**
8	**11.79**	**0.89**	**39.24**	**4.17**
9	**11.58**	**0.88**	**40.54**	**4.11**
10	**11.44**	**0.87**	**39.67**	**4.00**

In Figure 5.10, we observed that the OPV cells fabricated by using aged active solutions of PCDTBT:PC71BM. We found a common trend that OPV cell produced the best performance at the 7th day with a J_{SC} of 11.84 mA cm^{-2}, a V_{OC} of 0.90 V, and a PCE of 4.2% (Table 5.4). In the Figure, each data represent results from a single cell in the respected OPV devices. We observed that the FF value was peaking at the 9th day (40.54%) and was relatively stable over a prolonged period of the aged active solutions.

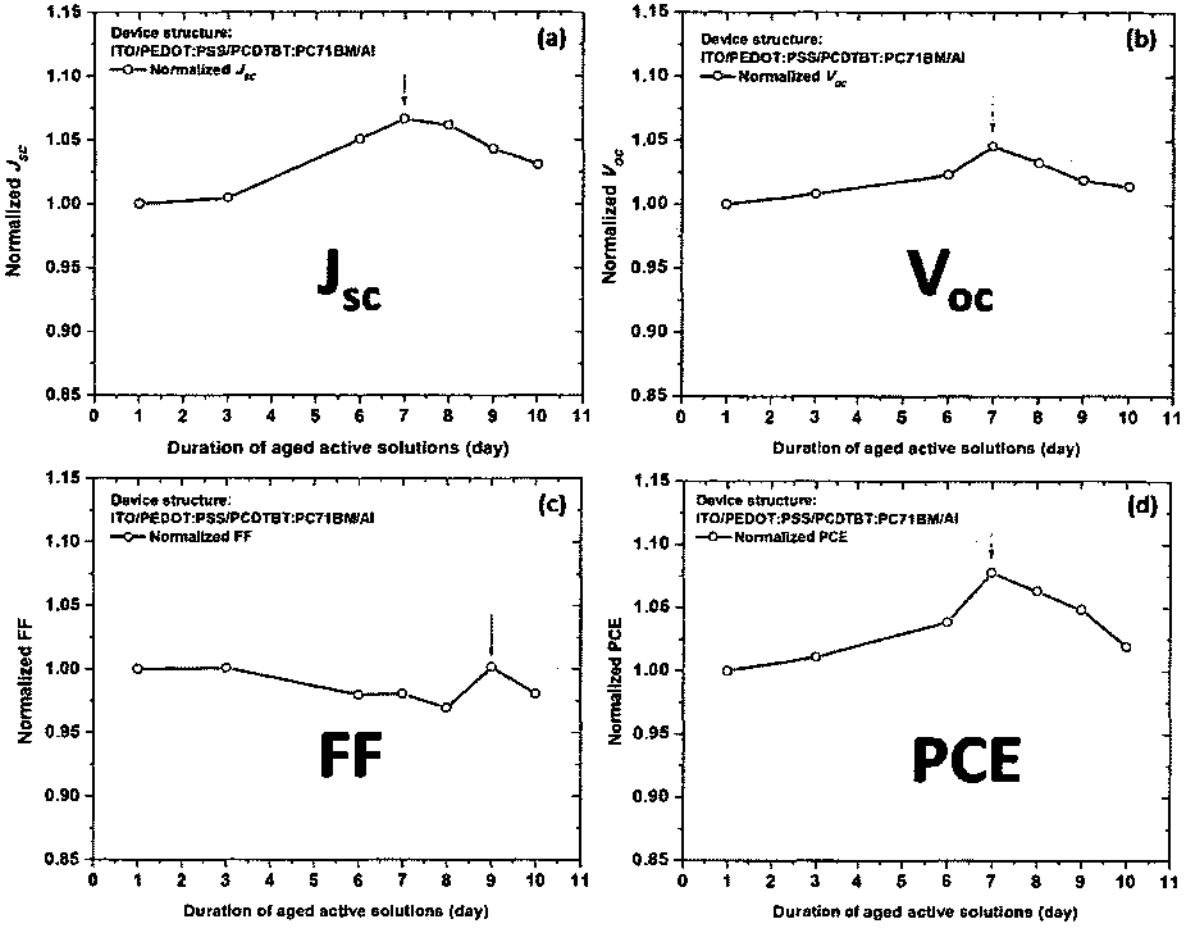

Figure 5.10: Parameters of PCDTBT:PC71BM OPV cells as a function of the aging time of the active solutions of PCDTBT:PC71BM.

Fill factor is a very sensitive OPV parameter and the most difficult parameter to control because it is impacted by phase separation, molecular ordering, charge mobility, morphology of the active layer, and recombination mechanisms in a BHJ OPV cell [135]. An important aspect of the aged active solution study is to find an optimal condition in which the demixing of the organic materials reaches a favorable state to better harvest excitons, to better charge carrier extraction, and to improve the photocurrent and efficiency of the OPV device. We found that seven days was the optimal time for aged active solutions of PCDTBT:PC71BM. It is likely due to a well mixed active solution

that improves the nanomorphology, the percolation path, and the interconnected transport network in the bulk heterojunction OPV cell. We observed, however, after 7 days using the aged active solution, the device performance decreased. The declining quality in the OPV devices after 7 days might be due to several factors. First, the active solution evaporates during the aging process resulting in a decrease in the concentration of donor and acceptor materials in the solution. Second, excessive stirring of the active solution might have causes the decrease in the quality of the nanomorphology of the active solution. Third, degradation of the active solution due to its exposure to light worsened each time the solution was exposed. However, we observed the declining qualities of the aged active solution after 7 days was not catastrophic; since the devices still functioned properly without disastrous failure.

5.8. The best PCDTBT:PC71BM OPV cell achieved in our experiment

From different optimization tests and adjusting several fabricating procedures, the best performance of the PCDTBT:PC71BM BHJ OPV device in our experiment was achieved with a J_{SC} of 12.73 mA cm^{-2}, a V_{OC} of 0.89 V, a FF of 45%, and a PCE of 5.13% as seen in Figure 5.11 (Table 5.5). While the average PCE value of all PCDTBT:PC71BM OPV devices is 3.21 ± 1.20 % (Table C.4). The performances of OPV devices on a regular basis are of course lower. The mean of the PCE value was reduced and the standard deviation was large due to data population with a large interval of PCE values. This study comprises early basic research on OPV devices and as a consequence variability of the fabrication process for the devices was excessive. The excessive process variability is attributed to the difficult fabrication processes and

limitations in a university laboratory. Morphology and reproducibility controls have been reported to be the major problems in OPV research. Moreover, the variation in fabrication conditions and parameters (the experimental facility also varies) from report to report also causes great difficulty in reproducing the optimal OPV devices in every fabrication process.

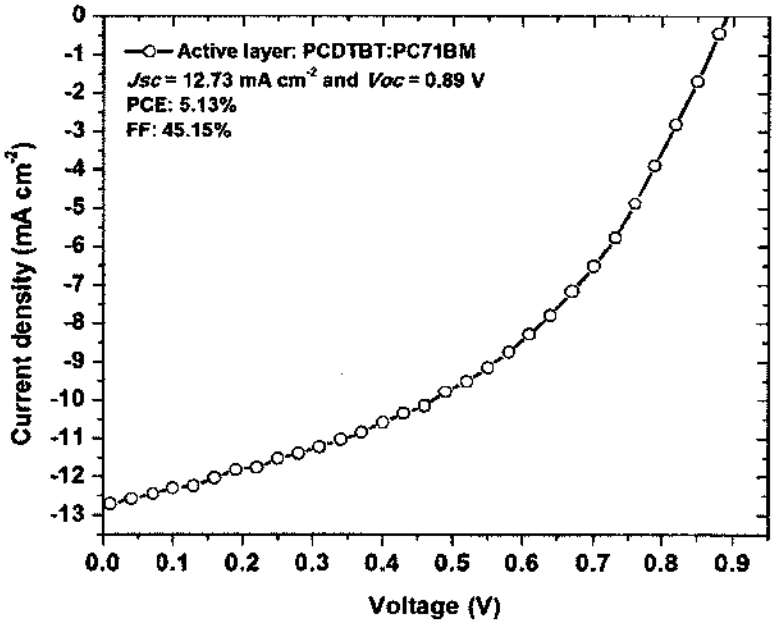

Figure 5.11: *J-V* characteristics of the best PCDTBT:PC71BM OPV cell achieved in our experiment.

Table 5.5: The parameters of the best PCDTBT:PC71BM OPV cell achieved in our experiment.

Active layer	J_{SC} (mA cm^{-2})	V_{OC} (V)	FF (%)	PCE (%)
PCDTBT:PC71BM	**12.73**	**0.89**	**45.15**	**5.13**

5.9. Summary

We tested and optimized the fabrication procedure on a widely used blend of active solution of PCDTBT:PC71BM (1:4 wt%). A weight concentration of 7 mg of PCDTBT and 28 mg of PC71BM in 2 mL of 1,2-dichlorobenzene solvent was used in our experiment. We investigated the blend solution of a low bandgap polymer PCDTBT:

PC71BM by fabricating OPV devices and monitoring their performances. We performed the optimization steps similar to the steps used in the high bandgap polymer. We found that the optimal thickness of the active layer was 80 nm, the optimal pre-annealing condition was at 140 °C for 2 min, and the optimal post-annealing condition was at 150 °C for 10 min. From the TEM measurement as seen in Figure 5.2, we found that in the PC71BM-rich environment, the nanocomposite of PCDTBT:PC71BM was dominated by the formation of PC71BM nanoclusters.

We studied the effect of the aging process of PCDTBT:PC71BM active solutions on the performance of OPV devices. We found that 7 days stirring was optimal for the aged active solution of PCDTBT:PC71BM and yielded a FF of 40% and a PCE of 4.3%. Over 100 OPV devices of PCDTBT:PC71BM were fabricated, with less than 10% of them resulting in PCE values of 5.04 ± 0.05 % (Table C.2). The average PCE value of PCDTBT:PC71BM OPV devices is 3.12 ± 1.20 % (Table C.4). By using optimum fabrication conditions, we found that the best performance of the PCDTBT:PC71BM BHJ OPV device in our experiment was achieved with a J_{SC} of 12.73 mA cm^{-2}, a V_{OC} of 0.89 V, a FF of 45%, and a PCE of 5.1%. This result is still slightly lower than the best performance of PCDTBT:PC71BM based OPV device with a PCE of 7% reported in the literature [84]. We concluded that our fabrication procedure for low bandgap polymer OPV devices is not optimal yet.

Chapter 6

Improving the Stability of the High Bandgap OPV Devices using a Solution Based Titanium Sub-oxide Interfacial Layer

6.1. Introduction

The degradation of the active layer was accelerated due to exposure to three primary factors; oxygen, air, and light [25,136]. To achieve OPV device stability, either the development of improved barrier materials for packing or the development of devices with less air sensitivity (or both) is required. Air stable OPV devices have reportedly been achieved by inserting a solution based metal oxide as a buffer layer between the active layer and the metal cathode [137,138]. For example, a solution based titanium sub-oxide (TiO_x) with a thickness less than 20 nm has been reported to effectively minimize physical and chemical damages [18]. The TiO_x layer serves as an effective barrier for oxygen permeation to improve device stability in an ambient atmosphere.

The improvement in device efficiency has brought OPV cells closer to commercial viability, highlighting the importance of studying the lifetime and reliability of OPV devices. The lifetime and degradation mechanisms of BHJ solar cells that employ the high bandgap polymer (P3HT) have been well studied [51,137,138,140]. We synthesized the solution based TiO_x material by using the sol-gel chemistry method as previously discussed in Section 3.5 [18,77]. We performed optimization tests on the TiO_x layer including a TiO_x layer thickness test and a TiO_x solution drying test. We used the

optimized TiO_x layer as the buffer layer in the OPV fabrication and performed a stability test.

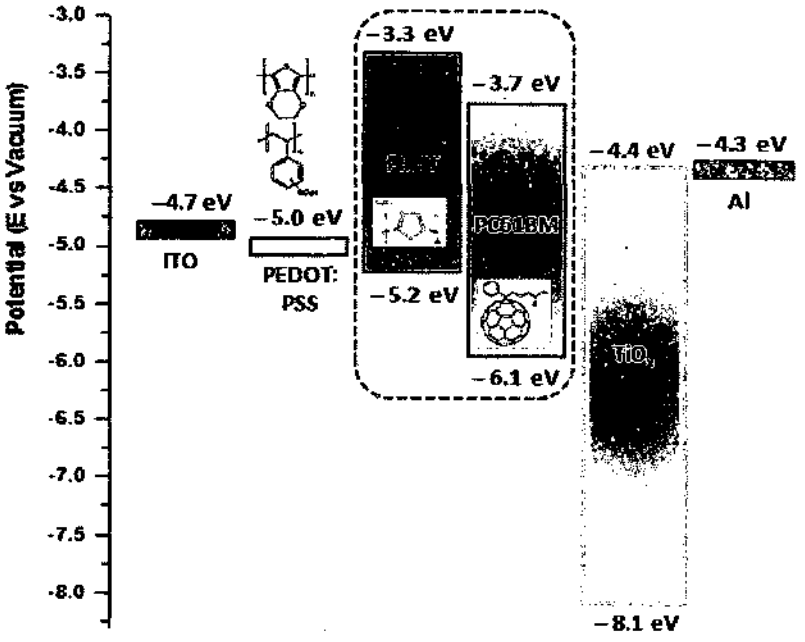

Figure 6.1: Energy level of an OPV device of P3HT:PC61BM with the TiO_x interfacial layer (with respect to the vacuum level).

To study the effect of the solution based TiO_x interfacial layer on the stability of the OPV device performance over a period of time, we fabricated OPV devices with a structure of ITO/PEDOT:PSS/P3HT:PC61BM/TiO_x/Al. An energy level diagram of OPV devices with the TiO_x layer is shown in Figure 6.1. The weight ratio for an active solution of P3HT:PC61BM is 1:0.8 with a weight concentration (mg) of 30:24 (in 2 mL chlorobenzene solvent). The active solution was spun inside a glove box to form a thickness of 100 nm. Immediately following, the active layer was annealed at 140 °C for 2 min. The substrate was then allowed to cool down to room temperature inside the glove box. The TiO_x solution was spun in air inside a fume hood environment. Al with an 80

nm thickness was used as the metal contact and deposited by an *e*-beam evaporator. For fabrication processes performed outside the glove box, the TiO_x layer deposition, drying of the TiO_x solution, and Al deposition, must be done carefully to protect the active solution from degradation. We first performed optimization tests including thickness and drying of TiO_x layer tests.

6.2. Absorption study on the P3HT:PC61BM/TiO_x layers

It has been reported that a solution based TiO_x layer has been used as the optical spacer to optimize absorption within the active layer, and to redistribute the light intensity inside the device between the active layer and the reflecting electrode [87]. In addition to exhibiting excellent electrical and physical properties, optical spacer material must also be transparent to light with wavelengths within the solar spectrum. Therefore, an understanding of the TiO_x absorption is very important. First, the photoactive layer we investigated was spun with TiO_x solutions at different spin speeds of 3000 rpm (TF1), 2000 rpm (TF2), and 1000 rpm (TF3). The thickness of the TiO_x layer coated at 1000 rpm was estimated to be less than 20 nm within the limitation of the accuracy measurement of the Dektak Stylus profilometer. A thin film of active layer coated without a TiO_x layer (TF0) was added as well. A pre-cleaned glass was used as the substrate. Second, we coated the TiO_x solution on separate glass substrates pre-coated with an active layer and annealed the TiO_x at 90 °C for 10 min.

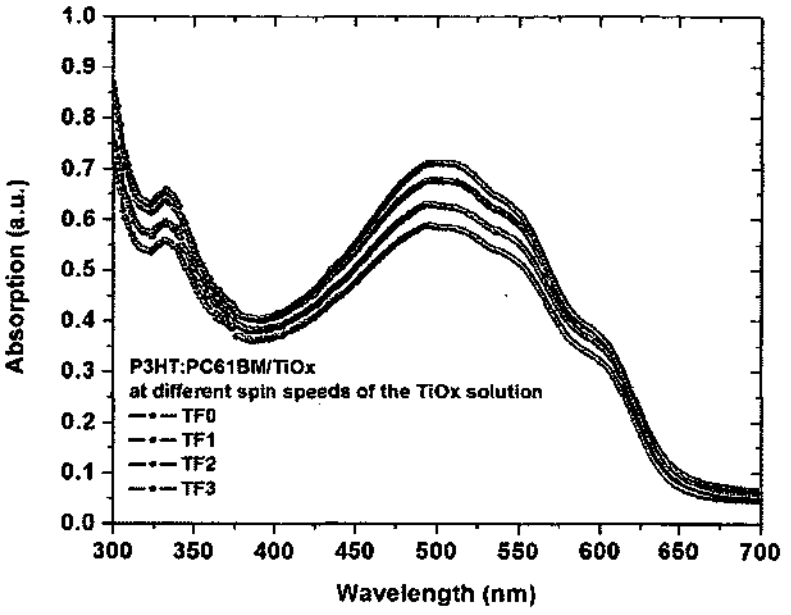

Figure 6.2: The UV-Vis absorption profile of P3HT:PC61BM immediately following fabrication (TF0, green) and P3HT:PC61BM/TiO_x at different spin speeds of the TiO_x solution: 3000 rpm (TF1, blue), 2000 rpm (TF2, red), and 1000 rpm (TF3, black).

The optical property of different thicknesses of TiO_x on the active layer was studied by observing the UV-visible absorption spectra of P3HT:PC61BM and P3HT:PC61BM/TiO_x immediately following fabrication as shown in Figure 6.2. In this picture, it shows the relative maximum points of absorption that are influenced by both the polymer and fullerene. There is one local peak in the UV range at 330 nm, influenced by the PC61BM in the blend, and three peaks in the visible ranges of 510, 555, and 605 nm, due to the presence of P3HT. These peaks are very consistent with published data, which also show the absorption peaking in the exact same ranges [103,141]. The absorbance of both materials was peaking at 500 nm and increased up to 25% when a TiO_x layer coated at a spin speed of 3000 rpm on the active layer.

6.3. TiO_x spin coating test

We used the absorption study as previously discussed and fabricated three OPV devices with a structure of ITO/PEDOT:PSS/P3HT:PC61BM/TiO_x/Al at different spin speeds of the TiO_x solution. By varying the spin speed, we indirectly varied the thickness of the TiO_x layer. However, our TiO_x layer was too thin and difficult to be measured precisely with the Dektak profilometer at the facility. Thicknesses of each layer in the OPV device were optimized to maximize light absorption by the active layer [142]. In the BHJ OPV cell, the light entering into the device from the glass side travels through the nearly transparent ITO and PEDOT:PSS layers, is partly absorbed in the photoactive BHJ layer, passes through the nearly transparent TiO_x layer, and is then reflected onto the Al surface for a second pass through the BHJ, PEDOT:PSS, and ITO layers. Another excellent property of the TiO_x layer is that it is non-absorbing in visible and infrared light and improves optical absorption of the light [85].

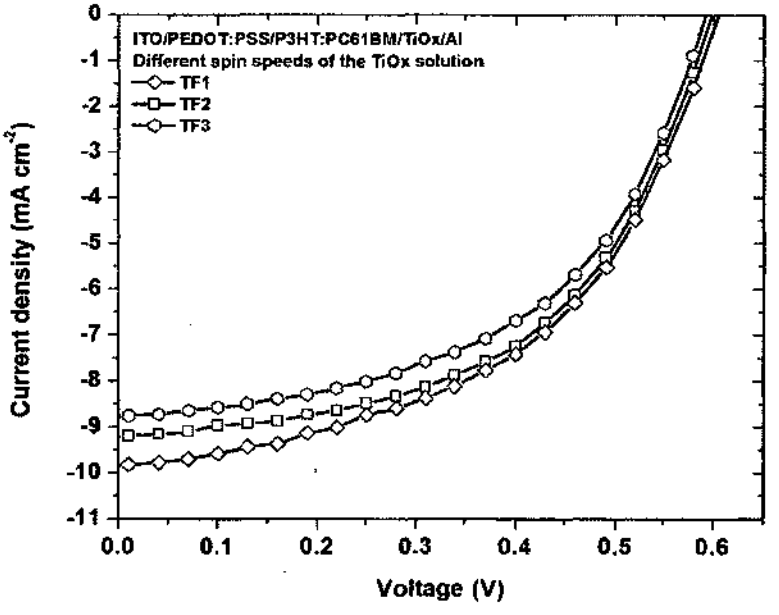

Figure 6.3: *J-V* characteristics of P3HT:PC61BM OPV cells fabricated at different spin speeds of the TiO_x solution: 3000 rpm (TF1, diamond), 2000 rpm (TF2, square), and 1000 rpm (TF3, circle).

Figure 6.3 shows the *J-V* characteristics of the OPV cells fabricated at different spin speeds of the TiO_x solution (the spin coating time was kept the same at 3 min). Each data represents the optimal performance of a single OPV cell in the respected OPV devices. In this Figure, the device fabricated a TiO_x layer (TF1) with the spin speed of 3000 rpm produced the best performance with an FF of 50% and PCE of 3.0% (see Table 6.1). The thickness of TF3 was measured to be less than 20 nm within the limitation of the Dektak Stylus profilometer. Other studies have reported that optimal thicknesses of the TiO_x layer for OPV devices are in the 5 nm – 20 nm ranges [82,143]. The OPV performance with the TiO_x layer thickness we tested agreed with those reports.

Table 6.1: The parameters of P3HT:PC61BM OPV cells fabricated at different spin speeds of the TiO_x solution.

Spin speed of the TiO_x solution	J_{SC} (mA cm^{-2})	V_{OC} (V)	FF (%)	PCE (%)
3000 rpm (TF1)	**9.88**	**0.61**	**50.28**	**3.00**
2000 rpm (TF2)	**9.21**	**0.60**	**52.37**	**2.89**
1000 rpm (TF3)	**8.78**	**0.59**	**52.34**	**2.72**

6.4. TiO_x solution drying test

The next optimization step is the TiO_x solution drying by means of thermal annealing. Hal and his coworkers reported that the conversion of $Ti(OC_3H_7)_4$ to TiO_2 was estimated to be 77% – 91% (the result is called a partial conversion process) [74]. In the drying test of the TiO_x layer, we compared four different drying conditions (1) at a room temperature (25 °C) for 60 min [77], (2) at 80 °C for 10 min [84], (3) at 90 °C for 10 min [144], and (4) at 100 °C for 10 min in the air. During the drying process, the substrate pre-coated with multi-layered films of ITO/PEDOT:PSS/P3HT:PC61BM/TiO_x was protected by a Petri dish covered with Al foil to shield the active layer from the light.

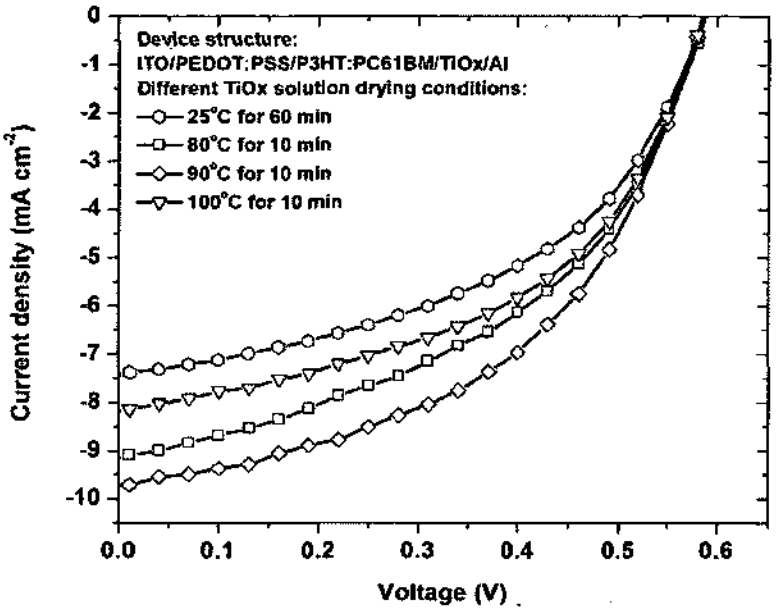

Figure 6.4: *J-V* characteristics of P3HT:PC61BM OPV cells fabricated at different TiO_x solution drying conditions.

Table 6.2: The parameters of P3HT:PC61BM OPV cells fabricated at different TiO_x solution drying conditions.

Drying condition	J_{SC} (mA cm^{-2})	V_{OC} (V)	FF (%)	PCE (%)
25 °C for 60 min	**7.42**	**0.59**	**47.33**	**2.08**
80 °C for 10 min	**9.15**	**0.59**	**45.67**	**2.46**
90 °C for 10 min	**9.75**	**0.59**	**48.63**	**2.78**
100 °C for 10 min	**8.17**	**0.59**	**48.99**	**2.34**

Figure 6.4 shows the *J-V* characteristics of the OPV cells fabricated at different drying conditions of the TiO_x layer. Each data represents the optimal performance of a single OPV cell in the respected OPV devices. The best performance was obtained with the device fabricated at a drying temperature of 90 °C for 10 min (see Table 6.2), while a device fabricated at room temperature and the high temperature at 100 °C showed a collapsing effect on J_{SC} and FF. The main drawback of thermal treatment is that active blends of the P3HT:PC61BM composite would be damaged at high temperatures

6.5. Surface topography of P3HT:PC61BM/TiO_x

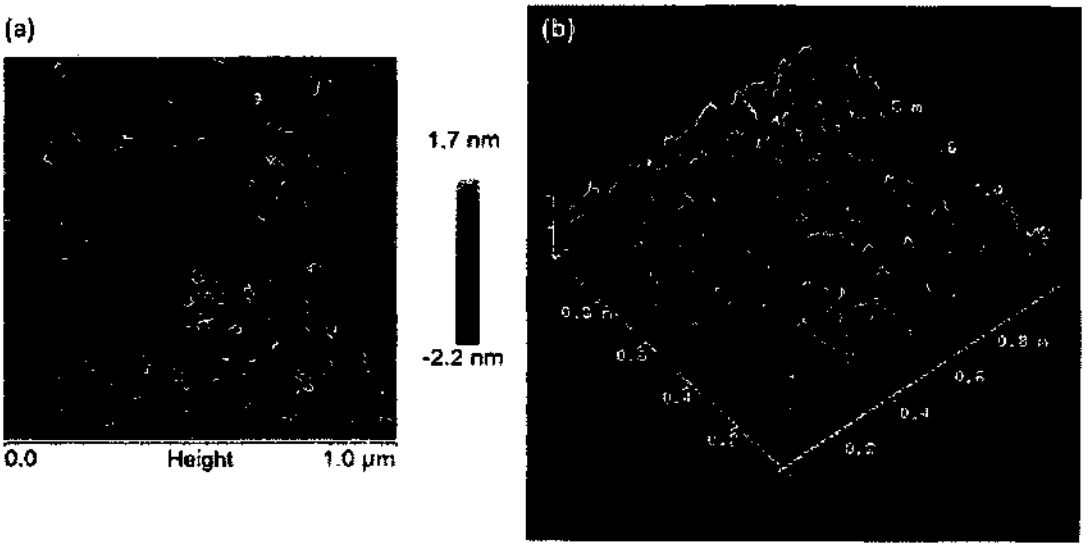

Figure 6.5: (a) 2-D and (b) 3-D AFM images of P3HT:PC61BM/TiO_x.

The photoactive layer of P3HT:PC61BM (100 nm) coated with a TiO_x layer (less than 20 nm) was created and subsequently annealed in the air at 90 °C for 10 min (as was shown in the drying process [142]). To observe the topography of the top surface of the P3HT:PC61BM/TiO_x layer, the sample was characterized under AFM (a scanned area of 1 µm × 1 µm and a scanned frequency of 512 MHz). The 2-D and 3-D images of the top of the layer are shown in Figure 6.5. Based on the AFM images, we observed a relatively smooth P3HT:PC61BM/TiO_x surface with an overall surface roughness (RMS roughness) of 0.494 nm. The smoothness of the TiO_x film, as we expected, was important in creating a good interface with the active layer.

6.6. Stability study on the P3HT:PC61BM OPV device

P3HT:PC61BM BHJ OPV devices stored in the air and in dark environments exhibit a decrease in the short circuit current with exposure to time [17,145]. The lifetime and

stability of OPV devices is a very important aspect in the commercialization of photovoltaic devices. The aim of this study is to produce an OPV device with air stability under a prolonged storage time by using a solution-based TiO_x material as the interfacial layer. We fabricated an OPV device with a structure of ITO/PEDOT:PSS/P3HT: PC61BM/TiO_x/Al by using optimal fabrication procedures as previously discussed. We investigated the lifetime and stability of the OPV device with the TiO_x layer.

The change of *J-V* characteristics of the P3HT:PC61BM OPV device fabricated with a TiO_x layer was monitored with a 70 day storage time. We compared the degradation trend of the device by evaluating their J_{SC}, V_{OC}, FF, and PCE values as a function of the storage time. To maintain the consistency of our results, for a total of 8 cells in the OPV device, we characterized the same cell showing the best performance over a period of time. The rest of the OPV cells were operating well with less than 10% lower in their performances comparing to the best cell.

In our experiment, we stored the OPV device fabricated with a TiO_x layer inside the glove box and characterized it periodically in the air for 70 days. We performed both a stability study using a solution based TiO_x layer to protect the active layer from moisture and oxygen and a stability study using an opaque Al cover to protect the device from light (Case (II)). Figure 6.6 shows the *J-V* characteristic of an OPV device with a TiO_x layer as a function of storage time. We found that semi-crystalline P3HT materials prove to be an excellent air stability material and are slow to degrade as reported elsewhere [146]. The degradation of OPV devices consisting of at least two active organic materials is a complex problem. Reactions of the organic materials with oxygen [12], water [147], and light [145] have been reported to accelerate degradation of the organic materials. For

example, the oxygen atom induces trap states in the polymer resulting in a strong decrease in charge carrier mobility and short circuit current [148].

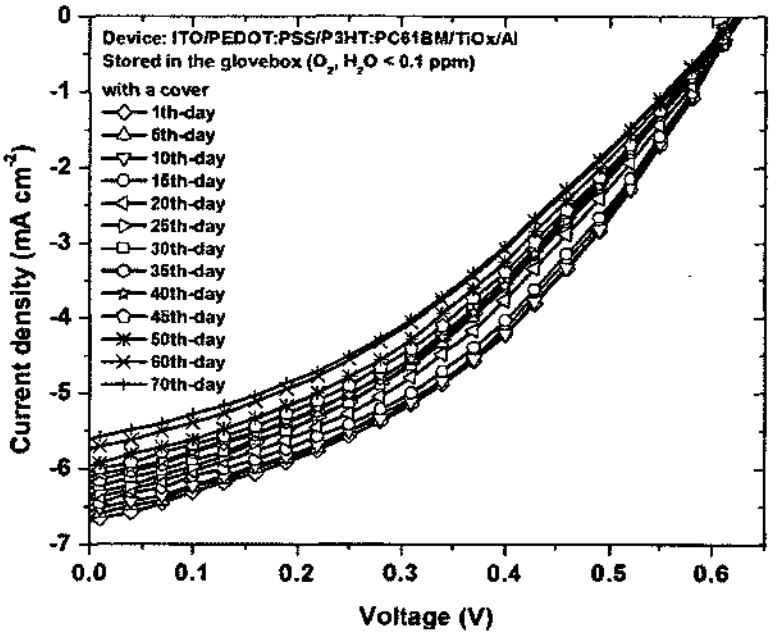

Figure 6.6: *J-V* characteristics of a P3HT:PC61BM OPV cell with a TiO_x layer and stored with an opaque Al cover up to 70 days of the storage time.

After 70 days of storage, we observed that the V_{OC} *was* relatively stable, the J_{SC} dropped 16%, the FF dropped 11%, and the PCE dropped approximately 25% in Figure 6.7. Hayakawa and his coworkers reported that the TiO_x layer played a significant role in preventing a reaction to a blend of active polymer with Al and a diffusion of Al into the active polymer [149]. Our stability study showed that the TiO_x layer alone could not completely block the oxygen from penetrating the OPV device at a prolonged storage time even when the device was stored inside a glove box atmosphere. In Figure 6.7, the values of OPV parameters were measured and calculated from the same OPV cell in the OPV device (Table D.1).

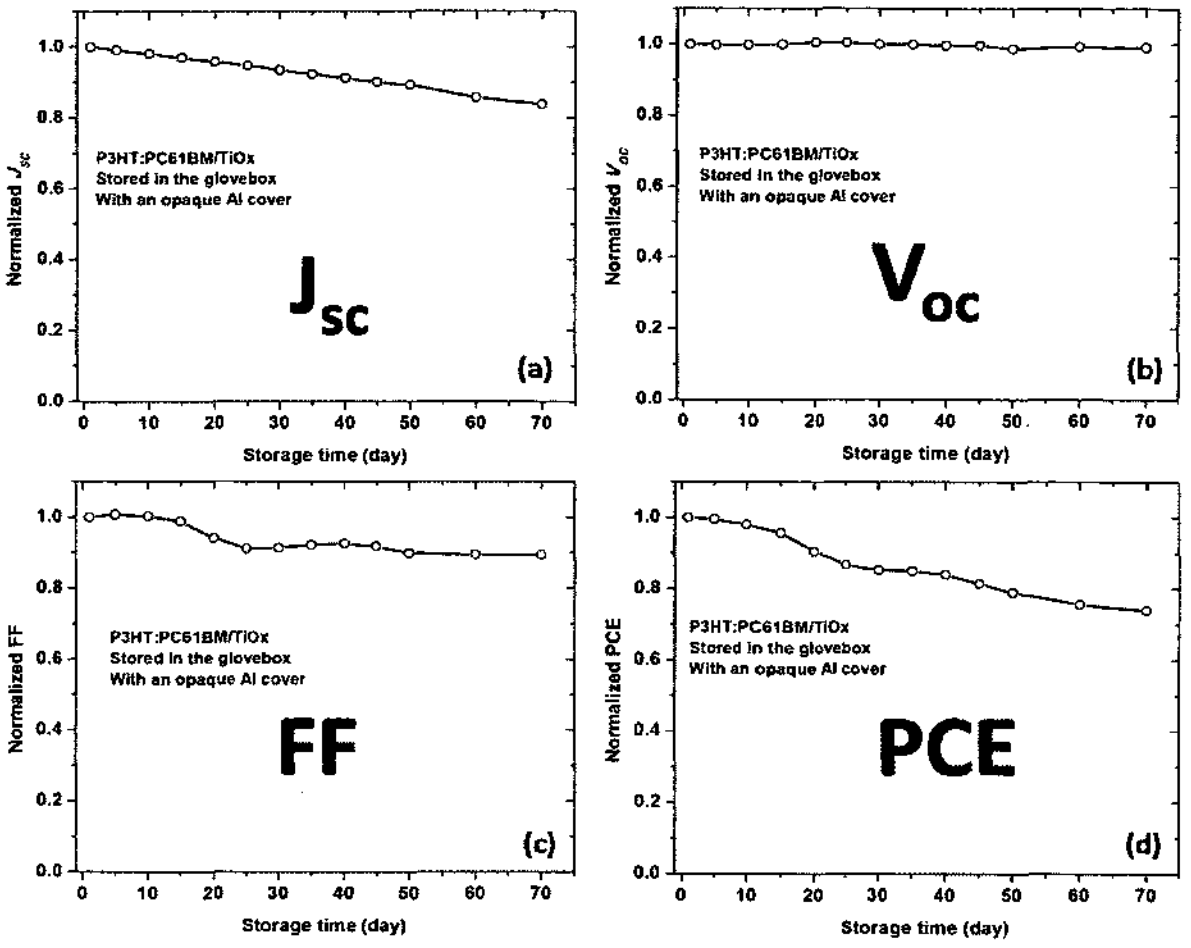

Figure 6.7: The change of the normalized OPV parameters, (a) J_{SC}, (b) V_{OC}, (c) FF, and (d) PCE, of a P3HT:PC61BM OPV cell with a TiO_x layer and stored with an opaque Al cover up to 70 days.

We observed that the J_{SC} value dropped linearly over the entire storage time with a loss rate of approximately -0.02 mA cm^{-2} per day. The FF and PCE values fluctuated slightly and dropped gradually over time. Hau and his coworkers reported that the FF value could improve slightly during a prolonged storage time due to the stability of the BHJ organic materials [46]. The V_{OC} value dropped slightly after 70 days of the storage time; therefore it could be considered the most stable OPV parameter. The V_{OC} value has been reported to be intrinsically dependent on the energy levels of the active materials and the morphology of the active layer [150,151].

6.7. Summary

We used a sol-gel TiO_x material as the interfacial layer between the active layer of P3HT:PC61BM and the Al cathode. We performed optimization tests on the TiO_x layer including a TiO_x spin coating test and a TiO_x solution drying test. We found that a solution based TiO_x layer coated at a spin speed of 3000 rpm (TF1) improved the photon absorption of the active layer. For the drying TiO_x solution test, we found that 90 °C for 10 min was the optimal drying condition for the TiO_x solution. A relatively smooth P3HT:PC61BM/TiO_x surface with an overall surface roughness (RMS roughness) of 0.494 nm was observed with an AFM measurement. An optimized TiO_x layer was used as the buffer layer in the OPV fabrication. We also performed a stability study using a solution based TiO_x layer to protect the active layer from moisture and oxygen and a stability study using an opaque Al cover to protect the device from the light (Case (II)). After 70 days of storage, we observed that the J_{SC} dropped 16%, FF dropped 11%, and PCE dropped approximately 25%, while the V_{OC} remained relatively stable. We concluded that a solution based TiO_x layer synthesized using a sol-gel chemistry method is effective in protecting the active layer from degradation.

Chapter 7

Improving the Stability of the Low Bandgap OPV Devices using a Solution Based Titanium Sub-oxide Interfacial Layer

7.1. Introduction

Stability and lifetime studies on recently developed low bandgap polymers (PCDTBT) are limited. Because of their inherent chemical and physical properties, low bandgap polymers generally exhibit different lifetimes and degradation pathways than do high bandgap polymers [152,153]. The PCDTBT is different from its high bandgap counterpart, P3HT. We assumed that the stability and the acceleration of physical and chemical degradation of the semi-crystalline polymer-based (P3HT) BHJ cell and an amorphous polymer-based (PCDTBT) BHJ cell might be different. In general, degradation can occur at the electrodes or within the photoactive layer of OPV devices. For example, a photochemical reaction in the photoactive layer of PCDTBT based OPV devices was reported to reduce the FF, V_{OC}, and J_{SC} [154].

We fabricated OPV devices with a structure of ITOPEDOT:PSS/PCDTBT: PC71BM/TiO_x/Al. The energy level diagram of OPV devices with a TiO_x layer is shown in Figure 7.1. The weight ratio for an active solution of PCDTBT:PC71BM is 1:4 with a weight concentration (mg) of 7:28 (in 2 mL 1,2-dichlorobenzene solvent). The active solution was spun inside the glove box to form an 80 nm thickness. Immediately following, the active layer was annealed at 140 °C for 2 min. The substrate was then allowed to cool down to room temperature inside the glove box. The TiO_x solution was

spun in the air inside the fume hood environment. An 80 nm thickness of Al deposited with the *e*-beam evaporator was used as the metal contact. We began by performing optimization tests including thickness and drying TiO_x film tests.

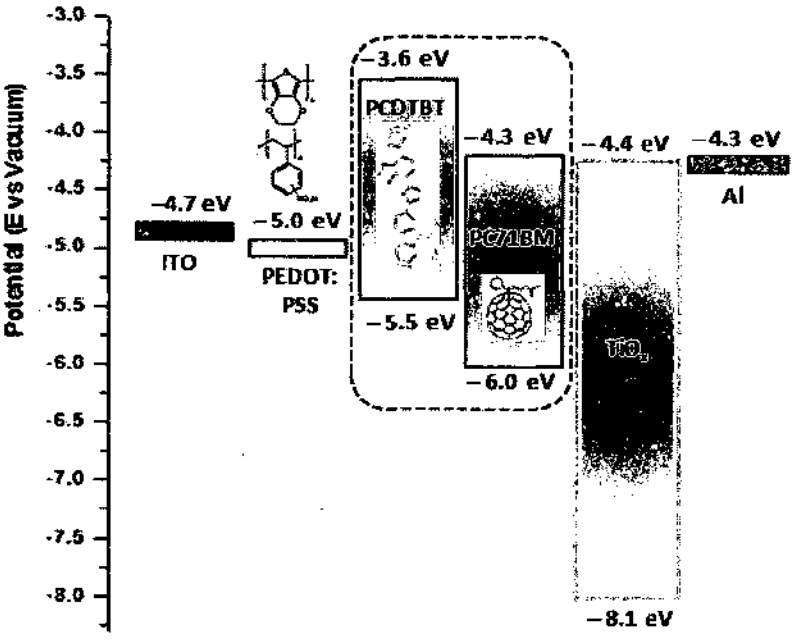

Figure 7.1: Energy level of an OPV device of PCDTBT:PC71BM with the TiO_x interfacial layer (with respect to the vacuum level).

7.2. Absorption study on the PCDTBT:PC71BM/TiO_x layers

The photoactive layer of PCDTBT:PC71BM we investigated was spun with TiO_x solutions at different spin speeds of TF1 (3000 rpm), TF2 (2000 rpm), and TF3 (1000 rpm) as discussed previously in Section 6.2. A thin film of active layer coated without a TiO_x layer (TF0) was added to our study. A pre-cleaned glass was used as the substrate. We then coated the TiO_x solution onto separate glass substrates pre-coated with an active layer and annealed the TiO_x at 90 °C for 10 min. Figure 7.2 shows the absorption spectra

of the blend of PCDTBT:PC71BM film coated with the TiO_x layer at different thicknesses.

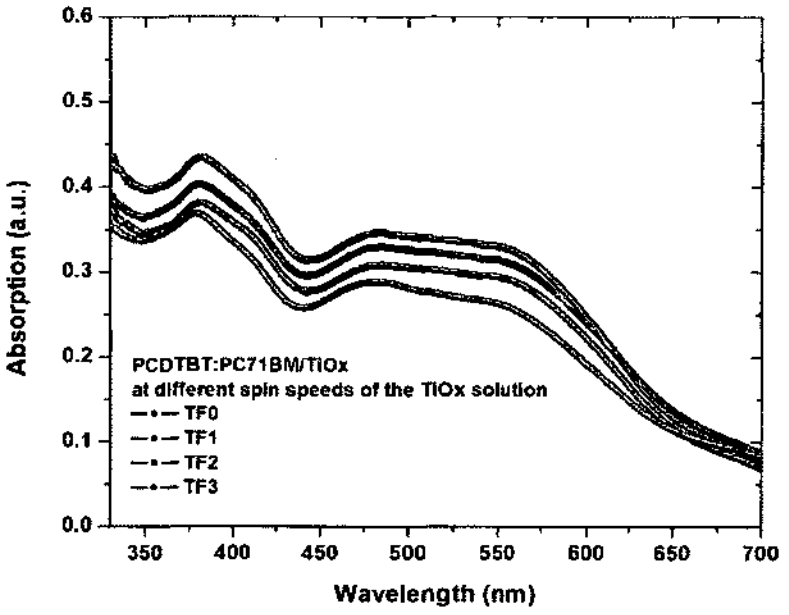

Figure 7.2: The UV-Vis absorption profile of PCDTBT:PC71BM immediately following fabrication (TF0, green) and PCDTBT:PC71BM/TiO_x at different spin speeds of the TiO_x solution: 3000 rpm (TF1, black), 2000 rpm (TF2, red), and 1000 rpm (TF3, blue).

The absorption spectrum of the PCDTBT:PC71BM film is a superposition of the polymer and the fullerene absorption spectra. The spectra exhibit two distinct absorption bands centered at approximately 400 nm and 580 nm, respectively. The two absorption peaks previously discussed were attributed to π–π^* transitions with the lower energy peak associated with an intra-chain charge transfer [120]. We observed that the absorbance of PCDTBT:PC71BM coated with a TiO_x layer at 3000 rpm (TF1) showed the best absorption intensity.

7.3. TiO_x spin coating test

We fabricated three OPV devices with a structure of ITO/PEDOT:PSS/PCDTBT: PC71BM/TiO_x/Al at different spin speeds of the TiO_x solution. As discussed in the previous section, the optimal spin speed of the TiO_x solution coated on the PCDTBT: PC71BM was 3000 rpm. Figure 7.3 shows the *J-V* characteristics of the OPV cells fabricated at different thicknesses of the TiO_x layer. In this study, the OPV device fabricated with a spin speed of the TiO_x solution of 3000 rpm yielded the best result with an FF of 40% and a PCE of 3.1%, while the V_{OC} values were relatively the same. The slight enhancement in the photocurrent observed in the OPV devices with TiO_x as the interfacial layer are not only due to the property of the TiO_x layer, the thickness and the optical constants, but are also due to the thickness and optical constants of all layers within the BHJ OPV cell including ITO, PEDOT:PSS, and active materials [85].

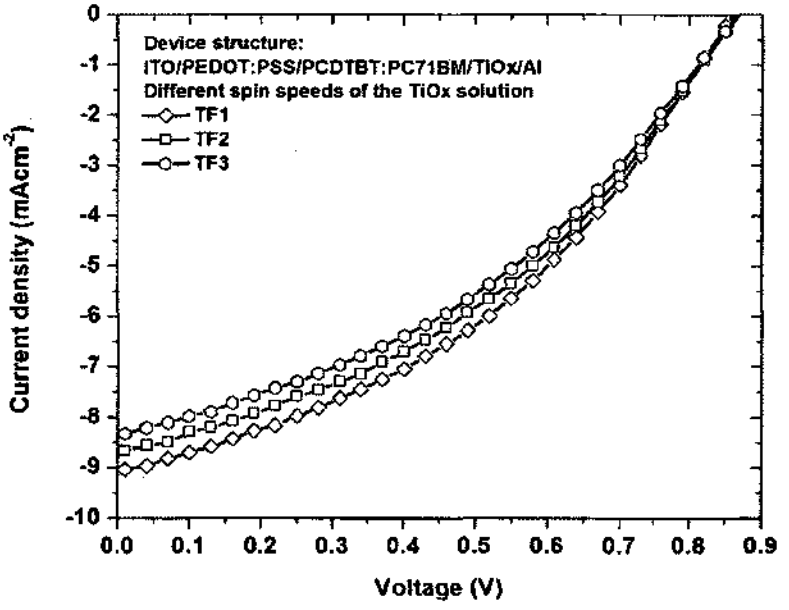

Figure 7.3: *J-V* characteristics of PCDTBT:PC71BM OPV cells fabricated at different spin speeds of the TiO_x solution: 3000 rpm (TF1, diamond), 2000 rpm (TF2, square), and 1000 rpm (TF3, circle).

Table 7.1: The parameters of PCDTBT:PC71BM OPV cells fabricated at different spin speeds of the TiO_x solution.

Spin speeds of the TiO_x solution	J_{SC} (mA cm^{-2})	V_{OC} (V)	FF (%)	PCE (%)
3000 rpm (TF1)	**9.09**	**0.86**	**39.80**	**3.12**
2000 rpm (TF2)	**8.72**	**0.87**	**39.01**	**2.94**
1000 rpm (TF3)	**8.39**	**0.87**	**38.34**	**2.78**

7.4. TiO_x solution drying test

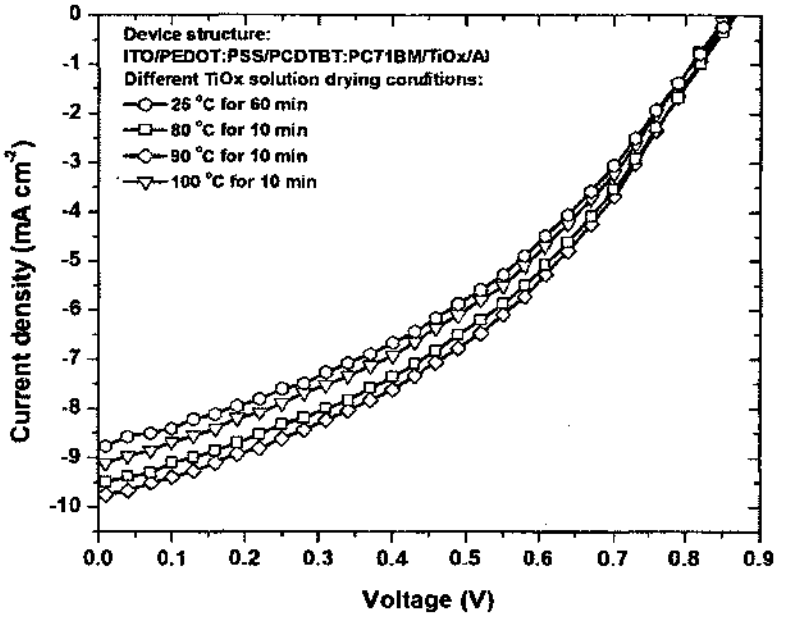

Figure 7.4: *J-V* characteristics of PCDTBT:PC71BM OPV cells fabricated at different TiO_x solution drying conditions.

For the TiO_x solution drying test, we fabricated OPV devices with drying conditions of the TiO_x layer used to optimize high bandgap polymer OPV devices. Figure 7.4 shows the *J-V* characteristics for low bandgap polymer OPV cells fabricated at different conditions; 25 °C for 60 min, 80 °C for 10 min, 90 °C for 10 min, and 100 °C for 10 min as discussed in Section 6.4. We observed that the V_{OC} value is not sensitive to variations in the drying conditions. We concluded that the optimal TiO_x solution drying condition in

a device structure of ITO/PEDOT:PSS/PCDTBT:PC71BM/TiO_x/Al was at 90 °C for 10 min which yielded a FF of 40% and a PCE of 3.4%.

Table 7.2: The parameters of PCDTBT:PC71BM OPV cells fabricated at different TiO_x solution drying conditions.

Drying condition	J_{SC} (mA cm^{-2})	V_{OC} (V)	FF (%)	PCE (%)
25 °C for 60 min	**8.82**	**0.86**	**38.16**	**2.91**
80 °C for 10 min	**9.55**	**0.87**	**39.06**	**3.23**
90 °C for 10 min	**9.81**	**0.86**	**39.91**	**3.37**
100 °C for 10 min	**9.15**	**0.86**	**38.57**	**3.02**

7.5. Surface topography of the PCDTBT:PC71BM/TiO_x layers

The photoactive layer of PCDTBT:PC71BM (80 nm) coated with a TiO_x film (less than 20 nm) was created and subsequently annealed in the air at 90° C for 10 min (as used in the drying process). To observe the topography of the top surface of the PCDTBT: PC71BM/TiO_x layer, the sample was characterized under AFM (a scanned area of 2 μm × 2 μm and a scanned frequency of 512 MHz). The 2-D and 3-D images of the top of the layer are shown in Figure 7.5. Based on the AFM images, we observed a few random bumps and spikes with approximately 6 nm in height of a freshly deposited a solution TiO_x material on a PCDTBT:PC71BM layer. Figure 7.5 clearly indicates the presence of large TiO_x grains at 90 °C annealing temperature. From this AFM surface morphology revealed in Figure 7.5 one can conclude that a 90 °C annealing temperature results already in a mixture of large grains embedded in a polycrystalline structure of the TiO_x film. The surface of the PCDTBT: PC71BM/TiO_x was a little bit rougher that of the P3HT:PC61BM/TiO_x as discussed in Section 6.5. However, the overall RMS roughness of the PCDTBT:PC71BM/TiO_x surface of 0.989 nm was observed.

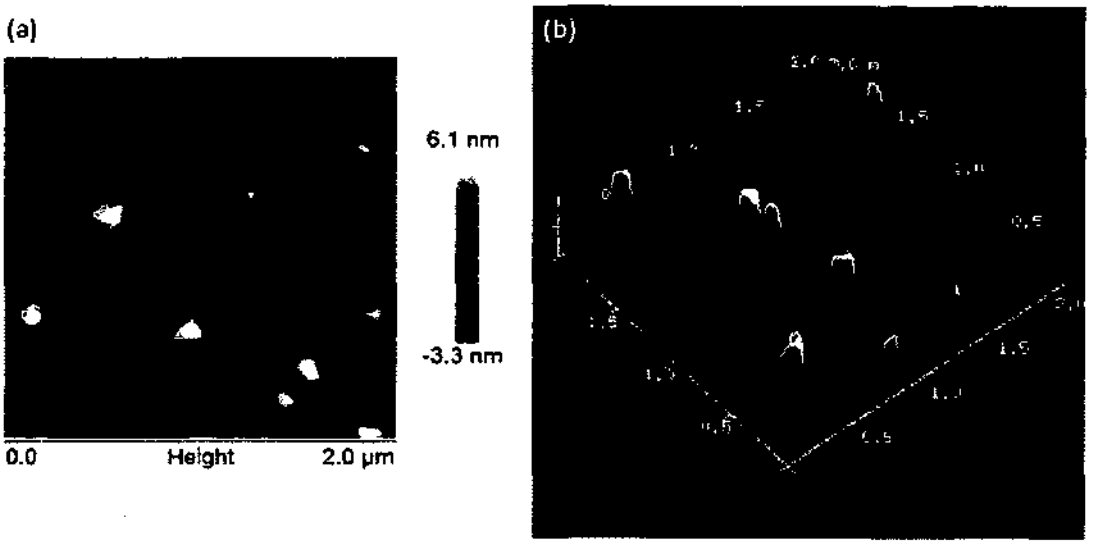

Figure 7.5: (a) 2-D and (b) 3-D AFM images of PCDTBT:PC71BM/TiO_x.

7.6. Stability studies on PCDTBT:PC71BM OPV devices

At the present time, the lifetime of OPVs is much shorter and the instability of the OPV device is the weakest point of OPV technology due to photo-degradation of the organic materials [16,134]. The instability of OPV devices is mainly caused by oxygen, and moisture resulting in the oxidation on low work function electrodes and the degradation of the morphology of the photoactive layer [16,155]. Furthermore, light has been reported to deteriorate the metal electrode and organic materials [33]. Since the mechanism of OPV device degradation is not yet fully understood and many different issues can lead to the same degradation trend of OPV cells, it is very difficult to determine specifically the exact cause of degradation. By observing the changes in important OPV device parameters, such as the J_{SC}, V_{OC}, FF, and PCE of the OPV devices as a function of time, we were able to make some intelligent guesses concerning the type of degradation taking place.

Table 7.3: Different stability study conditions for PCDTBT:PC71BM OPV devices.

Storage media	Temperature	With TiO_x		Without TiO_x
		With an opaque Al cover	Without an opaque Al cover	With an opaque Al cover
N_2-filled atmosphere (O_2, H_2O < 0.1 ppm)	25 °C	X		
			X	
				X
Ambient atmosphere	25 °C	X		
			X	
				X
Ante-chamber of a glove box	25 °C	X		
Refrigerator	3 – 5 °C	X		

To understand the behavior of the degradation of the low bandgap polymer, we performed important stability studies: (a) a stability study using a solution based TiO_x interfacial layer to protect the active layer from moisture and oxygen (Case (I)), (b) an stability study using an opaque Al cover to protect the OPV device from light (Case (II)), and (c) storage media study to study the degradation trend of OPV devices stored in the ambient and N_2-filled atmospheres, inside the ante-chamber of a glove box, and in a refrigerator (Case (III)) as seen in Table 7.3. We did not perform the study without an opaque Al cover for the device that did not have a TiO_x layer.

Figure 7.6 shows the OPV devices with and without an opaque cover. The temperature of the devices stored in the air, inside a glove box and in the ante-chamber of the glove box is maintained at a room temperature of (25 °C) in the laboratory, while the temperature of the refrigerator is at 3 – 5 °C. In this study, we fabricated 8 unencapsulated OPV devices and each device consisting of 8 OPV cells (a total of 64 cells must be characterized). The OPV devices were characterized in the air periodically

for 30 days. For the devices that were protected with an opaque Al cover, the characterization was done efficiently in a shorter time to avoid overexposure to light.

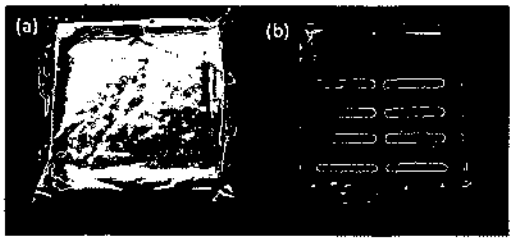

Figure 7.6: PCDTBT:PC71BM OPV devices (a) with and (b) without an opaque Al cover.

7.7. I-V measurements of OPV devices

It is important to discuss the I-V measurements of the OPV devices prior to discussing the stability study results. The OPV devices were fabricated with different stability study conditions and stored in their respective storage media conditions. We characterized the devices in the air daily for the first 7 days of storage time. For example, the devices stored in the N_2-filled atmosphere were taken out of the glove box for I-V measurements. After 7 days of consecutive I-V measurements, the devices were stored in their respective storage media environment and were taken out into the air atmosphere for characterization after 12, 18, 25, and 30 days. During measurements, O_2, H_2O, and light were inevitably introduced to the organic materials and devices that might accelerate the degradation process.

7.8. Case (I): Stability study of OPV devices with and without TiO_x layers

First, we studied the stability of the low bandgap OPV devices fabricated with and without TiO_x layer. The purpose of this study was to investigate the effectiveness of the TiO_x layer in protecting organic materials from degradation, especially from water and

oxygen. For an ideal intrinsically stable OPV device, both the organic materials and electrodes must be stable without using any encapsulation. We also performed a storage media study at the same time. We prepared four low bandgap OPV devices fabricated with and without a TiO_x protection layer (less than 20 nm) and stored them in the air and inside a glove box. We stored the fabricated OPV devices with and without opaque Al covers (with a high research grade quality).

We were interested in monitoring the change in the *J-V* characteristics of OPV cells with and without a TiO_x layer. We compared the relative degradation trend from device to device by evaluating their J_{SC}, V_{OC}, FF, and PCE values as a function of the storage time. Figure 7.7 shows the change in the *J-V* characteristics of four OPV cells fabricated without the TiO_x layer stored in the air and inside the glove box up to 7 days of storage time. The devices were protected with an opaque Al foil cover. To maintain the consistency of our results, Figure 7.7 shows the *J-V* characteristics of the same OPV cell (from the total of 8 cells in each OPV device) with the best performance on a periodic basis. The devices were characterized at a period of 30 days, but the *J-V* characteristics were only shown up to 7 days since the *J-V* curves were too crowded. We observed that the device with a TiO_x layer and stored inside the glove box is the most stable with both J_{SC} and FF values dropping only approximately 5% and 2% over 7 days of storage time, as seen in Figure 7.7(b). While for the device fabricated without the TiO_x layer and stored in the glove box, the J_{SC} and FF values dropped 20% and 23%, respectively, over 7 days of storage time as seen in Figure 7.7(d).

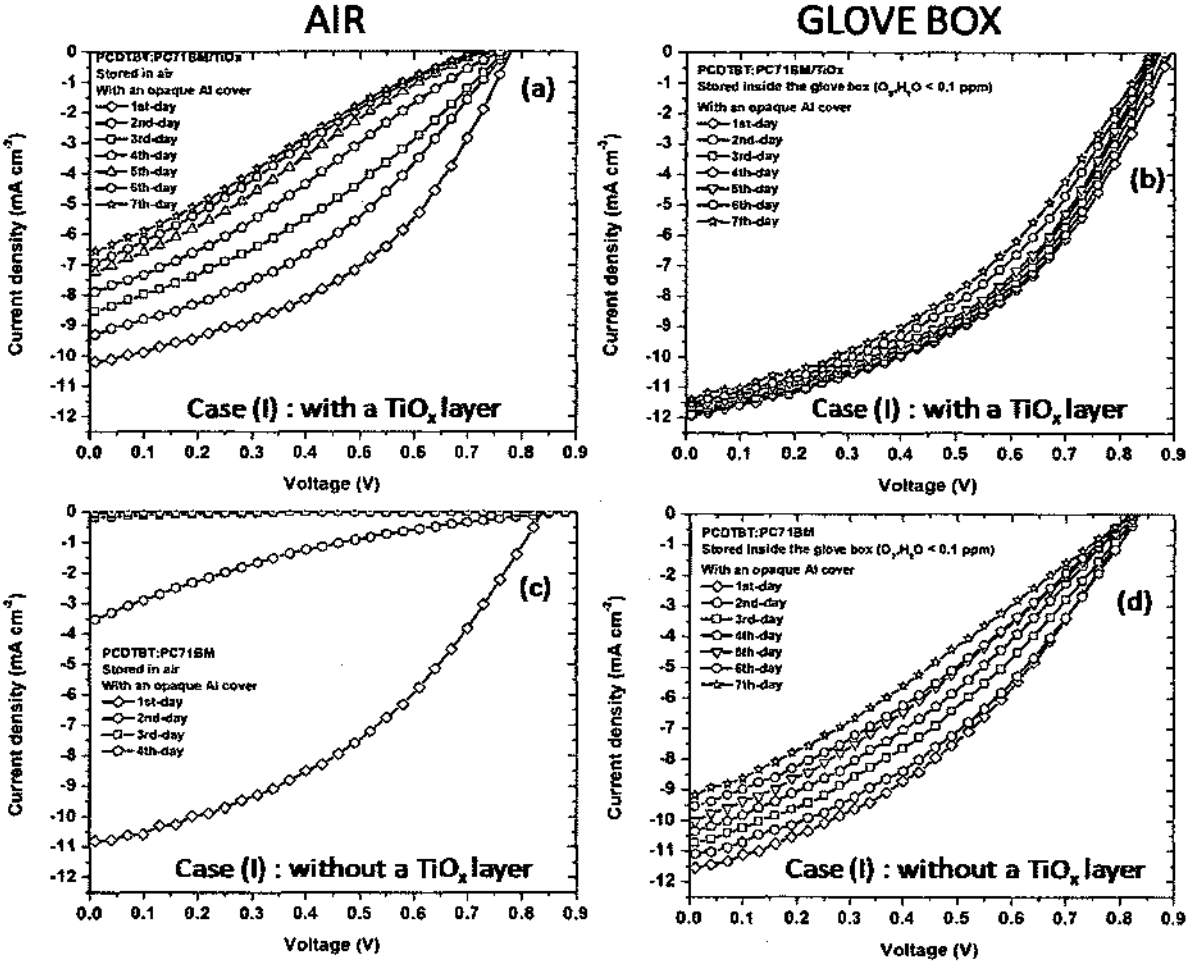

Figure 7.7: *J-V* characteristics of PCDTBT:PC71BM OPV cells fabricated with and without TiO_x layers (Case (I)) and stored in the air and glove box. The devices were protected with an opaque Al cover.

These results show us that both the TiO_x layer and the N_2-filled atmosphere significantly improved the stability of the low bandgap OPV devices. The inert gas environment has been reported to be a favorable place to store organic materials and to enhance the stability of OPV devices [14,86]. Improved device performance has been reported due to the reduction of series resistance and improved shunt resistance of the cell which can be attributed to improvement in the following three areas: (1) reduction of the contact resistance between the inorganic TiO_x layer and active organic layer by

passivation of surface trap states; (2) enhancement of the electronic coupling between the inorganic TiO_x and active organic layer to mediate better forward charge transfer and reduce back charge recombination at the interface, and (3) in affecting the upper organic layer growth mode and morphology [156].

We monitored the OPV device performances in the air as well. For the device with a TiO_x layer and stored in the air, the J_{SC} and FF values dropped 32% and 44%, respectively, over 7 days of storage time as seen in Figure 7.7(a). We observed that the degradation of the low bandgap OPV device fabricated without the TiO_x layer was the fastest when it was stored in the air, as seen in Figure 7.7(c), where the J_{SC} and FF values dropped 98% and 81%, respectively, after 3 days of storage time. The reactions between O_2 and H_2O and the Al cathode lead to metal oxidation and active layer damage [157]. An opaque Al foil cover was not enough to slow down the degradation. The degradation of the performance of the OPV device has been reported to be related to recombination of the charge carriers [113] and oxygen induced trap states in the polymer resulting in a strong decrease in charge carrier mobility [158].

We found that the TiO_x layer effectively improved the lifetime and stability of the OPV device. The polymers with low ionization potential and amorphous structure materials such as PCDTBT are the most susceptible to oxygen diffusion into the blend of the active solution [159]. The effect of the TiO_x material as the oxygen/water protection and as the oxygen scavenging agent for the OPV device application is reportedly due to the combination of photo-catalysis and inherent oxygen deficiency [160]. This study further highlights the importance of the TiO_x layer in the lifetime and stability of OPV devices.

7.9. Case (II): Stability study of OPV devices with and without opaque Al covers

We then performed a stability study of low bandgap OPV devices stored with and without opaque Al protection covers. The purpose of this study was to investigate the effects of the Al cover in protecting OPV device from degradation, especially from exposure to light. We prepared four low bandgap OPV devices with and without an Al cover (with a high research grade quality) stored in the air and inside the glove box. We fabricated OPV devices with a TiO_x layer (less than 20 nm) as the protection layer.

Similar to what we did in Case (I) stability study, we monitored the change in *J-V* characteristics of OPV devices with and without an opaque Al cover. In this study, all devices were fabricated with a TiO_x layer and we compared the relative degradation trend from device to device by evaluating their OPV parameter values. To maintain the consistency of our results, in a total of 8 cells in each OPV device, we characterized and monitored the same cell showing the best performance periodically.

Figure 7.8 shows the change in the *J-V* characteristics of four OPV cells fabricated with and without an opaque Al cover stored in the air and inside the glove box up to 7 days of storage time. The devices were fabricated with a TiO_x layer. Over 7 days of storage time, we observed that the device stored with an opaque Al cover inside the glove box was the most stable with both J_{SC} and FF values dropping only approximately 5% and 2% as seen in Figure 7.8(d). While the device stored without an opaque Al cover inside the glove box is relatively stable and gradually dropped its performance over time showing the J_{SC} and FF values dropping only 14% and 1%, respectively as seen in Figure 7.8(b).

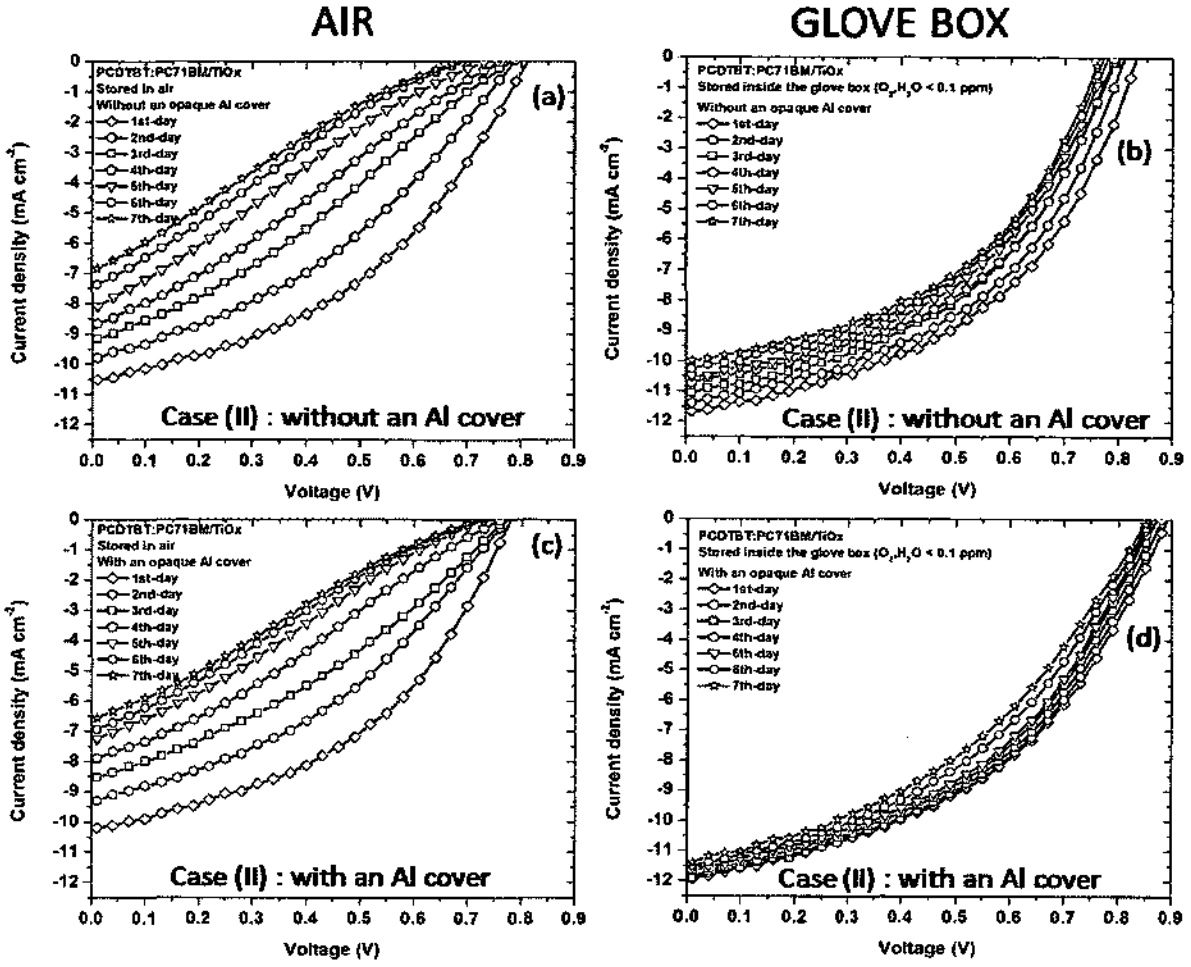

Figure 7.8: *J-V* characteristics of PCDTBT:PC71BM OPV cells stored with and without opaque Al covers (Case (II)) in the air and glove box. The devices were fabricated with a TiO_x layer.

In general, the condition and quality of OPV devices stored inside a glove box were preserved well regardless of the presence of an opaque Al cover due to the oxygen- and moisture-free environment which slows down degradation [17]. The relatively small dropping of the FF values (approximately 1%), of the OPV device stored without a cover for over 7 days of storage time was not a direct result of the effect of the Al cover; rather it was ascribed to the internal stable morphology of the BHJ active materials of PCDTBT:PC71BM.

We observed degradation of OPV devices stored with and without an opaque Al cover in an ambient atmosphere. We found that the device with an opaque Al cover showed that J_{SC} and FF values dropped 32% and 44%, respectively as seen in Figure 7.8(c). While the devices stored without an opaque Al cover, J_{SC} and FF values dropped 29% and 46%, respectively as seen in Figure 7.8(a). In general, we observed that the OPV devices stored in the air with and without Al covers degraded significantly faster under exposure to air and moisture compared to the ones stored inside the N_2-filled atmosphere. It seems that the Al cover was not as effective in protecting the OPV devices from photodegradation because the J_{SC} and FF values are relatively similar We believe the reason that the Al cover was ineffective in protecting the OPV devices were (1) the reaction between the organic materials or metal electrodes and O_2 and H_2O was stronger compared to the reaction between the organic materials/electrodes with the light and (2) the devices were not completely protected from the light because they were characterized in the air and under an intense solar illuminator on a periodic basis. In the latter case, the photodegradation inevitably deteriorated the performance and the quality of OPV devices.

7.10. Case (III): Stability study of OPV devices based on different storage media

We also investigated the degradation trend of the PCDTBT:PC71BM based OPV devices influenced by the storage media environment. Krebs and his coworkers had investigated different degradation variables affecting the lifetime and stability of OPV devices [22]. They studied the effects of different storage media on the lifetime of OPV device stored in extreme conditions such as outdoor and cool environments. In addition to

(1) the ambient and (2) N_2-filled atmosphere environments (as previously mentioned in Section 7.6 and 7.7), two separate storage media, (3) the ante-chamber and (4) refrigerator, were used. The refrigerator provided a controlled environment with temperatures of a 3 – 5 °C range.

The device stored inside the refrigerator also had limited exposure to light. The ante-chamber of the glove box was utilized when access was needed in and out of the glove box and also had a limited exposure to light. The ante-chamber of the glove box is not a moisture free or oxygen free environment; rather it is a partial environment which is sometimes an inert gas or ambient atmosphere. The ante-chamber environment might be useful if we do not have enough space to keep the OPV devices inside a glove box but we want to study them at a later time. It would be beneficial to manufacture an affordable partial glove box that does not require a completely O_2- and H_2O-free environment.

Similar to previous studies, we were interested in monitoring the change of *J-V* characteristics of OPV devices stored in different storage media environments. We compared the relative degradation trend from device to device by evaluating their J_{SC}, V_{OC}, FF, and PCE values as a function of storage time. To maintain the consistency of our results, for the total of 8 cells in each OPV device, we characterized and monitored the same cell showing the best performance over a period of time.

We fabricated four PCDTBT:PC71BM OPV devices with a TiO_x layers. Following fabrication, we protected the devices with Al foil and stored them in different storage environments; the ambient and N_2-filled atmosphere environment, a refrigerator and an in ante-chamber of the glove box as shown in Figure 7.9. We characterized the devices periodically in the air. As previously discussed, we found that the J_{SC} and FF values

dropped 32% and 44%, respectively, for the device stored in the air (Figure 7.9(a)), and approximately 5% and 2% for the devices stored inside the glove box (Figure 7.9(b)) over a period of 7 days in the storage media. For the device stored in the ante-chamber, we observed that the J_{SC} and FF values dropped 27% and 16%, respectively, over 7 days of the storage time (Figure 7.9(c)). And for the device stored in the refrigerator, J_{SC} and FF values dropped 16% and 5%, respectively, over 7 days of storage time (Figure 7.9(d)).

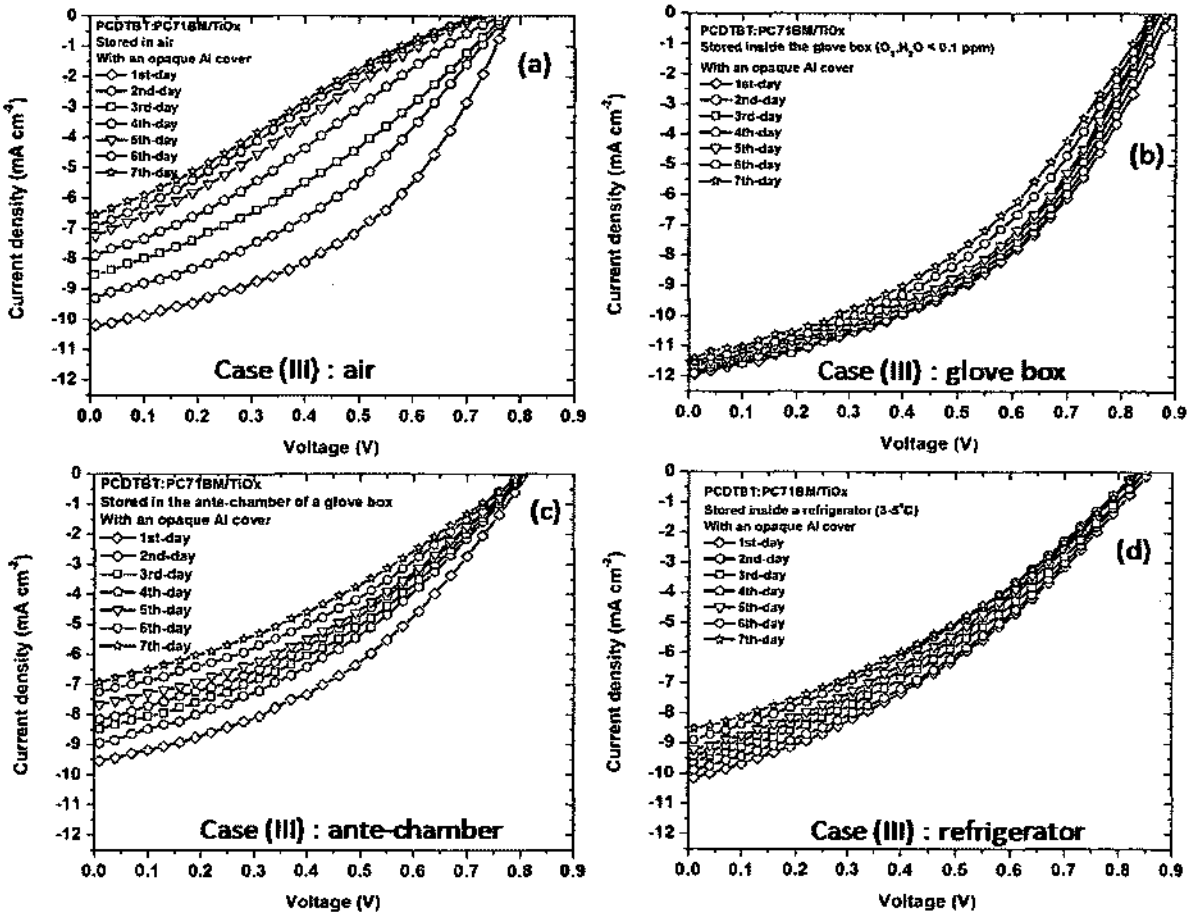

Figure 7.9: *J-V* characteristics of PCDTBT:PC71BM OPV devices fabricated with a TiO_x layer and stored with an opaque Al cover in different storage media : (a) air, (b) glove box, (c) ante-chamber of the glove box, and (d) refrigerator (Case (III)).

The results showed that the N_2-filled atmosphere environment was the best storage media to keep OPV devices from degradation. However, the degradation of the OPV

device was slowed down in the refrigerator. It has been reported that a low temperature storage environment has helped tremendously in keeping organic materials from degrading over long periods of time [161,162]. Moreover, the dark environment inside the refrigerator and the cool temperatures improved the stability and lifetime of the OPV device. While the ambient and ante-chamber environments deteriorated the quality of the OPV devices approximately 30% compared to their initial performances. The degradation of the OPV device performance stored in any place where O_2 and H_2O are available has been reported to be related to recombination of the charge carriers [113] and oxygen induced trap states in the polymer resulting in a strong decrease in charge carrier mobility [156].

7.11. Summary

We used the sol-gel TiO_x material as an interfacial layer between the active layer of PCDTBT:PC71BM and the Al cathode. We performed optimization tests on the TiO_x layer including the TiO_x solution spin coating test and the TiO_x solution drying test. We found that the TiO_x solution deposited at a spin speed of 3000 rpm (TF1) improved the photon absorption of the active layer. For the drying test, we found that 90 °C for 10 min was the optimal drying condition for the TiO_x solution. The surface roughness of PCDTBT:PC71BM/TiO_x of a 0.989 nm was observed with an AFM measurement.

We performed stability studies on the low bandgap OPV devices based on (1) with and without TiO_x layers (Case (I)), (2) with and without opaque Al protection covers (Case (II)), and (3) different storage media (Case (III)). We investigated the degradation of the OPV devices by observing the changes in the J_{SC}, V_{OC}, FF, and PCE values of the

OPV devices as a function of time. Figure 7.10 shows the change in the OPV parameters (J_{SC}, V_{OC}, FF, and PCE) of a single cell in respected OPV devices as a function of time for 30 days (Table D.2 – D.7). To maintain the consistency of our result, over the total of 8 cells in each OPV device, we characterized and monitored the same cell showing the best performance periodically.

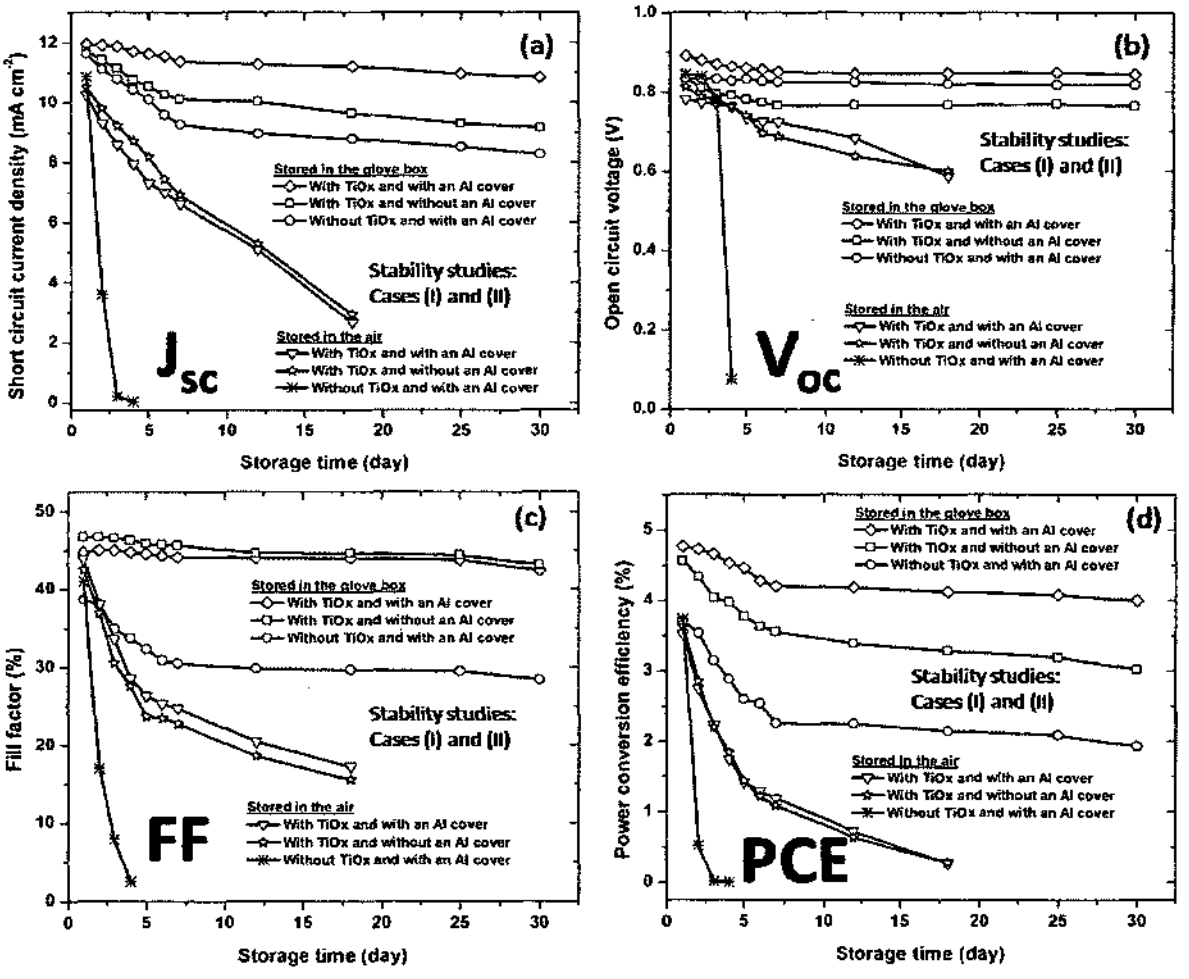

Figure 7.10: The change of parameters, (a) J_{SC}, (b) V_{OC}, (c) FF, and (d) PCE values of PCDTBT:PC71BM OPV cells fabricated with and without TiO_x layers (Case (I)). The devices were stored with and without Al opaque covers (Case (II)) in the air and glove box atmospheres for 30 days.

In general, the performance of OPV devices dropped relatively fast for the first 7 days because the devices were taken out of their respective storage media environments for I-

V measurements in the air. While measuring, OPV devices were exposed to O_2, H_2O, and light. After 7 consecutive days of I-V measurements, the devices were only taken out and characterized in the air periodically (every other 5 days) which significantly improved the stability of the devices. The decrease in the OPV device parameters (J_{SC}, FF, and PCE) correlates to the loss of the physical or chemical qualities of the device due to recombination, loss mechanism, or degradation. However, the V_{OC} value was relatively stable and was reported to be internally dependent on the energy levels of the active materials and the morphology of the active layer [12,148].

From the stability study of the low bandgap OPV devices with and without TiO_x layers (Case (I)), we found that the TiO_x layer was significantly effective in protecting the active solution and the OPV device from degradation especially from exposure to O_2 and H_2O. After 30 days of storage time, the PCE values dropped 16% for the device with a TiO_x layer and 48% for the device without the TiO_x layer stored in a N_2-filled atmosphere. While for the device stored in the air, the PCE values dropped 92% after 18 days of the storage time for the device with a TiO_x layer and 100% after 3 days for the device without the TiO_x layer. We concluded that the solution based TiO_x layer was effective in slowing down degradation by 300% for the device stored in the N_2-filled and ambient atmospheres. This study highlighted the effectiveness of the TiO_x layer as an oxygen/water protection and as an oxygen scavenging agent in improving the lifetime and stability of OPV devices.

From the stability study of the low bandgap OPV devices stored with and without opaque Al protection covers (Case (II)), we found that the Al cover was not effective in protecting the organic materials and OPV devices from degradation especially from the

light. After 30 days of storage, the PCE values dropped 16% in the device with an opaque Al cover and 34% in the device without a cover stored in the N_2-filled atmosphere. For the device stored in the air, the PCE values of both devices with and without an Al cover dropped approximately 92% after 18 days of storage time. We suggest the reasons for the ineffectiveness of the Al cover are (1) the reaction between the organic materials or metal electrodes and O_2 and H_2O was stronger comparing the reaction between the organic materials/electrodes with light and (2) the devices were not completely protected from light.

From the stability study of the low bandgap OPV devices with different storage media (Case (III)), we found that the N_2-filled atmosphere environment was the most optimum environment to store OPV devices and to keep them from degradation as seen in Figure 7.11. As observed in stability studies for Cases (I) and (II), the performance of OPV devices stored in different storage media environments also dropped relatively faster in the first 7 days compared to the later storage times because the devices were exposed to O_2, H_2O, and light more often during the I-V measurements. Figure 7.11 shows the change in the OPV parameters (J_{SC}, V_{OC}, FF, and PCE) of a single cell in respected OPV devices as a function of time for 30 days (Appendix D.2, D.4, D.8, and D.9). We characterized and monitored the same cell showing the best performance periodically.

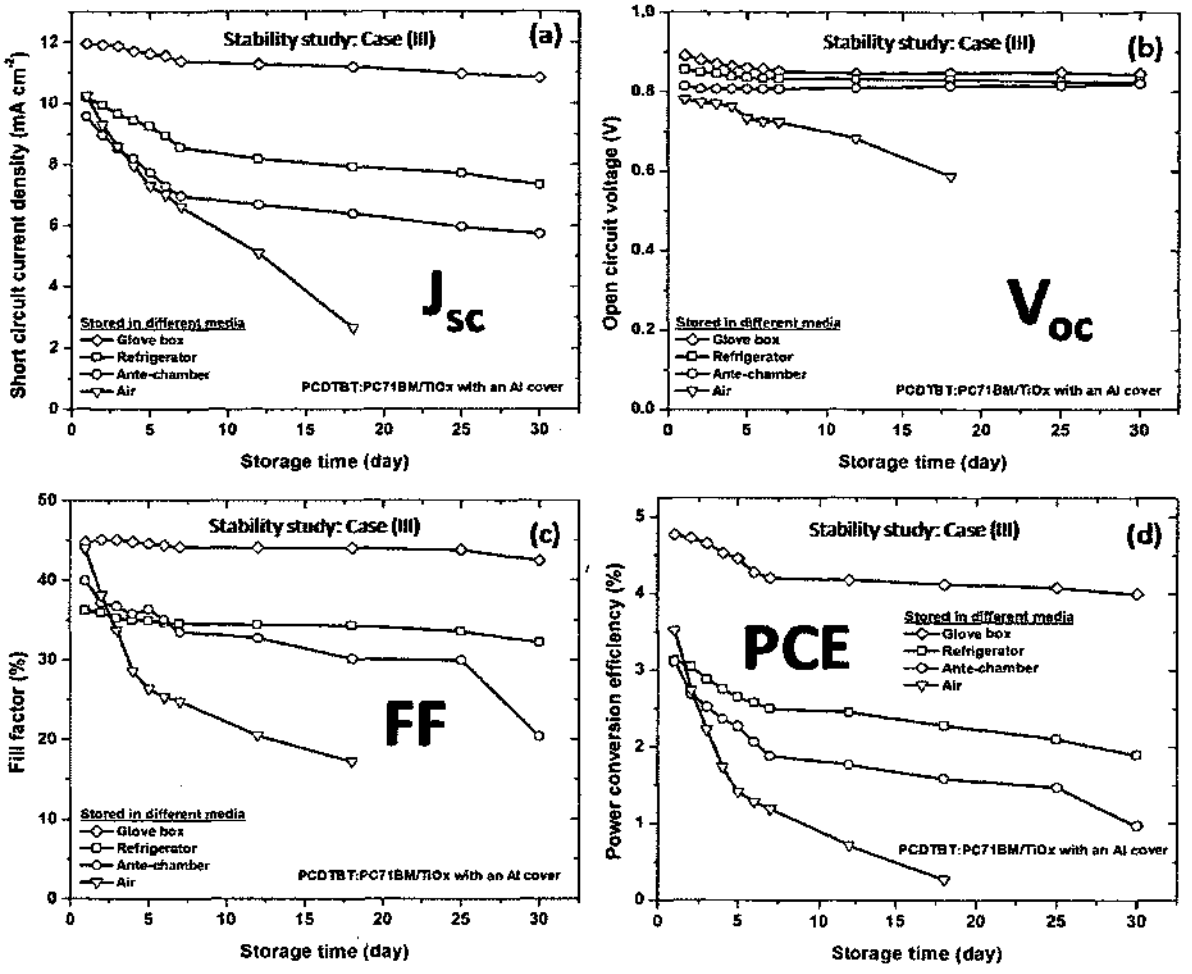

Figure 7.11: The change of parameters, (a) J_{SC}, (b) V_{OC}, (c) FF, and (d) PCE, of PCDTBT:PC71BM OPV cells fabricated with a TiO_x layer and stored with an opaque Al cover in different storage media: glove box (diamond), refrigerator (square), ante-chamber of a glove box (circle), and air (triangle) (Case (III)) for 30 days.

After 7 consecutive days of I-V characterizations, the devices were taken out and characterized in the air periodically (every other 5 days), which improved the stability of the devices. The PCE of the device stored in the glove box dropped only 16% after 30 days. The next optimum environment was the refrigerator maintained at low temperatures of 3 – 5 °C which was reported to be successful in slowing down degradation in the organic materials. The PCE value of the device stored in the refrigerator dropped 42% after 30 days.

We found that the condition in a partial inert environment of the antechamber would be a comprising optimum condition where the OPV device would be operational without causing any catastrophic failures (The PCE value dropped 75% after 30 days). After 25 days of storage time in the ante-chamber, the OPV device quality dropped significantly which might be caused by activity in the glove box during that period of storage time. The activity of the ante-chamber that introduced O_2, H_2O, and light to an OPV device certainly accelerates the degradation processes. Finally, the PCE of the device stored in the air dropped 100% after 18 days because the O_2 and H_2O aggressively reacted with the organic materials/electrodes. Similar to our previous findings, the V_{OC} was stable as expected since the V_{OC} values depended intrinsically on the energy level of the active materials.

Chapter 8

Conclusions and Future Work

In this thesis, we fabricated unencapsulated bulk heterojunction (BHJ) organic photovoltaic (OPV) devices based on the high and low bandgap polymers with structures of ITO/PEDOT:PSS/P3HT:PC61BM/Al and ITO/PEDOT:PSS/PCDTBT:PC71BM/Al, respectively. There are two major parts to this study. First, we fabricated conventional OPV devices without a TiO_x layer. Prior to fabrication, we spent significant time and effort in optimizing the fabrication processing steps including; the thickness of the active layer (using spin coating deposition), and the pre-annealing and post-annealing treatments. The majority of BHJ films were formed by spin coating where the initial phase morphology was determined by a complex combination of solvent removal and solidification of acceptor and donor materials. We found that although the principle of spin coating might sound simple, it can limit morphological controllability.

We fabricated the OPV devices by using the optimal fabrication procedure. In our experiment, we achieved that the best PCE value of 4.1% for the P3HT:PC61BM based OPV device and 5.1% for the PCDTBT:PC71BM OPV device as seen in Table 8.1. However, the fill factor for our low bandgap polymer based OPV devices was below 50% which means the control morphology for the PCDTBT:PC71BM layer was not fully optimized. Reproducibility of the OPV devices is another major issue in OPV research. The main reason for a reproducibility issue is the instability of the morphological donor

and acceptor phase separation. The reproducibility issue could be improved with an optimum fabricating and processing environment. Moreover, reproducing good results for BHJ OPV devices in a non dust free laboratory environment is even harder.

Table 8.1: The best P3HT:PC61BM and PCDTBT:PC71BM OPV parameters achieved in our experiment bench marked with literature values [85,163].

Active layer	Reference	E_g (eV)	J_{SC} (mA/cm^{-2})	V_{OC} (V)	FF (%)	PCE (%)
P3HT:PC61BM	[163]	1.8	11.3	0.64	69	5.2
	This work		10.5	0.63	63	4.1
PCDTBT:PC71BM	[85]	1.9	10.6	0.86	64	6.0
	This work		12.7	0.90	45	5.1

We then studied the long term stability trends of two different BHJ systems: semi-crystalline and amorphous polymer based BHJ cells. Since both the P3HT and the PCDTBT displayed distinctive morphological characteristics in BHJ OPV cells, we believe that the acceleration of physical and chemical degradation may occur at different speeds for the P3HT:PC61BM and the PCDTBT:PC71BM active layers. There are rarely any reports about the stability study on a low bandgap polymer, PCDTBT based OPV devices. Therefore we focused the stability study on the blend of PCDTBT:PC71BM based OPV devices in this study. We synthesized a solution based titanium sub-oxide (TiO_x) by using a sol-gel chemistry method. We inserted a solution based TiO_x layer coated at a spin speed of 3000 rpm (less than 20 nm) between the photoactive layer and the Al cathode in OPV devices. We studied the effectiveness of the TiO_x layer in protecting the photoactive layer from degradation and performed a stability study on the OPV devices by using the TiO_x solution.

Table 8.2: The stability study performance of OPV devices fabricated using different photoactive layers, different stability conditions: with and without TiO_x layers (Case (I)), with and without opaque Al protection covers (Case (II)), and different storage media ((1) glove box, (2) air, (3) ante-chamber of the glove box, and (4) refrigerator (Case (III)).

No	Active layer of BHJ OPV device	TiO_x layer	Storage condition of OPV device	Initial PCE (%)	Storage time (day)	Percentage of PCE reduction
1	P3HT:PC61BM	YES	Glove box with an Al cover	1.7	70	26.02
2	PCDTBT:PC71BM	YES	Glove box with an Al cover	4.8	30	16.16
3	PCDTBT:PC71BM	YES	Glove box without an Al cover	4.6	30	33.80
4	PCDTBT:PC71BM	NO	Glove box with an Al cover	3.7	30	48.04
5	PCDTBT:PC71BM	YES	Air with an Al cover	3.5	18	92.35
6	PCDTBT:PC71BM	YES	Air without an Al cover	3.6	18	92.48
7	PCDTBT:PC71BM	NO	Air with an Al cover	3.7	3	100.00
8	PCDTBT:PC71BM	YES	Ante-chamber with an Al cover	3.1	30	75.21
9	PCDTBT:PC71BM	YES	Stored in a refrigerator	3.1	30	42.93

We performed stability studies on PCDTBT:PC71BM OPV devices based on different stability conditions : (1) with and without TiO_x layers (Case (I)), (2) with and without opaque Al covers (Case (II)), and (3) different storage media conditions (Case (III)) as seen in Table 8.2. To determine the trend of the performance of OPV devices as a function of the storage time, we used normalized OPV parameters, J_{SC}, V_{OC}, FF, and PCE values. Normalized parameters of OPV devices would be useful in comparing the relative degradation effect from one device to another. Figure 8.1 shows the change in the normalized OPV parameters (J_{SC}, V_{OC}, FF, and PCE) as a function of time for 30 days. Each normalized data represents results of a single cell of OPV parameters reported in Figure 7.10 (Table D.2 – D.7). To maintain the consistency of our result, over the total of 8 cells in each OPV device, we characterized and monitored the same cell showing the

best performance periodically. All data of parameters of OPV cells were normalized to the initial values of the cells.

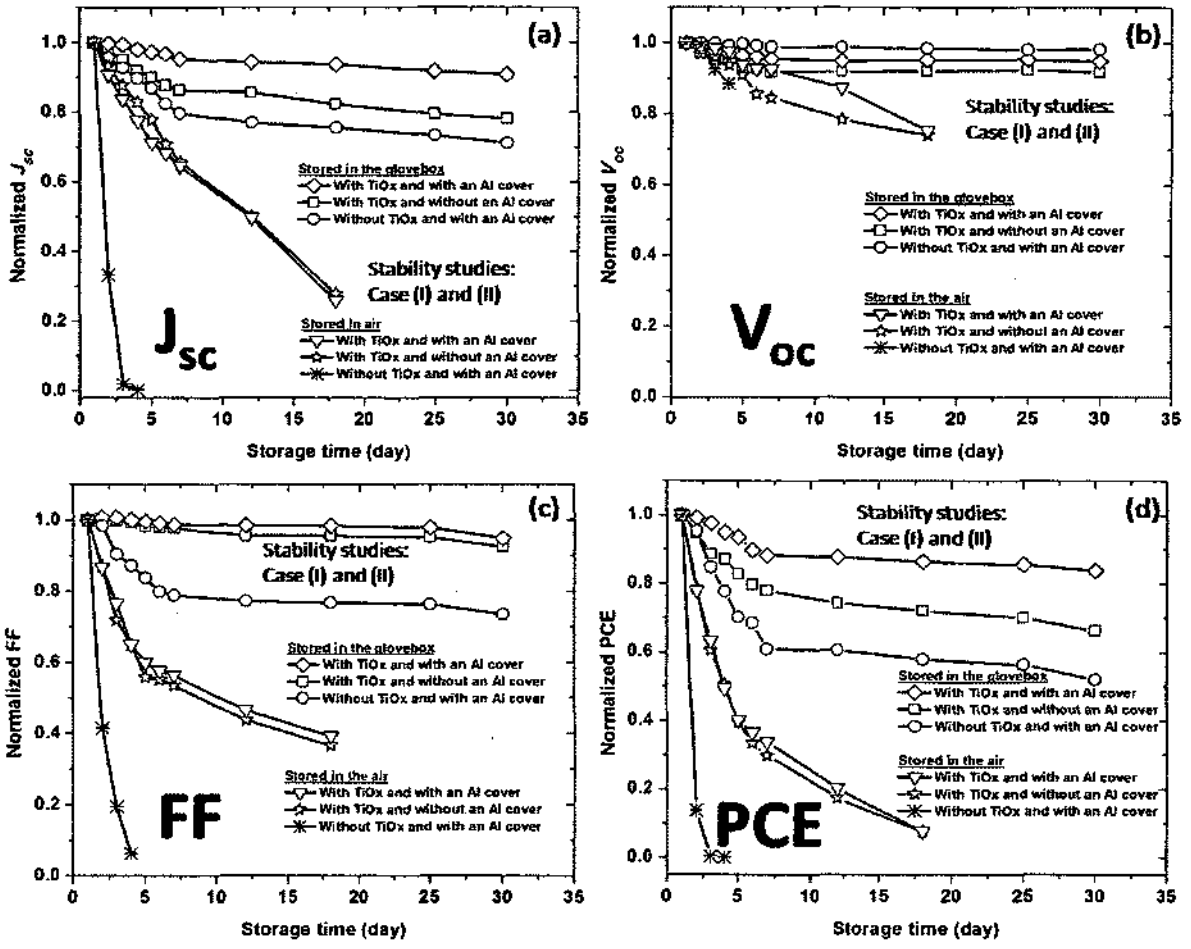

Figure 8.1: The change of the normalized OPV parameters, (a) J_{SC}, (b) V_{OC}, (c) FF, and (d) PCE values of PCDTBT:PC71BM OPV cells fabricated with and without TiO_x layers (Case (I)). The devices were stored with and without opaque Al covers (Case (II)) in the air and glove box atmospheres for 30 days.

In general, the performance of OPV devices dropped relatively fast for the first 7 days because the devices were taken out of their respective storage media environments for I-V measurements in the air. While measuring, OPV devices were exposed to O_2, H_2O, and light. After 7 consecutive days of I-V measurements, the devices were only taken out and characterized in the air periodically (every other 5 days) which significantly improved the

stability of the devices. The decrease in the OPV device parameters (J_{SC}, FF, and PCE) correlates to the loss of the physical or chemical qualities of the device due to recombination, loss mechanism, or degradation.

To evaluate the degradation trend of the low bandgap PCDTBT:PC71BM OPV devices, 5 different storage times were chosen: 1, 3, 7, 18, and 30 days. We compared the degradation trend of the device relatively with the first day as the device was fabricated (fresh). We chose the 3rd and 18th days because after those periods of time we observed some of low bandgap OPV devices were already dead due to degradation issues with unique fabrication and/or storage conditions, as discussed in previous chapter. The 30th day was chosen as the last day to perform the stability study of the device, and the 7th day was added to see the degradation trend of the device after a week.

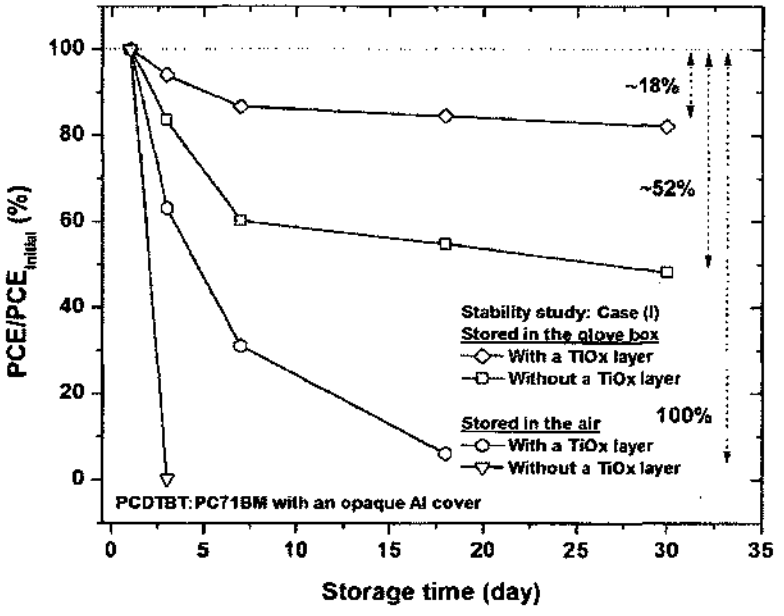

Figure 8.2: The stability study based on different stability conditions of low bandgap PCDTBT:PC71BM OPV cells fabricated with and without TiO_x layers (Case (I)). The devices were stored with an opaque Al cover in the air and glove box atmospheres for 30 days.

In the Case (I) stability study, we found that the TiO_x layer was significantly effective in protecting the organic materials from degradation especially from H_2O and O_2, and in improving the lifetime of the PCDTBT:PC71BM OPV device. The devices were stored with an opaque Al cover in two different storage conditions in ambient and inert gas atmospheres. We observed that the performance of OPV devices dropped relatively fast for the first 7 days as seen in Figure 8.2 because the devices were taken out daily from their respective storage media environments for I-V measurements in the air. During the measurements, the devices were exposed to O_2, H_2O, and light more often. After 7 consecutive days of I-V measurements, the devices were taken out and characterized in the air periodically (every other 5 days), which significantly improved the stability of the devices. The device spin coated with a TiO_x was able to extend the lifetime of the device by 15 days as compared to the device without the TiO_x layer which was already dead after 3 days in the air. After 18 days, the efficiency of the device with the TiO_x layer stored in the air was too small (dead).

We also found that the device with a TiO_x layer was able to retain 84% of the initial device performance (PCE), while the device without the TiO_x layer lost almost 50% over 30 days of storage time in the N_2-filled atmosphere. We concluded that the TiO_x layer is significantly effective in extending both the lifetime and the retaining performance of the OPV device by approximately 300% over the device without the TiO_x layer. The internal study of the PCDTBT:PC71BM devices emphasizes the effectiveness of the TiO_x layer as an oxygen/water protection and as an oxygen scavenging agent in improving the lifetime and stability of OPV devices.

In the Case (II) stability study, we found that the Al cover was relatively effective in protecting the organic materials from degradation especially from light. The devices were fabricated with a TiO_x layer and stored with an opaque Al cover in two different storage conditions: in ambient and inert gas atmospheres. Figure 8.3 shows the percentage ratio of PCE of devices stored with and without an Al cover, and measured at different storage times. For the devices stored in the glove box, we observed that the performance of the device with an opaque Al cover was improved by 50% compared to the device without the Al cover.

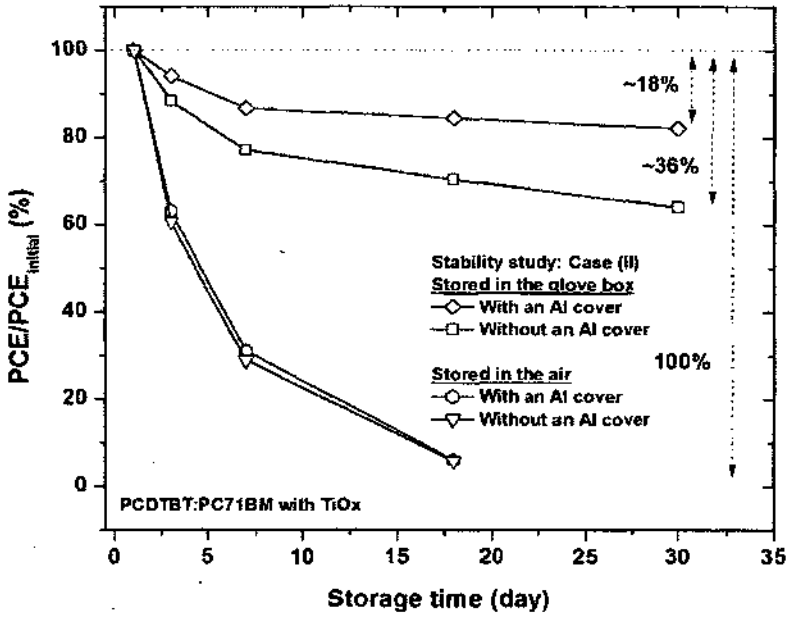

Figure 8.3: The stability study based on different stability conditions of low bandgap PCDTBT:PC71BM OPV cells stored with and without opaque Al covers (Case (II)) in the air and glove box atmospheres for 30 days. The devices were fabricated with a TiO_x layer.

The improvement in the lifetime is also attributed to the effectiveness of the TiO_x layer and the inert gas atmosphere in slowing down degradation. The OPV devices stored in the air, with and without an opaque Al cover, degraded at a relatively same degradation rate up to 18 days, but degraded faster than their counterparts stored in an

N_2-filled atmosphere. The reactions between O_2 and H_2O with the electrode and active layer were much stronger than the reactions between the electrode and active layer with light. The Al cover was not able to protect the device from the aggressive degradation due to O_2 and H_2O. Moreover, the devices were also not completely protected from the light, as they were characterized in the air and under an intense solar illuminator in a periodic basis.

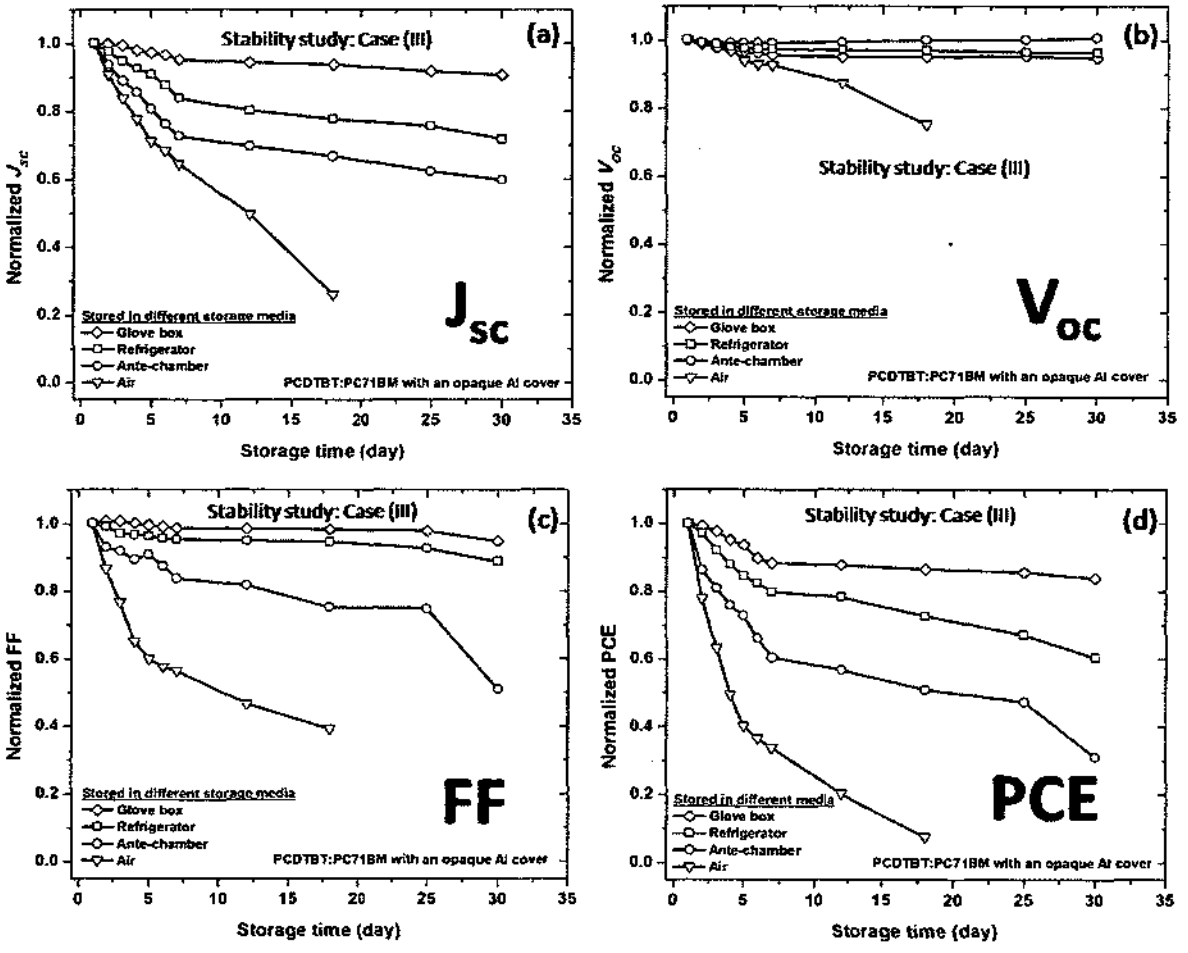

Figure 8.4: The change of normalized OPV parameters, (a) J_{SC}, (b) V_{OC}, (c) FF, and (d) PCE, of PCDTBT:PC71BM OPV cells fabricated with a TiO_x layer and stored with an opaque Al cover in different storage media : glove box (diamond), refrigerator (square), ante-chamber of a glove box (circle), and air (triangle) (Case (III)) for 30 days.

The final and last stability study was based on different storage media. The PCDTBT:PC71BM devices were fabricated with a TiO_x layer and stored with an opaque Al cover. We used different storage media: (1) air, (2) glove box, (3) ante-chamber of the glove box, and (4) refrigerator (Case (III)). As observed in the stability studies for Cases (I) and (II), the performance of OPV devices stored in different storage media environments also dropped relatively faster in the first 7 days compared to the later storage times because the devices were exposed to O_2, H_2O, and light more often during the I-V measurements. From the storage media study of the low bandgap OPV devices, we found that the N_2-filled atmosphere environment was the most optimum environment to store OPV devices and to keep them from degradation as seen in Figure 8.4. All data of parameters of OPV cells were normalized to the initial values of the cells. The values of OPV parameters reported in Figure 7.11 (Table D.2, D.4, D.8, and D.9) were used to produce the normalized data.

After 7 consecutive days of I-V characterizations, the devices were taken out and characterized in the air periodically (every other 5 days), which improved the stability of the devices. The PCE of the device stored in the glove box dropped only 16% after 30 days. The next optimum environment was the refrigerator maintained at low temperatures of 3 – 5 °C which was reported to be successful in slowing down degradation in the organic materials.

Figure 8.5 shows the percentage ratio of PCE of devices stored in different storage media conditions and measured at different storage times in the air. The performance of OPV devices was compared with the performance of the newly fabricated OPV devices in each condition. We observed that there was a "30% drop" rule as we studied the

performance of PCDTBT:PC71BM devices based on the different storage media conditions. The PCE value dropped the least (16%), when the device was stored in the glove box, dropped at a higher amount of 42% for the device stored in a refrigerator, and dropped at a rate of 75% for the device stored in an ante-chamber of the glove box. While the PCE of the device stored in the air dropped 100% after 18 days. We concluded that the N_2-filled atmosphere is the best storage media to keep OPV devices from degradation. And the degradation of the OPV device stored in the refrigerator was also relatively slow due to the low temperatures and dark storage environment. The devices stored in the ambient air and ante-chamber atmospheres degraded relatively fast due to the exposure to O_2 and H_2O.

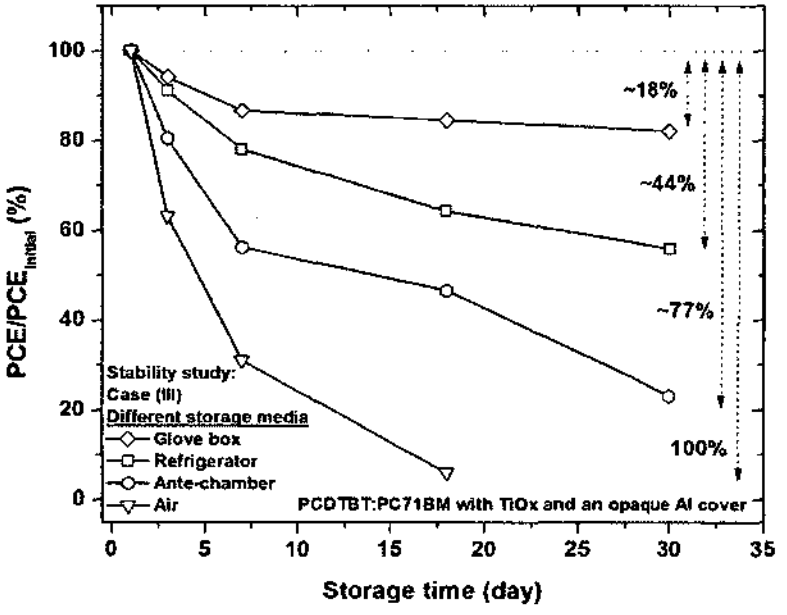

Figure 8.5: The stability study based on different storage media conditions of low bandgap PCDTBT:PC71BM OPV devices stored in the air, a glove box, an ante-chamber, and a refrigerator (Case (III)). The devices were fabricated with a TiO_x layer and stored with an opaque Al cover.

A highly stable OPV device was obtained by using a combination of the TiO_x layer as the protection layer and an Al cover stored in a N_2-filled atmosphere. The stability of the

OPV devices stored inside the inert atmosphere was improved because the inert (oxygen-free and moisture-free environment) conditions slow down degradation. The TiO_x layer acts as a diffusion barrier for oxygen which effectively further slows down the interaction between the oxygen with the active layer. From this study on stabilization of OPV devices with a TiO_x layer, we learned, (1) the device efficiency decreases with an increase in air and light exposure time, (2) a thin film of TiO_x layer on top of the active layer provides significant protection from degradation and (3) a higher rate of loss in cell efficiency for the devices without a TiO_x layer was noted when exposed to the combined effect of light and oxygen, as compared to other devices with a TiO_x layer. The incorporation of a solution based TiO_x layer into OPV devices is useful approach towards reducing the sensitivity of such devices to oxygen and water vapor. However, degradation still occurred for three reasons: (1) the organic materials decayed over time, (2) the fabrication was not performed in a dust-free manufactured environment, and (3) the characterization was performed in air.

Another important issue is the stability of the morphological donor/acceptor phase separation. The molecular order as well as the spatial dimensions of donor/acceptor demixing over a period of storage time can impact OPV performance [22]. Further phase separation observed at a longer storage time might lead to a spatial donor/acceptor distance exceeding the diffusion length of photogenerated excitons which results in loss of the photocurrent [132]. Progress in the encapsulation techniques in the OPV research is important in improving the stability of OPV devices, but the improvement in the morphological long-term stability is the key to OPV devices being competitive in the market.

We believe that the stability and lifetime of our OPV devices are relatively stable and excellent; although we cannot easily compare the stability of organic solar cells since its evaluation method is not standardized. This implies that the polycrystalline TiO_x plays an important role as the electron collection layer, the hole blocking layer, air stability, high performance, and as a long lifetime device. Minimizing exposure towards oxygen and water during processing should in principle contribute considerably to an increased lifetime of OPV cells. This can be achieved by working in a moisture free, inert atmosphere.

We suggest several approaches for future work in improving the stability of the OPV devices: (1) internal and (2) external approaches. The internal approach includes the use of newly developed donor and acceptor materials that improve the photon absorption in the near IR range, additional studies that optimize the solution based metal oxide interfacial layer such as ZnO_x and TiO_x to improve the photo catalytic properties by means of doping, the use additives to improve the solubility and the miscibility of the donor and acceptor materials, etc. The external approach includes the use of encapsulation techniques to protect the device from degradation. Another improvement would be in the fabrication and characterization conditions in the laboratory. Performing nanoscale multilayered BHJ OPV devices experiments in a non dust-free environment will introduce impurities into the OPV device. Small amounts of impurity, even one part in a thousand, in BHJ OPV cells can alter the electronic properties of the device. In addition, characterizing the OPV devices in the air assists in degradation due to exposure to oxygen and moisture which is proven to accelerate the deterioration of the organic materials and metal cathode oxidation.

In conclusion, we found that the TiO_x layer effectively improved the stability the OPV devices. The solution based TiO_x material is an excellent interfacial layer and a promising route in fabricating low cost and scalable long term stability in the OPV devices. The lifetime of organic solar cells is a very important topic for the commercialization of photovoltaic devices. We have demonstrated the application of the TiO_x protection layer internally in OPV cells. Our experimental results also show that the sol-gel derived TiO_x layer containing organic functionalities serves as an effective passivation layer for protection from oxygen when excited by photons, where the photo-oxidation of the bound organic moieties causes oxygen gas scavenging. However, degradation still occurs due to the imperfection of our processing, fabrication, and characterization conditions (some were performed in air which unfortunately introduced degradation issues) in our university laboratory. Multi-dimensional approaches must be performed in order to significantly improve the stability of OPV devices. Those approaches include the choice of internally smart materials (stable under storage, under sunlight, and under reduction or oxidation conditions); the use of effective purification methods; the choice of high glass-transition temperature (T_g) materials and structures (stable under outdoor cooling or heating); a water and oxygen free fabrication technique (for example, under a N_2-filled glove box, for instance), or encapsulation techniques, etc. In order to discover optimum performance, the stabilities need to be enhanced and must become the foci of research efforts in OPV devices.

REFERENCES

[1] United Nations Environment Program (UNEP), "Global Environment Outlook (GEO) – 2000", Earth-scan Publications Ltd., London (2000).

[2] J. Nelson, "The Physics of Solar Cells", 1st ed., Imperial College Press (2003).

[3] M.I. Hoffert, K. Caldeira, A.K. Jain, E.F. Haites, L.D.D. Harvey, S.D. Potter, M.E. Schlesinger, S.H. Schneider, R.G. Watts, T.M.L. Wigley, and D.J. Wuebbles, *Nature,* **395**, 881 (1998).

[4] M.A. Green, "Solar Cells: Operating Principles, Technology and System Applications", Kensington: The University of New South Wales (1998).

[5] H. Akamatsu, H. Inokuchi, and Y. Matsunaga, *Nature,* **173**, 168 (1954).

[6] C.W. Tang, *Appl. Phys. Lett.*, **48**, 183 (1986).

[7] The Nobel Prize in Chemistry 2000 was awarded jointly to Alan J. Heeger, Alan G. MacDiarmid and Hideki Shirakawa.

[8] M. Pope and C. E. Swenberg, "Electronic Processes in Organic Crystals and Polymers", Oxford University, Press, USA, 2nd edition (1999).

[9] T. Stubinger and W. Brutting, *J. Appl. Phys.,* **90,** 3632 (2001).

[10] National Renewable Energy Laboratory (2011).

[11] (a) M. Gratzel, *Inorg. Chem.*, **44**, 6841 (2005); (b) Y. Chiba, A. Islam, Y. Watanabe, R. Komiya, N. Koide, and L. Han, *Japanese J. Appl. Phys.*, **45**, 638 (2006).

[12] (a) M.C. Scharber, D. Muhlbacher, M. Koppe, P. Denk, C. Waldauf, A.J. Heeger, and C.J. Brabec, *Adv. Mater.*, **18**, 789 (2006); (b) J. You, L. Dou, K. Yoshimura, T. Kato, K. Ohya, T. Moriarty, K. Emery, C.-C. Chen, J. Gao, G. Li, and Y. Yang, *Nat. Comm.*, DOI: 10.1038/ncomms2411, 1 (2013).

[13] D.W. Zhao, X.W. Sun, C.Y. Jiang, A.K.K. Kyaw, G.Q. Lo, and D.L. Kwong, *Appl. Phys. Lett.*, **93**, 083305 (2008).

[14] T. Jeranko, H. Tributsch, N.S. Sariciftci, and J.C. Hummelen, *Sol. Energy Mater. Sol. Cells*, **83**, 247 (2004).

[15] H. Neugebauer, C.J. Brabec, J.C. Hummelen, and N.S. Sariciftci, *Sol. Energy Mater. Sol. Cells*, **61**, 35 (2000).

[16] F.C. Krebs, J.E. Carlé, N. Cruys-Bagger, M. Andersen, M.R. Lilliedal, M.A. Hammond, and S. Hvidt, *Sol. Energy Mater. Sol. Cells*, **86**, 499 (2005).

[17] M.O. Reese, A.J. Morfa, M.S. White, N. Kopidakis, S.E. Shaheen, G. Rumbles, and D.S. Ginley, *Sol. Energy Mater. Sol. Cells*, **92**, 746 (2008).

[18] K. Lee, J.Y. Kim, S.H. Park, S.H. Kim, S. Cho, and A.J. Heeger, *Adv. Mater.*, **19**, 2445 (2007).

[19] S. Wakim, S. Beaupré, N. Blouin, B.-R. Aich, S. Rodman, R. Gaudiana, Y. Tao, and M. Leclerc, *J. Mater. Chem.*, **19**, 5351 (2009).

[20] T.M. Clarke and J.R. Durrant, *Chem. Rev.*, **110**, 6736 (2010).

[21] S.R. Cowan, A. Roy, and A.J. Heeger, *Phys. Rev. B*, **82**, 245207 (2010).

[22] M. Jørgensen, K. Norrman, and F.C. Krebs, *Sol. Energy Mater. Sol. Cells*, **92**, 686 (2008).

[23] J. Jo, S. Kim, S. Na, B. Yu, and D. Kim, *Adv. Funct. Mater.*, **19**, 866 (2009).

[24] B. Ray and M.A. Alam, *Appl. Phys. Lett.*, **99**, 033303 (2011).

[25] K. Kawano, R. Pacios, D. Poplavskyy, J. Nelson, D.D.C. Bradley, and J.R. Durrant, *Sol. Energy Mater. Sol. Cells*, **90**, 3520 (2006).

[26] M. Wohlers, H. Werner, D. Herein, T. Schedel-Niedrig, A. Bauer, and R. Schlögl, *Synth. Met.*, **77**, 299 (1996).

[27] A. Tapponnier, I. Biaggio, and P. Günter, *Appl. Phys. Lett.*, **86**, 112114 (2005).

[28] G. Koller, R.I.R. Blyth, S.A. Sardar, F.P. Netzer, and M.G. Ramsey, *Appl. Phys. Lett.*, **76**, 927 (2000).

[29] K. Seki, N. Hayashi, H. Oji, E. Ito, Y. Ouchi, and H. Ishii, *Thin Solid Films*, **393**, 298 (2001).

[30] P. Dannetun, M. Boman, S. Stafstrom, W.R. Salaneck, R. Lazzaroni, C. Fredriksson, J.L. Bredas, R. Zamboni, and C. Taliani, *J. Chem. Phys.*, **99**, 664 (1993).

[31] J. Kim, J.-S. Kim, S.-W. Kwak, J.-S. Yu, Y. Jang, J. Jo, T.-M. Lee, and I. Kim, *Appl. Phys. Lett.*, **101**, 213304 (2012).

[32] K. Norrman, N.B. Larsen, and F.C. Krebs, *Sol. Energy Mater. Sol. Cells*, **90**, 2793 (2006).

[33] Y.J. Suh, S.Y. Park, T.H. Lee, W.S. Chung, K.K. Kim, and M.J. Kim, *Microsc. Microanal.*, **16** (Suppl. 2), 1378 (2010).

[34] G. Li, V. Shrotriya, J. Huang, Y. Yao, T. Moriarty, K. Emery, and Y. Yang, *Nat. Mater.*, **4**, 864 (2004).

[35] Y.-H. Kim, S.-H. Lee, J. Noh, and S.-H. Tan, *Thin Solid Films*, **510**, 305 (2006).

[36] C. Ionescu-Zanetti, A. Mechler, S.A. Carter, and R. Lal, *Adv. Mater.*, **16**, 385 (2004).

[37] J.C Wang, W.T. Weng, M.Y. Tsai, M.K. Lee, S.F. Hong, T.P. Peng, C.C. Kei, C.C. Yu, and H.F. Meng, *J. Mater. Chem.*, **20**, 862 (2010).

[38] M.P. de Jong, L.J. van Ijzendoorn, and M.J.A. de Voigt, *Appl. Phys. Lett.*, **77**, 2255 (2000).

[39] The material information is available from The Heraeus Company's website.

[40] C. Waldauf, M. Morana, P. Denk, P. Schilinsky, K. Coakley, S.A. Choulis, and C.J. Brabec, *Appl. Phys. Lett.*, **89**, 233517 (2006).

[41] G. Li, C.-W. Chu, V. Shrotriya, J. Huang, and Y. Yang, *Appl. Phys. Lett.*, **88**, 253503 (2006).

[42] H. Schmidt, F. Flugge, T. Winkler, T. Bulow, T. Riedl, and W. Kowalsky, *Appl. Phys. Lett.*, **94**, 243302 (2009).

[43] Z. Xu, L.M. Chen, G. Yang, C.H. Huang, J. Hou, Y. Wu, G. Li, C.H. Hsu, and Y. Yang, *Adv. Funct. Mater.*, **19**, 1 (2009).

[44] M.D. Irwin, D.B. Buchholz, A.W. Hains, R.P.H. Chang, and T.J. Marks, *Proc. Natl. Acad. Sci. U.S.A.*, **105**, 2783 (2008).

[45] D.E. Gallardo, C. Bertoni, S. Dunn, N. Gaponik, and A. Eychmuller, *Adv. Mater.*, **19**, 3364 (2007).

[46] S.K. Hau, H.-L. Yip, O. Acton, N.S. Baek , H. Ma, and A.K.-Y. Jen, ***J. Mater. Chem.***, **18**, 5113 (2008).

[47] M.S. White, D.C. Olson, S.E. Shaheen, N. Kopidakis, and D.S. Ginley, *Appl. Phys. Lett.*, **89**, 143517 (2006).

[48] W.J. Potscavage, S. Yoo, B. Domercq, and B. Kippelen, *Appl. Phys. Lett.*, **90**, 253511 (2007).

[49] N. Kim, W.J. Potscavage, B. Domercq, B. Kippelen, and S. Graham, *Appl. Phys. Lett.*, **94**, 163308 (2009).

[50] C.-Y. Chang, C.-T. Chou, Y.-J. Lee, M.-J. Chen, and F.-Y. Tsai, *Org. Electron.*, **10**, 1300 (2009).

[51] C. Lungenschmied, G. Dennler, H. Neugebauer, S.N. Sariciftci, M. Glatthaar, T. Meyer, and A. Meyer, *Sol. Energy Mater. Sol. Cells*, **91**, 379 (2007).

[52] R. Steim, F. Kogler, and C.J. Brabec, *J. Mater. Chem.*, **20**, 2499 (2010).

[53] J.H. Lee, S. Cho, A. Roy, H.-T. Jung, and A.J. Heeger, *Appl. Phys. Lett.*, **96**, 163303 (2010).

[54] D.W. Zhao, P. Liu, X.W. Sun, S.T. Tan, L. Ke, and A.K.K. Kyaw, *Appl. Phys. Lett.*, **95**, 153304 (2009).

[55] N.N. Greenwood and A. Earnshaw, "Chemistry of the Elements" Butterworth-Heinemann, Oxford (1997).

[56] The DuPont™ Company, "Ti-Pure® Titanium Oxide: Titanium Oxide for Coating" (2007).

[57] S.L. Pugh and J.T. Guthrie, *Dyes Pigments*, **55**, 109 (2002).

[58] T. Corralles, C. Peinado, N.S. Allen, M. Edge, G. Sandoval, and F. Catalina, *J. Photochem. Photobiol. A: Chem.*, **156**, 151 (2003).

[59] Y. Kubota, C. Niwa, T. Ohnuma, Y. Ohko, T. Tatsuma, T. Mori, and A. Fujishima, *J. Photochem. Photobiol. A: Chem.*, **141**, 225 (2001).

[60] L.G. Philips and D.M. Barbano, *J. Diary Sci.*, **80**, 2726 (1997).

[61] V.A. Schwaz, S.D. Klein, R. Hornung, R. Knochenmuss, P. Wyss, and D. Fink, *Lasers Surg. Med.*, **29**, 252 (2001).

[62] O. Carp, C.L. Huisman, and A. Reller, *Prog. Sol. State Chem.*, **32**, 33 (2004).

[63] R.M. Alberci and W.F. Jardim, *Appl. Catal. B: Environ.*, **14**, 55 (1997).

[64] K.J. Hadjiivanov and D.G. Kissurski, *Chem. Soc. Rev.*, **25**, 61 (1996).

[65] D. Chen and A.K. Ray, *Chem. Eng. Sci.*, **56**, 1561 (2001).

[66] H.A. Macleod, "Thin Film Optical Filters", MacMillan, New York, 2nd Edn., p.370 (1986).

[67] A. Fujishima and K. Honda, *Nature*, **238**, 37 (1972).

[68] A.L. Linsebigler, G. Lu, and J.T. Yates, Jr., *Chem. Rev.*, **95**, 735 (1995).

[69] V.E. Henrich and P.A. Cox, "The Surface Science of Metal Oxides", Cambridge University Press, Cambridge (1994).

[70] C. Noguera, "Physics and Chemistry of Oxide Surfaces", Cambridge University Press, Cambridge (1996).

[71] B. O'Regan and M. Grätzel, *Nature*, **353**, 737 (1991).

[72] U. Bach, D. Lupo, P. Comte, J.E. Moser, F. Weissörtel, J. Salbeck, H. Spreitzer, and M. Grätzel, *Nature*, **395**, 583 (1998).

[73] A.J. Breeze, Z. Schlesinger, S.A. Carter, and P.J. Brock, *Phys. Rev. B*, **64**, 125205 (2001).

[74] P.A. van Hal, M.M. Wienk, J.M. Kroon, W.J.H. Verhees, L.H. Slooff, W.J.H. van Gennip, P. Jonkheijm, and R.A.J. Janssen, *Adv. Mater.*, **15**, 118 (2003).

[75] H. Hansel, H. Zettl, G. Krausch, R. Kisselev, M. Thelakkat, and H.W. Schmidt, *Adv. Mater.*, **15**, 2056 (2003).

[76] M. Thelakkat, C. Schmitz, and H.-W. Schmidt, *Adv. Mater.*, **14**, 577 (2002).

[77] J.Y. Kim, S.H. Kim, H.-H. Lee, K. Lee, W. Ma, X. Gong, and A.J. Heeger, *Adv. Mater.*, **18**, 572 (2006).

[78] U. Diebold, *Surf. Sci. Rep.*, **48**, 53 (2003).

[79] M. Gratzel, *Nature*, **414**, 338 (2001).

[80] S.H. Kim, J.Y. Kim, S.H. Park, and K. Lee, *Proc. SPIE-Int. Soc. Opt. Eng.*, **5937**, 59371G1 (2005).

[81] D.H. Wang, S.H. Im, H.K. Lee, O.O. Park, and J.H. Park, *J. Phys. Chem. C*, **113**, 17268 (2009).

[82] C.J. Ko, Y.K. Lin, F.C. Chen, and C.W. Chu, *Appl. Phys. Lett.*, **90**, 063509 (2007).

[83] H.J. Snaith, N.C. Greenham, and R.H. Friend, *Adv. Mater.*, **16**, 1640 (2004).

[84] S.H. Park, A. Roy, S. Beaupre, S. Cho, N. Coates, J.S. Moon, D. Moses, M. Leclerc, K. Lee, and A.J. Heeger, *Nat. Photonics*, **3**, 297 (2009).

[85] A. Roy, S.H. Park, S. Cowan, M.H. Tong, S. Cho, K. Lee, and A.J. Heeger, *Appl. Phys. Lett.*, **95**, 013302 (2009).

[86] E.A. Katz, S. Gevorgyan, M.S. Orynbayev, and F.C. Krebs, *Eur. Phys. J. Appl. Phys.*, **36**, 307 (2006).

[87] J.K. Lee, N.E. Coates, S. Cho, N.S. Cho, D. Moses, G.C. Bazan, K. Lee, and A.J. Heeger, *Appl. Phys. Lett.*, **92**, 243308 (2008).

[88] S. Cho, K. Lee, and A.J. Heeger, *Adv. Mater.*, **21**, 1941 (2009).

[89] P. Boland, Jr., Dissertation, Old Dominion University (2012).

[90] J. Kim, G. Kim, Y. Choi, J. Lee, S.H. Park, and K. Lee, *J. Appl. Phys.*, **111**, 114511 (2012).

[91] M. Kallala, C. Sanchez, and B. Cabane, *Phys. Rev. E*, 48, 3692 (1993).

[92] O. Bikondoa, C.L. Pang, R. Ithnin, C.A. Muryn, H. Onishi, and G. Thornton, *Nat. Mater.*, 5, 189 (2006).

[93] L.-M. Chen, Z. Hong, G. Li, and Y. Yang, *Adv. Mater.*, **21**, 1434 (2009).

[94] J. Peet, M. L. Senatore, A. J. Heeger, and G.C. Bazan, *Adv. Mater.*, **21**, 1521 (2009).

[95] Private discussion with Dr. H. Baumgart (2013).

[96] S. Marchaut and P.J.S. Foot, *Polymer*, **38**, 1749 (1997).

[97] S. Hugger, R. Thomann, T. Heizel, and T. Thurn-Albiecht, *Colloid Polym. Sci.*, **282**, 932 (2004).

[98] X. Yang, J. Loos, S.C. Veenstra, W.J.H. Verhees, M.M. Wienk, J.M. Kroon, M.A.J. Michels, and R.A.J. Janssen, *Nano Lett.*, **5**, 579 (2005).

[99] H. Kim, W.-W. So and S.-J. Moon, *J. Korean Phys. Soc.*, **48**, 441, (2006).

[100] V. D. Mihailetchi, H. Xie, B. de Boer, L. J. A. Koster, and P.W. M. Blom, *Adv. Funct. Mater.*, **16**, 699 (2006).

[101] W. Ma, C. Yang, X. Gong, K. Lee, and A.J. Heeger, *Adv. Funct. Mater.*, **15** ,1617 (2005).

[102] J. Clark, C. Silva, R.H. Friend, and F.C. Spano, *Phys. Rev. Lett.*, **98**, 206406 (2007).

[103] G. Li, V. Shrotriya, Y. Yao, and Y. Yang, *J. Appl. Phys.*, **98**, 043704 (2005).

[104] H.Z. Yu, *Synth. Met.*, **160**, 2505 (2010).

[105] C. Muller, T.A.M. Ferenczi, M. Campoy-Quiles, J.M. Frost, D.D.C. Bradley, P. Smith, N. Stingelin-Stutzmann, and J. Nelson, *Adv. Mater.*, **20,** 3510 (2008).

[106] C.J. Brabec, S.E. Shaheen, T. Fromherz, F. Padinger, J.C. Hummelen, A. Dhanabalan, R.A.J. Janssen, and N. S. Sariciftci, *Synth. Met.*, **121**, 1517 (2001).

[107] J. Nelson, *Phys. Rev. B*, **67**, 155209 (2003).

[108] J. M. J. Frechet and B. C. Thompson, *Angew. Chem. Int. Ed.*, **47**, 58 (2008).

[109] T. Erb, U. Zhokhavets, G. Gobsch, R. Raleva, B. Stuhn, P. Schilinsky, C. Waldauf, and C.J. Brabec, *Adv. Funct. Mater.*, **15**, 1193 (2005).

[110] Y. Zhao, Z. Xie, Y. Qu, Y. Geng, and L. Wang, *Appl. Phys. Lett.*, **90**, 043504 (2007).

[111] F. Padinger, R.S. Rittberger, and N.S. Sariciftci, *Adv. Funct. Mater.*, **13**, 85 (2003).

[112] S.J. Yoon, J.H. Park, H.K. Lee, and O.O. Park, *Appl. Phys. Lett.*, **92**, 143504 (2008).

[113] J. Nelson, J. Kirkpatrick, and P. Ravirajan, *Phys. Rev. B*, **69**, 035337 (2004).

[114] C. Yang, J.G. Hu, and A.J. Heeger, *J. Am. Chem. Soc.*, **128**, 12007 (2006).

[115] N. Blouin, A. Michaud, and M. Leclerc, *Adv. Mater.*, **19**, 2295 (2007).

[116] G. Lu, L. Li, and X. Yang, *Small*, **4**, 601 (2008).

[117] G. Kalita, M. Masahiro, W. Koichi, and M. Umeno, *Solid-State Electron.*, **54**, 447 (2010).

[118] A.J. Heeger, S. Kivelson, J.R. Schrieffer, and W.-P. Su, *Rev. Mod. Phys.*, **60,** 781 (1988).

[119] M. Svensson, F. Zhang, S.C. Veenstra, W.J.H. Verhees, J.C. Hummelen, J.M. Kroon, O. Inganas, and M.R. Andersson, *Adv. Mater.* (Weinheim, Ger.), **15,** 988 (2003).

[120] K.G. Jespersen, W. Beenken, Y. Zaushitsyn, A. Yartse, M. Anderson, T. Pullerits, and V. Sundstrom, *J. Chem. Phys.*, **121**, 12613 (2004).

[121] N. Blouin, A. Michaud, D. Gendron, S. Wakim, E. Blair, R. Neagu-Plesu, M. Belletete, G. Durocher, Y. Tao, and M. Leclerc, *J. Am. Chem. Soc.*, **130**, 732 (2008).

[122] S. Cho, J.H. Seo, S.H. Park, S. Beaupre, M. Leclerc, and A.J. Heeger, *Adv. Mater.*, **22**, 1253 (2010).

[123] J.H. Kim, J.H. Park, J.H. Lee, J.S. Kim, M. Sim, C. Shim, and K. Cho, *J. Mater. Chem.*, **20**, 7398 (2010).

[124] J.S. Kim, J.H. Lee, J.H. Park, C. Shim, M. Sim, and K. Cho, *Adv. Funct. Mater.*, **21**, 480 (2011).

[125] D. Watters, J. Kinsley, H. Yi, T. Wang, A. Iraqi, and D. Lidzey, *Org. Electron.*, **13**, 1401 (2012).

[126] L. Huo, J. Hou, S. Zhang, H.-Y. Chen, and Y. Yang, *Angew. Chem. Int. Ed.*, **49**, 1500 (2010).

[127] S.R. Cowan, R.A. Street, S. Cho, and A.J. Heeger, *Phys. Rev. B*, **83**, 035205 (2011).

[128] S.-P. Yang, W.-G. Kong, B.-Y. Liu, W.-Y. Zheng, B.-M. Li, X.-H. Liu, and G.-S. Fu, *Chin. Phys. Lett.*, **28**, 128401 (2011).

[129] J. H. Seo, H. Kim, and S. Cho, *Phys. Chem. Chem. Phys.*, **14**, 4062 (2012).

[130] C. Shim, M. Kim, S.-G. Ihn, Y.S. Choi, Y. Kim, and K. Cho, *Chem. Comm.*, **48**, 7206 (2012).

[131] T. Wang, A.J. Pearson, A.D.F. Dunbar, P.A. Staniec, D.C. Watters, H. Yi, A.J. Ryan, R.A.L. Jones, A. Iraqi, and D.G. Lidzey, *Adv. Funct. Mater.*, **22**, 1399 (2012).

[132] T.-Y. Chu, S. Alem, S.-W. Tsang, S.-C. Tse, S. Wakim, J. Lu, G. Dennler, D. Waller, R. Gaudiana, and Y. Tao, *Appl. Phys. Lett.*, **98**, 253301 (2011).

[133] L. Chang, H.W.A. Lademann, J.-B. Bonekamp, K. Meerholz, and A.J. Moulé, *Adv. Funct. Mater.*, **21**, 1779 (2011).

[134] S. Schuller, P. Schilinsky, J. Hauch, and C.J. Brabec, *Appl. Phys. A*, **79**, 37 (2004).

[135] L.J.A. Koster, V.D. Mihailetchi, and P.W.M. Blom, *Appl. Phys. Lett.*, **88**, 052104 (2006).

[136] F.C. Krebs and K. Norrman, *Prog. Photovolt: Res. Appl.*, **15**, 697 (2007).

[137] J.A. Hauch, P. Schilinsky, S.A. Choulis, R. Childers, M. Biele, and C.J. Brabec, *Sol. Energy Mater. Sol. Cells*, **92**,727 (2008).

[138] S.A. Gevorgyan and F.C. Krebs, *Chem. Mater.*, **20**, 4386 (2008).

[139] M.T. Lloyd, D.C. Olson, P. Lu, E. Fang, D.L. Moore, M.S. White, M.O. Reese, D.S. Ginley, and J.W.P. Hsu, *J. Mater. Chem.*, **19**, 7638 (2009).

[140] M.O. Reese, A.M. Nardes, B.L. Rupert, R.E. Larsen, D.C. Olson, M.T. Lloyd, S.E. Shaheen, D.S. Ginley, G. Rumbles, and N. Kopidakis, *Adv. Funct. Mater.*, **20**, 3476 (2010).

[141] R. Friend, R. Gymer, A. Holmes, J. Burroughes, R. Marks, C. Taliani, D. Bradley, D. Dos Santos, J. Bredas, M. Logdlund, and W. Salaneck, *Nature*, **397**, 121 (1999).

[142] T.-Y. Chu, S. Alem, P.G. Verly, S. Wakim, J. Lu, Y. Tao, S. Beaupré, M. Leclerc, F. Bélanger, D. Désilets, S. Rodman, D. Waller, and R. Gaudiana, *Appl. Phys. Lett.*, **95**, 063304 (2009).

[143] A. Bauer, T. Wahl, J. Hanisch, and E. Ahlswede, *Appl. Phys. Lett.*, **100**, 073307 (2012).

[144] J. Li, S. Kim, S. Edington, J. Nedy, S. Cho, K. Lee, A.J. Heeger, M.C. Gupta, and J.T. Yates Jr., *Sol. Energy Mater. Sol. Cells*, **95**, 1123 (2011).

[145] J. Schafferhans, A. Baumann, A. Wagenpfahl, C. Deibel, and V. Dyakonov, *Org. Electron.*, **11**, 1693 (2010).

[146] B. Liu, R.-Q Peng, L.-H. Zhao, L.-L. Chua, R.H. Friend, and P.K.H. Ho, *Nat. Comm.*, **3**, 1321 (2012).

[147] K. Norrman, S.A. Gevorgyan, and F.C. Krebs, *ACS Appl. Mater. Interfaces*, **1**, 102 (2009).

[148] R. Pacios, A.J. Chatten, K. Kawano, J.R. Durrant, D.D.C. Bradley, and J. Nelson, *Adv. Funct. Mater.*, **16**, 2117 (2006).

[149] A. Hayakawa, O. Yoshikawa, T. Fujieda, K. Uehara, and S. Yoshikawa, *Appl. Phys. Lett.*, **90**, 163517 (2007).

[150] A. Gadisa, M. Svensson, M.R. Andersson, and O. Inganas, *Appl. Phys. Lett.*, **84,** 1609 (2004).

[151] J.L. Brédas, D. Beljonne, V. Coropceanu, and J. Cornil, *Chem. Rev.*, **104**, 4917 (2004).

[152] C. Piliego, T.W. Holcombe, J.D. Douglas, C.H. Woo, P.M. Beaujuge, and J.M.J. Fréchet, *J. Am. Chem. Soc.*, **132**, 7595 (2010).

[153] Z.M. Beiley, E.T. Hoke, R. Noriega, J. Dacuña, G.F. Burkhard, J.A. Bartelt, A. Salleo, M.F. Toney, and M.D. McGehee, *Adv. Energy Mater.*, **1**, 954 (2011).

[154] C.H. Peters, I.T. Sachs-Quintana, W.R. Mateker, T. Heumueller, J. Rivnay, R. Noriega, Z.M. Beiley, E.T. Hoke, A. Salleo, and M.D. McGehee, *Adv. Mater.*, **24**, 663 (2012).

[155] H. Neugebauer, C.J. Brabec, J.C. Hummelen, and N.S. Sariciftci, *Sol. Energy Mater. Sol. Cells*, **61**, 35 (2000).

[156] C. Noguera, "Physics and Chemistry of Oxide Surfaces", Cambridge University Press, Cambridge (1996).

[157] K. Norrman and F.C. Krebs, *Sol. Energy Mater. Sol. Cells*, **90**, 213 (2006).

[158] J. Schafferhans, A. Baumann, C. Deibel, and V. Dyakonov, *Appl. Phys. Lett.*, **93**, 093303 (2008).

[159] M.S.A. Abdou, F.P. Orfino, Y. Son, and S. Holdcroft, *J. Am. Chem. Soc.*, **119**, 4518 (1997).

[160] R.W. Lof, M.A van Veenendaal, B. Koopmans, H.T. Jonkman, and G.A. Sawatzky, *Phys. Rev. Lett.*, **68**, 3924 (1992).

[161] A.T. Ram, *Polym. Degrad. Stability*, **29**, 3 (1990).

[162] M. Edge. N.S. Allen, T.S. Jewitt, and C.V. Horie, *Polymer Degrad. Stability*, **25**, 345 (1989).

[163] C.J. Brabec, S. Gowrisanker, J.J.M. Halls, D. Laird, S.J. Jia, and S.P. Williams, *Adv. Mater.*, **22**, 3839 (2010).

APPENDIX A

Materials Preparation and Fabrication OPV Devices

A.1. Preparation of ITO substrates

In OPV devices, the most commonly used anode which is pre-coated on glass, is indium tin oxide (ITO). ITO is a composite solid thin film of indium oxide (In_2O_3) and tin oxide (SnO_2), typically 90% In_2O_3, 10% SnO_2 by weight. In our experiment, an excellent quality of ITO thin film was used. This ITO glass film has a high transmittance (~ 90%) and a low sheet resistance (10 – 15 Ω/□) and was purchased from NanoCS [1]. The low sheet resistance of electrode materials is essential to transport the photogenerated carriers with little loss. The thickness of the ITO thin film was about 100 nm. Two parallel strips of high electrical performance polyimide tape of 6.35 mm wide [2] were used to mask and protect the ITO thin film from the acidic nature of the etching solution. Subsequently, the polymide tape was rubbed with a gentle pressure to make sure that the tape adhered well on the ITO glass substrate. A conventional mixture solution of 5% of nitric acid (HNO_3), 20% of hydrochloric acid (HCl), and 75% of de-ionized (DI) water (with a high resistivity of 18.2 MΩ.cm) was used as the wet etching solution in order to remove the exposed ITO films. The wet etching process was conducted at a temperature of 80 ^{o}C for 60 – 90 s inside a fume hood environment.

Prior to depositing the solution of organic materials on the patterned ITO glass substrate, a thorough cleaning of the substrate is mandatory to remove any native surface

impurities or residual tape on the substrates. The substrate was cleaned for 10 min in an aqueous Mucasol® solution with a concentration of 3% in an ultrasonic bath. Subsequently it was cleaned in multi step ultrasonic bath process using various solvents, in the following order: (1) DI water, (2) isopropanol, and (3) acetone. Each solvent was pre-heated at temperature of 60 °C. The substrate was then rinsed with the DI water, and it was dried up by using a N_2-gun. Finally, it was annealed on a hot plate at a temperature of 100 °C for 10 min to remove any residual moisture inside a N_2-filled glove box environment (O_2, H_2O < 0.1 ppm).

A.2. Preparation of active solutions

We used two separate active solutions in our experiment. First, a blend solution of poly(3-hexylthiophene) or P3HT and [6,6]-phenyl-C_{61}-butyric acid methyl ester or PC61BM. P3HT (4002-EE with regio-regularity of 91 – 94%) purchased from Rieke Metals, Inc. and PC61BM from Nano-C. The active layer composition was fixed to a P3HT:PC61BM weight ratio of 1:0.8 [3,4,5,6]. A combination of 30 mg of P3HT and 24 mg of PC61BM was dissolved in 2 ml of chlorobenzene (C_6H_5Cl) or CB and stirred at a low speed of 100 rpm at 50 °C in a N_2-filled glove box (O_2, H_2O < 0.1 ppm) overnight. During the stirring process, the vial containing the blend of P3HT:PC61BM solution was covered with aluminum foil to protect organic solutions from photodegradation caused by light [7]. All materials were used as received. Figure A.1(a) shows the active solution of P3HT:PC61BM.

Second, a blend active solution of poly([9-(1-octylnonyl)-9H-carbazole-2,7-diyl]-2,5-thiophenediyl-2,1,3-benzothiadiazole-4,7-diyl-2, 5-thio-phenediyl) or PCDTBT from 1-

Material Company and [6,6]-phenyl-C_{71}-butyric acid methyl ester or PC71BM from Nano-C. Unlike its high bandgap counterpart, the weight ratio of PCDTBT and PC71BM used was 1:4 [8,9,10,11]. A mixture of 7 mg of PCDTBT and 28 mg of PC71BM dissolved in 2 ml of 1,2-dichlorobenzene ($C_6H_4Cl_2$) or DCB was prepared. The blend solution of PCDTBT:PC71BM was stirred at a higher speed of 250 rpm and at 120 °C for a much longer period and protected from light inside a N_2-filled glove box atmosphere (O_2, H_2O < 0.1 ppm). All materials were used as received. Figure A.1(b) shows the active solution of PCDTBT:PC71BM.

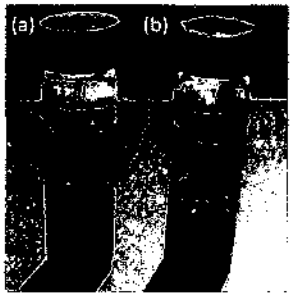

Figure A.1: Vials with active solutions of (a) P3HT:PC61BM (yellowish color) and (b) PCDTBT:PC71BM (reddish color).

A3. Fabrication diagrams

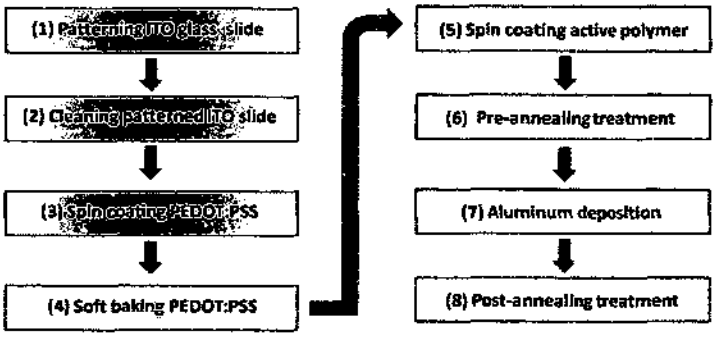

Figure A.2: A schematic diagram of fabricating an OPV device without the TiO_x layer.

Since two types of OPV devices, with and without solution-based TiO_x, were fabricated, we developed two different fabrication diagrams. The first diagram is shown in Figure A.2. The diagram is color coded to identify where the processes take place. The green color is for a process taking place in the air (a controlled fume hood environment), the orange color is for a process taking place in a N_2-filled glove box (O_2, H_2O < 0.1 ppm), and the gray color is for the metallization process under a vacuum environment (~2.0×10^{-7} Torr) inside the electron beam evaporator chamber.

While OPV cells with a solution-based TiO_x interfacial layer required additional processes, there was a longer fabrication time. The fabrication diagram for this particular OPV is shown in Figure A.3. The additional processes are related to the TiO_x interfacial layer treatments which are the spin coating and the drying of the TiO_x layer in the air. The main purpose of the drying process is to convert the solution-based TiO_2 precursor into a TiO_x layer [12]. Different drying TiO_x solution conditions at (1) a room temperature of 25 °C for 60 min [13], (2) 80 °C for 10 min [10,14], and (3) 90 °C for 10 min [15] in the air, have been reported. The main potential drawback of the thermal treatment is that active organic materials will be damaged at high temperatures.

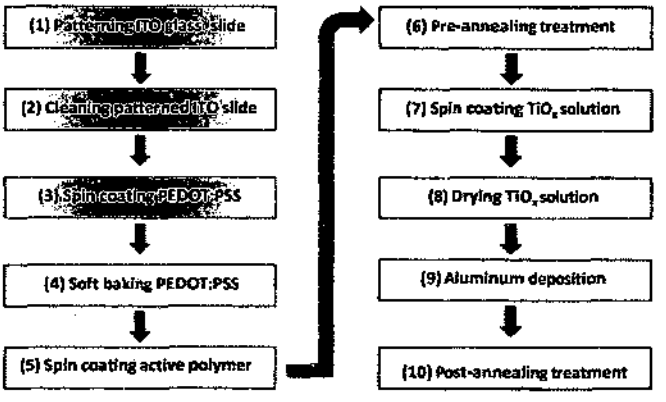

Figure A.3: A schematic diagram of fabricating an OPV device with the TiO_x layer.

A4. Application of the PEDOT:PSS solution

The poly(3,4-ethylene dioxythiophene):poly(styrene sulfonate) or PEDOT:PSS, having a Fermi level of -5.0 eV, has an advantage in contacting polymers with a wide range of HOMO levels. In our experiment, an electronic grade of PEDOT:PSS was deposited onto a patterned ITO substrate by using a spin coating technique. This process took place in air and the spin coater equipment (a vacuum controlled system) used was manufactured by Laurell®. The PEDOT:PSS (Clevios® P VP Al 4083) was purchased from Heraeus. The PEDOT:PSS was spun onto the patterned ITO substrate for 3 min at an optimal velocity of 3000 rpm and a ramp speed of 500 rpm/s. Figure A.4 shows the spin coating set up for PEDOT:PSS. After the PEDOT:PSS solution was deposited on the front side of the substrate, the backside of the substrate was cleaned by using a Q-tip dipped with acetone. To get rid of any moisture on the film and to increase the conductivity of the PEDOT:PSS [16], the substrate was annealed at 100 °C for 10 min in a N_2-filled glove box (O_2, H_2O < 0.1 ppm).

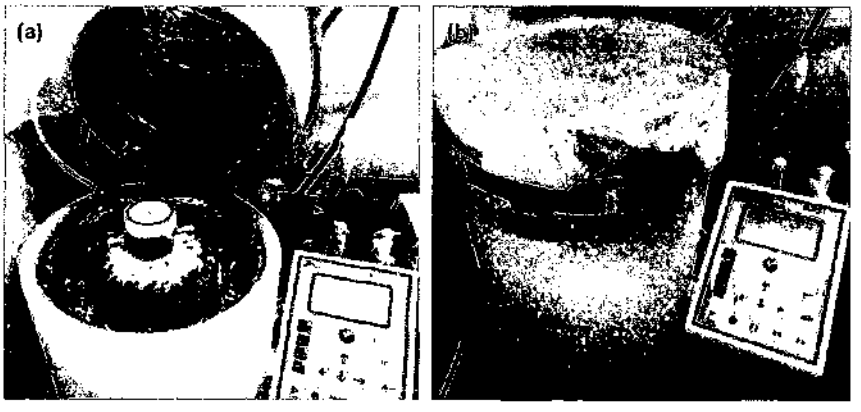

Figure A.4: Spin coater set ups: (a) Prior to spin coating the PEDOT:PSS and (b) during the spin coating process (Al foils protect the PEDOT:PSS layer from the light).

A.5. Application of the active solutions

Prior to use, the blend organic solution of P3HT:PC61BM was run through a 0.45 μm PTFE filter, while the PCDTBT:PC71BM solution was used without a filter. Then the photoactive solution was deposited on the substrate by using a special mechanical spin coater, SPIN150® as shown in Figure A.5, inside the N_2-filled glove box (O_2, H_2O < 0.1 ppm). Several optimization steps and tests were performed to optimize the use of the SPIN150® mechanical coater since the substrate was placed on the holding stopper without any vacuum system as in a typical spin coater system. After the active layer has been deposited, the anode area was cleaned to expose the ITO anode, and the backside was cleaned of any organic solution excesses with Q-tip dipped in acetone. Prior to the metal contact deposition using an electron beam evaporating system, the pre-cleaned OPV substrate was kept inside the ante-chamber of the glove box to allow any residual solvent to degas. The thickness of the active layer was varied and optimized to achieve the best power conversion efficiency (PCE).

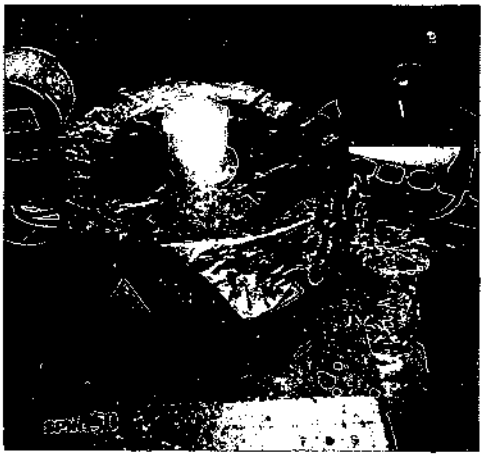

Figure A.5: A SPIN150® mechanical spin coater unit (the lid covered by the Al foil to protect the active layer from the light).

A.6. Application of the Al metal cathode

In general, there are three steps in an *e*-beam evaporation process; (1) the evaporation of the source material, (2) the transportation of evaporant from the source to the substrate (item to be coated), and (3) condensation of the evaporant onto the substrate to form the thin film deposit. Figure A.6 shows the *e*-beam evaporator system in our laboratory. The inset figure shows the metal evaporation and transportation processes observed through the *e*-beam observation window. The *e*-beam technology has been used in optical coating of metal oxide thin films [17] and organic photovoltaics [18,19].

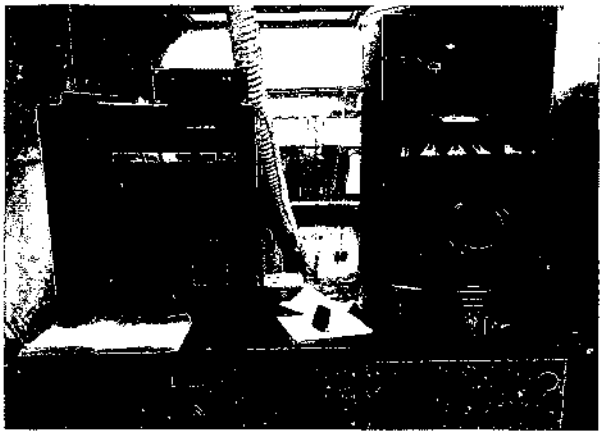

Figure A.6: An *e*-beam unit in our laboratory. The inset picture shows the metal evaporation and transportation processes taking place inside the *e*-beam deposition chamber (taken from the observation window).

It has been reported that a good quality of metal contact electrodes coated by *e*-beam evaporation improves the V_{OC} value of OPV devices [20]. The work function of the metal electrodes plays a critical role on the high PCE. It should present the smallest barrier for charge carriers to make Ohmic contact between the metal electrode and the photo-active material. Thus, the work function of metal electrodes should be aligned with the acceptor material LUMO to effectively maximize V_{OC} of the OPV cell [21].

The substrate was placed in a shadow mask holder and loaded into a high-vacuum electron-beam (*e*-beam) evaporator's chamber. The *e*-beam evaporating system was pumped down to at least until the *e*-beam chamber's pressure approximately 2.0×10^{-7} Torr was achieved. Aluminum pellets with a 99.999% purity grade purchased from The Kurt J. Lesker Company were used as the metal target inside the *e*-beam crucible. Aluminum was deposited onto the substrate through the use of a shadow mask at a deposition rate of approximately 1.5 Å/s until the final thickness of an Al layer of 80 nm was reached. Finally, the substrate was removed from the *e*-beam chamber, and was annealed at 150 °C for 10 min in the N_2-filled glove box (O_2, H_2O < 0.1 ppm). Figure A.7 shows OPV devices fabricated with active layers of (a) a 30:24 weight ratio of P3HT:PC61BM and (b) a 7:28 of PCDTBT:PC71BM after Al metal deposition.

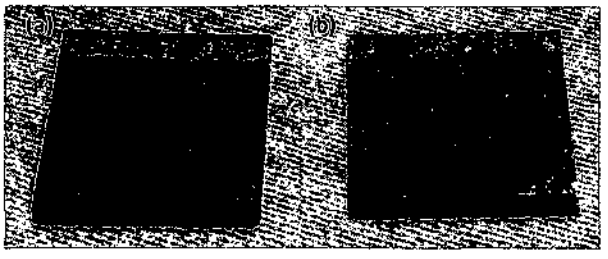

Figure A.7: OPV devices with active layers of (a) P3HT:PC61BM and (b) PCDTBT:PC71BM fabricated without the TiO_x layer.

A.7. Summary

We described preparation steps include patterning and cleaning ITO glass substrates, and stirring active solutions. To obtain a consistent and excellent result, the preparation steps must be performed with standard and optimal conditions. A standard cleaning procedure was used in our experiment. The stirring procedure is unique based on different active solutions. For a high bandgap active solution of P3HT:PC61BM (30 mg

of P3HT and 24 mg of PC61BM in 2 mL chlorobenzene), a combination of low speed stirring condition (100 rpm) and an annealing temperature of 50 °C was used. And for the low bandgap of PCDTBT:PC71BM (7 mg of PCDTBT and 28 mg of PC71BM in 2 mL 1,2-dichlorobenzene), a combination of a higher stirring speed of 250 rpm and a temperature of 120 °C was used.

Organic materials were deposited onto the substrate by means of spin coating. Since organic materials are sensitive to degradation issues like O_2, H_2O, and light, the spin coaters were covered with Al coil to protect organic materials. The condition of the glove box and the electron beam evaporator must be in an optimum quality to avoid any contamination. A lot of efforts had been performed to maintain the glove box and electron beam evaporator in a great working condition.

Two processing procedures were developed to fabricate device with and without the TiO_x layer. Introducing a TiO_x layer as an interfacial layer between the organic materials and the Al cathode means additional processing procedures have to be optimized. A good interfacial morphology between the TiO_x layer-organic materials and the TiO_x layer-Al metal cathode plays a key role in the device performance and the stability of the device.

APPENDIX B

Optimization Processes

B.1. Introduction

The J_{SC}, V_{OC}, FF, and PCE of the OPV devices can be enhanced by various fabrication procedures (morphology control, buffer layers, processing conditions, etc.) and the annealing treatments (pre- and post-annealing, etc.) [22,23]. For the OPV device fabricated with a solution based buffer layer, it is important to obtain an excellent quality of the buffer layer used at an optimum condition.

It must be kept in mind that most of the optimization of the OPV device is not well understood. The optimization results varied from report to report and so far they have been empirical. Tuning fabrication variables further is often required to improve the morphology of the active layer and to ensure that efficient exciton dissociation results in efficient charge separation and collection as well. Several external treatments have been reported to be effective in optimizing native composite films.

B.2. Optimizing the active layer deposition

Spin coating is the most successful and widely employed method for the highly reproducible fabrication of organic thin films with high structural uniformity [24]. The uniformity of the resulting thin film is affected and thus controlled mainly by the choice of solvent [25]. The final thin film morphology will be determined the time allowed for

phase separation to occur during the spin coating. The irregular thickness issue is more prominent in the 1:4 PCDTBT:PC71BM solution. It has been reported that a slow spin speed and a low bandgap polymer showed a better quality of thin film and better performance of the low bandgap polymer devices [10]. The quality issue for the low bandgap polymer might be due to the composition of the organic materials; the molecular weight of PCDTBT (389 kg/mol [26]) which is ~ 700% heavier than the high bandgap counterpart (P3HT) and the higher concentration of PC71BM (80%) in the solution. We observed the edge effect and the irregular thickness on PCDTBT:PC71BM film. Following sections discuss these two problems.

B.2.1 Optimizing the substrate stopper

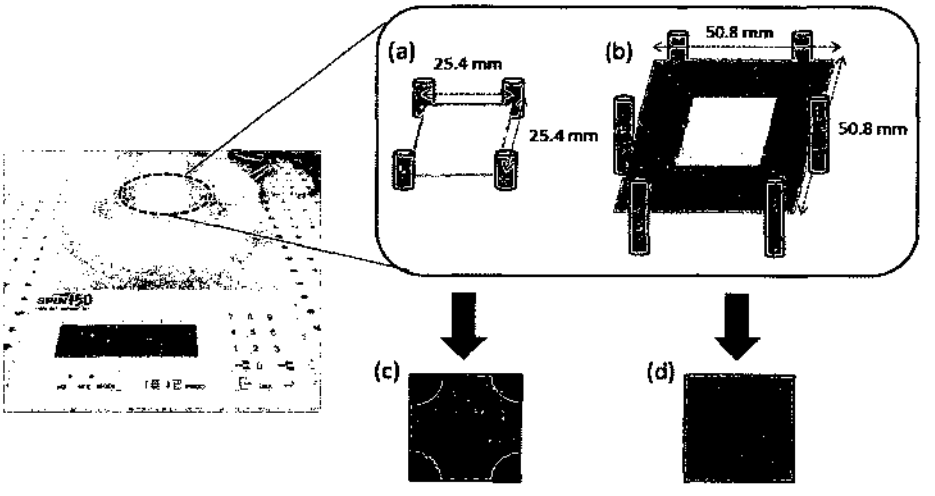

Figure B.1: (a) 25.4 mm × 25.4 mm and (b) 50.8 mm × 50.8 mm sample holders of the SPIN150® mechanical spin coater. Thin film images (c) with and (d) without edge effects.

The photoactive solution was deposited on an ITO glass substrate by using a special mechanical spin coater SPIN150® inside the N_2-filled glove box. The mechanical coater has two different set ups of the substrate stopper (as received from the manufacturer). First, we used the conventional 25.4 mm × 25.4 mm substrate stopper as seen in Figure

B.1(a). After the active solution was spun on the substrate, we observed a significant "edge effect" at every corner of the substrate as seen in Figure B.1(c). We observed that the edge effect was caused by non-equilibrium morphologies due to the disturbance from the four small cylindrical bars (as received from the manufacturer) functioned as substrate stoppers. When the solution was spun, the planar motion caused by the centrifugal force pushed the solution away from the center of the substrate. And the solution that hit the bars did not made its way to escape the substrate; instead it was pushed back and created the edge effect. The active solution concentrated at the edges gets thicker and wider as the spin speed is slower, especially for the low bandgap polymer solution. The widening edge effect has been observed to be overlap with the active area of the OPV devices which caused a serious problem of the thickness irregularity of the active layer across the substrate.

Secondly, we used the alternative set up which we had to incorporate a 50.8 mm × 50.8 mm glass substrate (did not come with the set up) as the base for the ITO glass substrate, as seen in Figure B.1(b). After depositing the solution, as seen in Figure B.1(d), we found that the deposited thin film is more uniform in thickness and more importantly, there are no more edge effects. Unlike in the first setup, the active solution was spun on the substrate without making any contact to any substrate stoppers of the SPIN150® spin coater. A common defect in spin coated films is radial lines representing thickness undulations (non uniform in the film thickness), referred to as striations [27], parallel to the direction of the flow. Because of the flow in the spin coating process the instabilities may lead to local differences in the surface tension at the top surface.

B.2.2. Optimizing the substrate mounting holder

We designed three different substrate mounting holders, as seen in Figure B.2(a) – (c), to achieve a better quality of the active layer films and to solve the irregular thickness issue. As previously mentioned in the previous section, the 50.8 mm × 50.8 mm glass substrate was used as the base in all designs. For the substrate mounting holder Design #1, the 25.4 mm × 25.4 mm substrate was mounted on the 50.8 mm × 50.8 mm glass base with 0.25 in of silicone polyimide tape [2] as seen in Figure B.2(a). In Design #2, we used a double coated foam tape [28] to mount the substrate to the base as seen in Figure B.2(b), and for Design #3, we used a double coated carbon conductive tape [29] to mount the substrate to the base as seen in Figure B.2(c). The cross sectional images of each design are shown in Figure B.2(d) – (f).

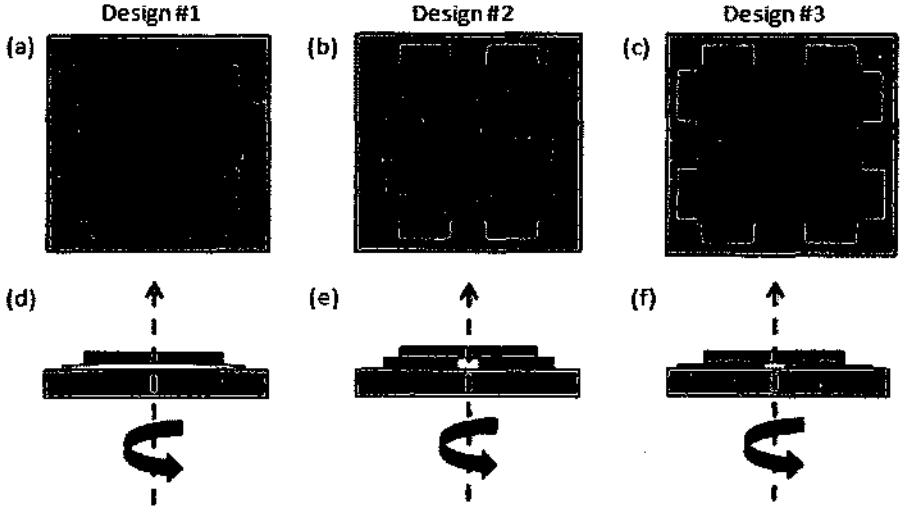

Figure B.2: Different designs of sample mounting holder (a) with a polyimide tape, (b) a foam tape, and (c) a carbon tape.

To test the substrate mounting holder designs, we fabricated three PCDTBT:PC71BM BHJ OPV devices by using different substrate holder designs (we used the same

fabrication conditions). In the test, the spin speed for the active solution was 400 rpm for 120 s inside the glove box. The active layer was then annealed at 140 °C for 2 min. The thickness of Al metal contact was 80 nm. For the post-production thermal treatment, the OPV devices were annealed at 150 °C for 10 min inside the glove box.

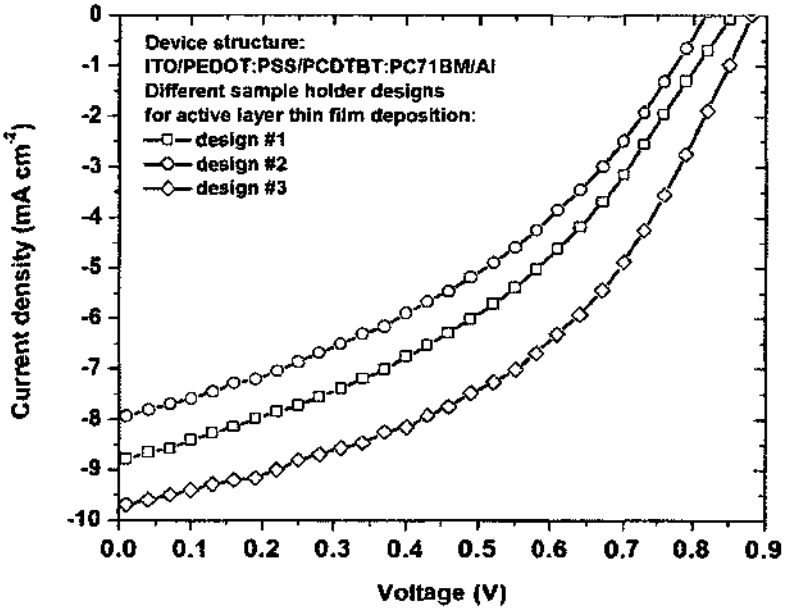

Figure B.3: *J-V* characteristics of PCDTBT:PC71BM OPV cells fabricated with different designs of the substrate mounting holder.

The *J-V* characteristics of the OPV devices are shown in Figure B.3. We observed that the OPV device fabricated with Design #3 shows the best quality of active layer thin film; thus, the best performance. Design #3 produced a FF of 45%, a J_{SC} of 9.72 mA cm^{-2}, and a PCE of 3.9%. Design #1 produced a PCE of 3.0% and Design #2 the lowest PCE of 2.5%, while their FF values were approximately 40%. We conclude that the substrate mounting holder in Design #3 shows the optimal morphology and optimal quality of the thin film of the PCDTBT:PC71BM BHJ cells.

Table B.1: The parameters of PCDTBT:PC71BM OPV cells fabricated with different substrate holder designs.

Substrate holder design	J_{SC} (mA cm^{-2})	V_{OC} (V)	FF (%)	PCE (%)
#1	8.84	0.85	39.51	3.00
#2	7.98	0.82	39.72	2.54
#3	9.72	0.88	45.20	3.87

B.3. Pre- and post-annealing treatments

The best annealing temperature achieving the most favorable morphological development of the OPV cell is normally above the glass-transition temperature, T_g, but below the melting point of the polymer [30]. The crystallinity of the polymer could also be improved by using a pre-annealing or a solvent removing treatment process. This approach aims at maintaining the polymer ordering during the film formation stage. Reducing the solvent removal accelerates results in self-organization in polymer chains by controlling the active polymer layer growth rate from solution to a solid state. The pre-annealed films consist of highly ordered polymer chains, which cannot be achieved through thermal annealing, the extra step of annealing the films provides further enhancement in device performance [31].

It is common to employ another annealing treatment after the fabrication of the OPV device. This process is called a post-annealing treatment. The main problem with controlling the morphology of all the layers in the device at the same time is typically surpassed by the overall improvements in the PV performance. Ma and his co-workers reported that the optimal post-annealing temperature was reported to be 150 °C [32]. We used the post-annealing temperature of 150 °C in our experiment and varied the post-annealing times to find the optimum result.

B.4. Interfacial layer thickness

The thickness of the highly conductive interlayer can be tuned to optimize the optical field distribution in the solar cell, and the increase in overall thickness of the devices allows higher stability and a lower probability for short circuiting the device [33]. Interfacial phenomena are largely independent of the cell design but must specifically accommodate the particular donor and acceptor materials being employed. In our study, we used the solution based TiO_x layer as an interfacial layer between the active layer and the metal cathode. The optimal thickness of the TiO_x film for OPV devices has been reported to be in the range of 5 – 20 nm [34,35,36,37].

B.5. Summary

It is mandatory to perform optimization steps to achieve an optimum and a good reproducible quality result of OPV devices. At present, the optimization results are empirical and varied from report to report. We developed optimization steps based on the following processing variables such as the active layer thickness, pre- and post-annealing treatments. When a TiO_x layer is introduced, additional optimization steps, the thickness of TiO_x layer and the TiO_x solution drying condition, must be performed.

We developed a spin coating procedure for the low bandgap active solution of PCDTBT:PC71BM since we observed a non-uniformity and an irregularity in the active layer thickness. We observed that the quality issue for the low bandgap polymer might be due to the composition of the organic materials; the molecular weight of PCDTBT and the higher concentration of PC71BM (80%) in the solution. We developed several sample holder mounting designs to solve the edge effect and the irregular thickness of the active

layer. We conclude that Design #3 with a conductive carbon tape was the best mounting design that improve the quality of the active layer. We used Design #3 in depositing both high and low bandgap active solutions of P3HT:PC61BM and PCDTBT:PC71BM in our experiment.

APPENDIX C

Statistical Method

In our experiment, although all 8 OPV cells in an OPV device were fabricated at the same processing condition, their qualities and performances might be different due to random variability issues such as the complexity on how the bulk heterojunction networks were formed on each OPV cell, the interface between the metal contact and the organic layer, etc. Moreover, in addition to the random variability, the data indicate among others a location effect affecting the outcome either due to mask design or process design.

The I-V characterization of OPV cells was measured in the air. In OPV research, if n measurements in a sample are denoted by x_1, x_2, ..., and x_n, the sample mean, standard deviation, and standard error of the population of the sample are defined as

$$\bar{x} = \frac{x_1 + x_n + \ldots + x_n}{n} = \frac{\sum x_i}{n} \tag{A.1}$$

$$s = \sqrt{\frac{\sum (x_i - \bar{x})^2}{n-1}} \tag{A.2}$$

By using Equations A.1 and A.2, we determined the mean and standard deviation of the cell's OPV parameter. Error bars are a graphical representation of the variability of data and are used on graphs to indicate the error, or uncertainty in a reported measurement.

They often represent one standard deviation of uncertainty, one standard error, or a certain confidence interval.

Table C.1. Lists the parameter variability of the best 20 OPV cells out of 200 high bandgap polymer of P3HT:PC61BM OPV devices tested with PCE values equal or larger than 4%.

P3HT:PC61BM	J_{SC} (mA cm^{-2})	V_{OC} (V)	FF (%)	PCE (%)
1	10.60	0.61	61.91	4.00
2	10.53	0.63	61.82	4.10
3	10.49	0.62	63.66	4.14
4	11.10	0.62	58.60	4.03
5	11.31	0.62	57.64	4.04
6	11.60	0.61	57.46	4.06
7	11.10	0.64	56.76	4.03
8	11.00	0.63	57.66	4.03
9	11.14	0.62	58.72	4.06
10	11.64	0.62	56.73	4.05
11	11.99	0.63	54.65	4.13
12	11.88	0.63	54.07	4.05
13	11.34	0.63	56.58	4.04
14	11.66	0.63	55.66	4.09
15	12.10	0.63	53.46	4.08
16	12.40	0.61	53.91	4.08
17	11.52	0.60	57.90	4.00
18	10.73	0.62	60.61	4.03
19	11.41	0.64	55.87	4.08
20	10.90	0.62	61.08	4.13
Average	11.32 ± 0.54	0.62 ± 0.01	57.74 ± 2.88	4.06 ± 0.04

Table C.2. Lists the parameter variability of the best 10 OPV cells of 100 low bandgap polymer of PCDTBT:PC71BM OPV devices tested with PCE values equal or larger than 5%.

PCDTBT:PC71BM	J_{SC} (mA cm^{-2})	V_{OC} (V)	FF (%)	PCE (%)
1	12.75	0.90	43.70	5.02
2	12.75	0.89	44.19	5.02
3	13.03	0.87	45.25	5.13
4	12.24	0.87	47.05	5.01
5	13.96	0.89	40.37	5.02
6	13.54	0.90	41.35	5.04
7	13.24	0.86	44.15	5.03
8	13.45	0.89	41.81	5.01
9	12.56	0.88	45.64	5.05
10	12.85	0.88	45.10	5.10
Average	13.04 ± 0.51	0.88 ± 0.01	43.86 ± 2.10	5.04 ± 0.04

Table C.3. List of experimentally determined PCE values of all 200 high bandgap of P3HT:PC61BM OPV devices that were fabricated for this thesis work. The overall average of all 200 PCE values for high bandgap polymers is 2.46 ± 0.97 %.

Device	PCE (%)	Device	PCE (%)	Device	PCE (%)	Device	PCE (%)	Device	PCE (%)
1	4.00	41	3.95	81	2.62	121	2.70	161	1.98
2	4.10	42	3.48	82	2.66	122	2.52	162	1.83
3	4.14	43	3.52	83	2.46	123	2.28	163	1.71
4	4.03	44	3.60	84	2.70	124	2.89	164	1.38
5	4.04	45	3.34	85	2.41	125	2.72	165	1.91
6	4.06	46	3.51	86	2.29	126	2.08	166	1.76
7	4.03	47	3.63	87	2.20	127	2.46	167	1.91
8	4.03	48	3.85	88	2.15	128	2.78	168	1.90
9	4.06	49	3.65	89	2.87	129	2.34	169	1.37
10	4.05	50	3.56	90	2.99	130	2.73	170	1.27
11	4.13	51	3.42	91	2.95	131	2.25	171	1.33
12	4.05	52	3.52	92	2.38	132	2.15	172	1.25
13	4.04	53	3.73	93	2.67	133	2.42	173	1.44
14	4.09	54	3.39	94	2.74	134	2.30	174	1.36
15	4.08	55	3.15	95	2.66	135	1.56	175	1.26
16	4.08	56	3.04	96	2.45	136	1.61	176	1.31
17	4.00	57	2.53	97	2.73	137	1.69	177	1.43
18	4.03	58	2.59	98	2.69	138	1.60	178	1.39
19	4.08	59	2.56	99	2.60	139	1.55	179	1.45
20	4.13	60	2.22	100	2.73	140	1.44	180	1.44
21	3.74	61	2.72	101	2.61	141	1.59	181	1.25
22	3.89	62	2.69	102	2.33	142	1.49	182	1.22
23	3.83	63	2.04	103	2.37	143	1.46	183	1.01
24	3.66	64	2.45	104	2.25	144	1.62	184	1.13
25	3.78	65	2.53	105	2.34	145	1.57	185	1.22
26	3.68	66	2.34	106	2.40	146	1.85	186	1.21
27	3.50	67	2.23	107	2.17	147	1.74	187	1.38
28	3.66	68	2.35	108	2.73	148	1.76	188	1.04
29	3.44	69	2.10	109	2.46	149	1.89	189	1.07
30	3.54	70	2.17	110	2.62	150	1.71	190	0.59
31	3.33	71	2.16	111	2.70	151	1.85	191	0.66
32	3.62	72	2.40	112	2.35	152	1.81	192	0.75
33	3.59	73	2.20	113	2.09	153	1.92	193	0.81
34	3.39	74	2.11	114	2.01	154	1.49	194	0.63
35	3.82	75	2.00	115	2.52	155	1.79	195	0.73
36	3.45	76	2.16	116	2.00	156	1.71	196	0.71
37	3.48	77	2.02	117	2.66	157	1.62	197	0.79
38	3.72	78	2.08	118	2.90	158	1.77	198	0.68
39	3.92	79	2.14	119	2.71	159	1.66	199	0.82
40	3.63	80	2.76	120	2.02	160	1.87	200	0.73

Table C.4. List of experimentally determined PCE values of all 100 low bandgap of PCDTBT:PC71BM OPV devices that were fabricated for this thesis work. The overall average of all 100 PCE values for low bandgap polymers is 3.21 ± 1.20 %.

Device	PCE (%)	Device	PCE (%)	Device	PCE (%)	Device	PCE (%)	Device	PCE (%)
1	5.02	21	4.39	41	3.03	61	3.39	81	2.87
2	5.02	22	4.77	42	3.52	62	3.32	82	2.34
3	5.13	23	4.86	43	3.00	63	3.34	83	2.11
4	5.01	24	4.54	44	3.12	64	3.39	84	2.95
5	5.02	25	4.17	45	3.23	65	3.21	85	2.31
6	5.04	26	3.67	46	3.37	66	2.40	86	1.23
7	5.03	27	3.86	47	3.02	67	2.15	87	1.11
8	5.01	28	3.36	48	3.35	68	2.69	88	1.70
9	5.05	29	3.63	49	3.48	69	2.68	89	1.59
10	5.10	30	3.88	50	3.50	70	2.09	90	1.33
11	4.16	31	3.48	51	3.65	71	2.10	91	1.15
12	4.13	32	3.95	52	3.03	72	2.85	92	1.93
13	4.37	33	3.86	53	3.52	73	2.20	93	1.53
14	4.42	34	3.90	54	3.73	74	2.74	94	1.88
15	4.04	35	3.89	55	3.25	75	2.23	95	0.30
16	4.55	36	3.87	56	3.22	76	2.60	96	0.51
17	4.27	37	3.53	57	3.32	77	2.54	97	0.77
18	4.09	38	3.35	58	3.36	78	2.24	98	0.97
19	4.19	39	3.48	59	3.45	79	2.27	99	0.27
20	4.93	40	3.65	60	3.56	80	2.64	100	0.65

In summary, we calculated the statistical values, the mean x-bar and standard deviations, of the OPV devices discussed in the thesis by using A1 and A2. The average PCE values in this study are low and the standard deviation values because the yield of OPV devices in our university was law due to multiple factors and impediments. Overall, the mean PCE value was significantly reduced and the standard was large due to the random variability. The root cause for low yield and low average PCE is attributed to the non-optimized device design and process technology, the difficult fabrication processes and the technical limitations in a university laboratory. The poor performance of OPV devices is generally attributed to a poorly developed morphology that consists of an intimately mixed composite of donor and acceptor materials rather than a bi-continuous network of well-developed and ordered pathways for the charge transport. The random

variability in OPV cells in a device fabricated with similar processing steps and affected by the experimental condition during the OPV fabrication results is still difficult to control in our study.

APPENDIX D

Stability Tests

D.1. High bandgap polymer of a P3HT:PC61BM OPV device

Table D.1. The parameters of a P3HT:PC61BM OPV cell with a TiO_x layer at stored in the glove box and with an opaque Al cover.

Storage time (day)	J_{SC} (mA cm^{-2})	V_{OC} (V)	FF (%)	PCE (%)
1	6.69	0.62	40.39	1.69
5	6.63	0.62	40.64	1.68
10	6.56	0.62	40.47	1.65
15	6.49	0.62	39.88	1.61
20	6.41	0.63	37.99	1.53
25	6.34	0.63	36.79	1.46
30	6.25	0.62	36.85	1.44
35	6.17	0.62	37.22	1.43
40	6.10	0.62	37.37	1.42
45	6.02	0.62	37.04	1.38
50	5.97	0.62	36.27	1.33
60	5.73	0.62	36.10	1.28
70	5.61	0.62	36.12	1.25

D.2. Low bandgap polymer of PCDTBT:PC71BM devices

Table D.2: The parameters of a PCDTBT:PC71BM OPV cell with a TiO_x layer stored in the air and with an opaque Al cover.

Storage time (day)	J_{SC} (mA cm^{-2})	V_{OC} (V)	FF (%)	PCE (%)
1	10.25	0.78	43.95	3.52
2	9.31	0.77	38.10	2.74
3	8.59	0.77	33.68	2.23
4	7.96	0.76	28.58	1.74
5	7.31	0.73	26.35	1.41
6	7.00	0.73	25.30	1.28
7	6.62	0.72	24.80	1.19
12	5.09	0.68	20.47	0.71
18	2.66	0.59	17.22	0.27

Table D.3: The parameters of a PCDTBT:PC71BM OPV cell with a TiO_x layer stored in the air and without an opaque Al cover.

Storage time (day)	J_{SC} (mA cm^{-2})	V_{OC} (V)	FF (%)	PCE (%)
1	10.51	0.81	42.52	3.63
2	9.80	0.79	36.94	2.85
3	9.22	0.78	30.57	2.20
4	8.72	0.76	27.60	1.83
5	8.18	0.74	23.71	1.43
6	7.44	0.70	23.49	1.22
7	6.92	0.69	22.78	1.08
12	5.28	0.64	18.60	0.63
18	2.93	0.61	15.56	0.27

Table D.4: The parameters of a PCDTBT:PC71BM OPV cell with a TiO_x layer stored in the glove box and with an opaque Al cover.

Storage time (day)	J_{SC} (mA cm^{-2})	V_{OC} (V)	FF (%)	PCE (%)
1	11.95	0.89	44.77	4.77
2	11.92	0.88	45.06	4.73
3	11.88	0.87	45.04	4.65
4	11.71	0.86	44.80	4.53
5	11.63	0.86	44.59	4.46
6	11.55	0.86	44.16	4.28
7	11.38	0.85	44.06	4.20
12	11.28	0.85	44.01	4.18
18	11.20	0.85	43.79	4.17
25	10.96	0.85	42.43	4.08
30	10.84	0.85	42.14	4.00

Table D.5: The parameters of a PCDTBT:PC71BM OPV cell with a TiO_x layer stored in the glove box and without an opaque Al cover.

Storage time (day)	J_{SC} (mA cm^{-2})	V_{OC} (V)	FF (%)	PCE (%)
1	11.71	0.83	46.25	4.56
2	11.43	0.81	46.39	4.33
3	11.14	0.79	45.31	4.04
4	10.76	0.79	46.35	3.97
5	10.54	0.78	45.40	3.77
6	10.27	0.77	45.37	3.63
7	10.03	0.77	45.83	3.56
12	9.91	0.77	44.66	3.38
18	9.64	0.77	44.41	3.28
25	9.30	0.77	44.65	3.19
30	9.15	0.76	43.16	3.02

Table D.6: The parameters of a PCDTBT:PC71BM OPV cell without a TiO_x layer stored in the air and with an opaque Al cover.

Storage time (day)	J_{SC} (mA cm^{-2})	V_{OC} (V)	FF (%)	PCE (%)
1	10.86	0.84	41.02	3.73
2	3.60	0.84	17.02	0.51
3	0.20	0.78	7.96	0.01
4	0.02	0.75	2.50	0.00

Table D.7: The parameters of a PCDTBT:PC71BM OPV cell without a TiO_x layer stored in the glove box and with an opaque Al cover.

Storage time (day)	J_{SC} (mA cm^{-2})	V_{OC} (V)	FF (%)	PCE (%)
1	11.63	0.83	38.68	3.71
2	11.12	0.83	38.10	3.53
3	10.79	0.83	34.94	3.14
4	10.44	0.82	33.75	2.88
5	10.10	0.83	30.91	2.60
6	9.59	0.82	30.52	2.54
7	9.25	0.83	29.88	2.26
12	8.96	0.82	29.84	2.24
18	8.78	0.82	29.51	2.14
25	8.52	0.82	29.68	2.09
30	8.27	0.82	28.42	1.93

Table D.8: The parameters of a PCDTBT:PC71BM OPV cell with a TiO_x layer stored in the ante-chamber and with an opaque Al cover.

Storage time (day)	J_{SC} (mA cm^{-2})	V_{OC} (V)	FF (%)	PCE (%)
1	9.57	0.81	39.98	3.12
2	8.96	0.81	37.15	2.69
3	8.52	0.81	36.68	2.52
4	8.20	0.81	35.71	2.36
5	7.73	0.81	36.34	2.27
6	7.30	0.81	35.00	2.06
7	6.96	0.81	33.49	1.88
12	6.68	0.81	32.71	1.77
18	5.96	0.82	29.91	1.47
25	5.73	0.82	20.36	0.97
30	5.22	0.82	17.79	0.77

Table D.9: The parameters of a PCDTBT:PC71BM OPV cell with a TiO_x layer stored in the refrigerator and with an opaque Al cover.

Storage time (day)	J_{SC} (mA cm^{-2})	V_{OC} (V)	FF (%)	PCE (%)
1	10.19	0.86	36.23	3.13
2	9.94	0.85	35.90	3.04
3	9.65	0.85	35.18	2.88
4	9.44	0.83	35.01	2.75
5	9.26	0.83	34.88	2.64
6	8.94	0.84	34.65	2.58
7	8.55	0.84	34.55	2.50
12	8.18	0.83	34.38	2.45
18	7.71	0.83	33.56	2.10
25	7.33	0.83	32.15	1.89
30	7.05	0.82	31.06	1.80

APPENDIX E

Copyrighted Materials

E.1. M. Jørgensen, K. Norrman, and F.C. Krebs, "Stability/degradation of polymer solar cells", *Sol. Energy Mater. Sol. Cells*, **92**, 686-714 (2008).

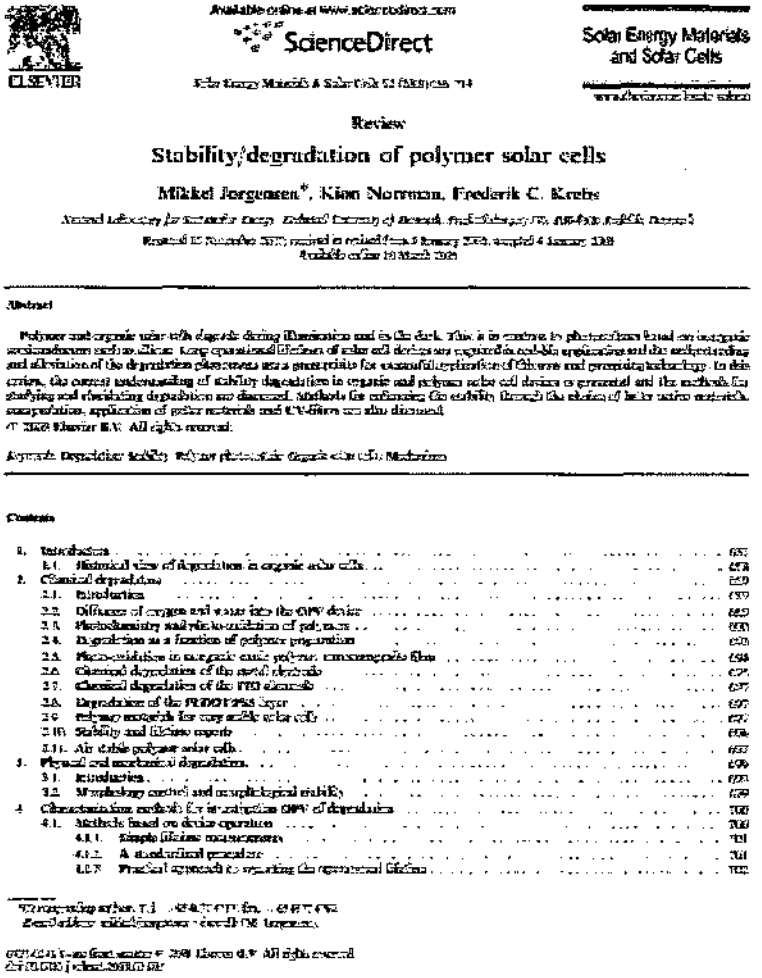

Available online at www.sciencedirect.com
ScienceDirect
Solar Energy Materials & Solar Cells 92 (2008) 686–714
Solar Energy Materials and Solar Cells
www.elsevier.com/locate/solmat

Review

Stability/degradation of polymer solar cells

Mikkel Jørgensen*, Kion Norrman, Frederik C. Krebs
Risø National Laboratory for Sustainable Energy, Technical University of Denmark, Frederiksborgvej 399, DK-4000 Roskilde, Denmark

Received 15 November 2007; received in revised form 5 January 2008; accepted 4 January 2008
Available online 10 March 2008

Abstract

Polymer and organic solar cells degrade during illumination and in the dark. This is in contrast to photovoltaics based on inorganic semiconductors such as silicon. Long operational lifetimes of solar cell devices are required to enable optimization and the understanding and alleviation of the degradation processes are a prerequisite for successful optimization of efficiency and promising technology. In this review, the current understanding of stability/degradation in organic and polymer solar cell devices is presented and the methods for studying and elucidating degradation are discussed. Methods for enhancing the stability through the choice of inherently more stable materials, encapsulation, application of solar materials and UV-filters are also discussed.

Keywords: Degradation; Stability; Polymer photovoltaic; Organic solar cells; Modules; Review

Contents

* Corresponding author. Tel.: +45 4677 4701; fax: +45 4677 4756.
E-mail address: mikkel.jorgensen@risoe.dk (M. Jørgensen).

doi:10.1016/j.solmat.2008.01.005

E.2. K. Lee, J.Y. Kim, S.H. Park, S.H. Kim, S. Cho, and A.J. Heeger, "Air-Stable Polymer Electronic Devices", *Adv. Mater.*, **19**, 2445 (2007).

ADVANCED MATERIALS

Air-Stable Polymer Electronic Devices**

By Kwanghee Lee, Jin Young Kim, Sung Heum Park, Sun Hee Kim, Shinuk Cho, and Alan J. Heeger

E.3. J.Y. Kim, S.H. Kim, H.-H. Lee, K. Lee, W. Ma, X. Gong, and A.J. Heeger, "New Architecture for High-Efficiency Polymer Photovoltaic Cells Using Solution-Based Titanium Oxide as an Optical Spacer", *Adv. Mater.*, **18**, 572 (2006).

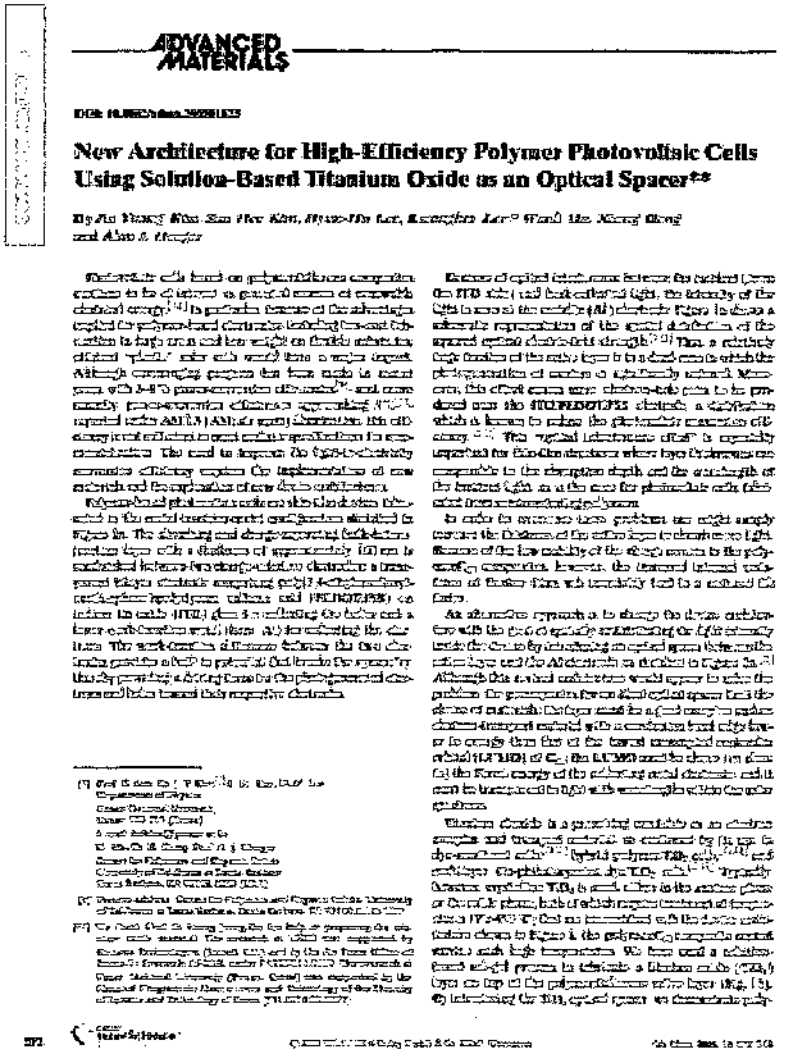

ADVANCED MATERIALS

New Architecture for High-Efficiency Polymer Photovoltaic Cells Using Solution-Based Titanium Oxide as an Optical Spacer

APPENDIX REFERENCES

[1] ITO coated glass (1.1 mm thick) is a product of The NanoCS Company.

[2] Kapton polyimide electrical tape is a product of The Tape Depot Company.

[3] S.-In Na, S.-S. Kim, S.-S. Kwon, J. Jo, J. Kim, T. Lee, and D.-Y. Kim, Appl. Phys. Lett., **91**, 173509 (2007).

[4] R. Radbeh, E. Parbaile, A. Bouche, C. Di Bin, A. Moliton, V. Coudert, F. Rossignol, and B. Ratier, *Nanotechnology*, **21**, 035201 (2010).

[5] N.D. Treat, M.A. Brady, G. Smith, M.F. Toney, E.J. Kramer, C.J. Hawker, and M.L. Chabinyc, *Adv. Energy Mater.*, **1**, 82 (2011).

[6] Y. Wang, S.W. Tong, X.F. Xu, B. Özyilmaz, and K.P. Loh, *Adv. Mater.*, **23**, 1514 (2011).

[7] J. Schafferhans, A. Baumann, A. Wagenpfahl, C. Deibel, and V. Dyakonov, *Org. Electron.*, **11**, 1693 (2010).

[8] C.H. Peters, I.T. Sachs-Quintana, J.P. Kastrop, S. Beaupre´, M. Leclerc, and M.D. McGehee, *Adv. Energy Mater.*, **1**, 491 (2011).

[9] M. Tong, N.E. Coates, D. Moses, A.J. Heeger, S. Beaupre, and M. Leclerc, *Phys. Rev. B*, **81**, 125210 (2010).

[10] S.H. Park, A. Roy, S. Beaupre, S. Cho, N. Coates, J.S. Moon, D. Moses, M. Leclerc, K. Lee, and A.J. Heeger, *Nat. Photonics*, **3**, 297 (2009).

[11] J.-L. Brédas, J.E. Norton, J. Cornil, and V. Coropceanu, *Acct. Chem. Res.*, **42**, 1691 (2009).

[12] P.A. van Hal, M.M. Wienk, J.M. Kroon, W.J.H. Verhees, L.H. Slooff, W.J.H. van Gennip, P. Jonkheijm, and R.A.J. Janssen, *Adv. Mater.*, **15**, 118 (2003).

[13] J.Y. Kim, S.H. Kim, H.-H. Lee, K. Lee, W. Ma, X. Gong, and A.J. Heeger, *Adv. Mater.*, **18**, 572 (2006).

[14] J.K. Lee, N.E. Coates, S. Cho, N.S. Cho, D. Moses, G.C. Bazan, K. Lee, and A.J. Heeger, *Appl. Phys. Lett.*, **92**, 243308 (2008).

[15] J. Li, S. Kim, S. Edington, J. Nedy, S. Cho, K. Lee, A.J. Heeger, M.C. Gupta, and J.T. Yates Jr., *Sol. Energy Mater. Sol. Cells*, **95**, 1123 (2011).

[16] J. Huang, P. Miller, J. Mello, A. Mello, and D. Bradley, *Synth. Met.*, **139**, 569 (2003).

[17] R.W. Phillips and A. Argoitia, 48th Annual Technical Conference Proceedings of the Society of Vacuum Coaters, 145 (2005).

[18] M. Glatthaar, M. Niggemann, B. Zimmermann, P. Lewer, M. Riede, A. Hinsch, and J. Luther , *Thin Solid Films*, **491**, 298 (2005).

[19] J. Kim, J.-S. Kim, S.-W. Kwak, J.-S. Yu, Y. Jang, J. Jo, T.-M. Lee, and I. Kim, *Appl. Phys. Lett.*, **101**, 213304 (2012).

[20] C. Zhang, S.W. Tong, C. Zhu, C. Jiang, E.T. Kang, and D.S.H. Chan, *Appl. Phys. Lett.*, **94**, 103305 (2009).

[21] Y.S. Eo, H.W. Rhee, B.D. Chin, and J.-W. Yu, *Synth. Met.*, **159**, 1910 (2009).

[22] D. Chirvase, J. Parisi, J.C. Hummelen, and V. Dyakonov, *Nanotechnology,* **15,** 1317 (2004).

[23] F. Padinger, R.S. Rittberger, and N.S. Sariciftci, *Adv. Funct. Mater.*, **13**, 85 (2003).

[24] K. Norrman, N.B. Larsen, and A. Ghanbari-Siahkali, *Ann. Rep. Prog. Chem. Sect. C: Phys. Chem.*, **101**, 174 (2005).

[25] R.A.L. Jones, "Polymers at Surfaces and Interfaces", University Press, Cambridge (1999).

[26] Z. Li and C.R. McNeill, *J. Appl. Phys.*, **109**, 074513 (2011).

[27] D.P. Birnie, III, *J. Mater. Res.*, **16**, 1145 (2001).

[28] Double coated Scotch foam tape is a product of The 3M Tape Company.

[29] Double coated conductive tape is a product of The Ted Pella Tape Company.

[30] J. M. J. Frechet and B. C. Thompson, *Angew. Chem. Int. Ed.*, **47**, 58 (2008).

[31] T. Erb, U. Zhokhavets, G. Gobsch, R. Raleva, B. Stuhn, P. Schilinsky, C. Waldauf, and C.J. Brabec, *Adv. Funct. Mater.*, **15**, 1193 (2005).

[32] W. Ma, C. Yang, X. Gong, K. Lee, and A.J. Heeger, *Adv. Funct. Mater.*, **15** ,1617 (2005).

[33] P.D. Andersen, J.C. Skarhoj, J.W. Andreasen, and F.C. Krebs, *Opt. Mater.*, **31**, 1007 (2009).

[34] K. Lee, J.Y. Kim, S.H. Park, S.H. Kim, S. Cho, and A.J. Heeger, *Adv. Mater.*, **19**, 2445 (2007).

[35] D.H. Wang, S.H. Im, H.K. Lee, O.O. Park, and J.H. Park, *J. Phys. Chem. C*, **113**, 17268 (2009).

[36] A. Hayakawa, O. Yoshikawa, T. Fujieda, K. Uehara, and S. Yoshikawa, *Appl. Phys. Lett.*, **90**, 163517 (2007).

[37] A. Bauer, T. Wahl, J. Hanisch, and E. Ahlswede, *Appl. Phys. Lett.*, **100**, 073307 (2012).

VITA

KURNIAWAN FOE

1730 Tulane Rd.
Norfolk, VA, 23518
kurniafoe@gmail.com

EDUCATION

- PhD., Electrical and Computer Engineering, Old Dominion University [August 2013]
- M.S., Physics, Old Dominion University [May 2006]
- M.Sc., Physics, University of Indonesia, Indonesia [May 2000]
- B.Sc., Physics, University of Indonesia, Indonesia [May 1998]

HONOR AND AWARD

- The best 5% top graduates, University of Indonesia, 1998.
- Recipient of University Research for Graduate Education from Indonesian government and USAID education program, 1998.
- Old Dominion University Teaching and Research Assistantship (Department of Physics): 2005 – 2008.
- Old Dominion University Research Assistantship (Department of Electrical and Computer Engineering): 2008 – 2012.
- Second prize for the poster presentation presented at Tidewater Virginia Chapter & Washington, D.C area Chapter of Sigma Xi-10th Annual Student Research Poster Session, Christopher Newport University, 2008.
- Nominated for The Outstanding Graduate Teaching Assistant Award in Department of Electrical and Computer Engineering for Spring 2012.
- Selected to present a research poster at ODU Research Achievement Day 2012 "Application of nanoscale thin film titanium sub-oxide in high and low band-gap organic photovoltaics".

PUBLICATION

- K. Foe, D. Kusno, Y. Surya, "Amplitudo multikutub fotoproduksi pion pada daerah resonansi delta", Kumpulan Fisika Teori dan Fisika Nuklir, Himpunan Fisikawan Indonesia, FMIP, UGM (1998).
- K. Foe, "Pion photoproduction up to the second resonance region", Proceedings of the 16th and 17th Annual Hampton University Graduate Studies, World Scientific Publishing Co. Pte. Ltd. (2004).
- K. Foe, P. Boland, Jr., G. Namkoong, D. Gu, H. Baumgart, and T.F. Abdel-Fattah, "Self-organized crystal growth of nanostructured ZnO morphologies by hydrothermal synthesis", *ECS Trans.*, **25**, 3 (2009).
- K. Foe, P.M. Boland, D. Gu, H. Baumgart, T.M. Abdel-Fattah, M. Jeong, and G. Namkoong, "Controlled synthesis of ZnO nanospheres using hydrothermal process", *ECS Trans.*, **33**, 51 (2010).

- K. Foe, H. Baumgart, T.M. Abdel-Fattah, and G. Namkoong, "Organic photovoltaics by using a nanoscale thin film of solution-based titanium sub-oxide", ECS Conference Poster, (2012).
- K. Foe and G. Namkoong, "Aluminum cathodic thin film as a metal contact in organic solar cells", Mid-Atlantic American Vacuum Society Conference Poster, (2012).
- K. Foe, T.M. Abdel-Fattah, H. Baumgart, D.-S. Lee, M. Jeong, and G. Namkoong, "Controlled synthesis of zinc oxide sphere using structure directing agents", *Thin Solid Films*, **534**, 76 (2013).
- K. Foe, M. Samson, T.M. Abdel-Fattah, and G. Namkoong, "Stability of high band-gap P3HT:PCBM organic solar cells using TiO_x interfacial layer", *International Journal of Photoenergy* (in progress).